OPEN ACCESS

CLINICAL SCIENCE

circPDE4B prevents articular cartilage degeneration and promotes repair by acting as a scaffold for RIC8A and MID1

Shuying Shen,[1,2] Yute Yang,[1,2] Panyang Shen,[1,2] Jun Ma,[1,2] Bin Fang,[3] Qingxin Wang,[4] Kefan Wang,[1,2] Peihua Shi,[1,2] Shunwu Fan ,[1,2] Xiangqian Fang [1,2]

Handling editor Josef S Smolen

► Additional supplemental material is published online only. To view, please visit the journal online (http://dx.doi.org/10.1136/annrheumdis-2021-219969).

[1]Department of Orthopaedic Surgery, Sir Run Run Shaw Hospital, Zhejiang University school of medicine, Hangzhou, China
[2]Key Laboratory of Musculoskeletal System Degeneration and Regeneration Translational Research of Zhejiang Province, Hangzhou, China
[3]Department of Spine Surgery, The Central Hospital Affiliated to Shaoxing University, Shaoxing, China
[4]Department of Spine Surgery, The Hospital of the Marine Police Corps of the Chinese people's Armed Police Force, Jiaxing, China

Correspondence to
Dr Xiangqian Fang and Dr Shunwu Fan, Department of Orthopaedic Surgery, Sir Run Run Shaw Hospital, Zhejiang University school of medicine, Hangzhou, People's Republic of China; orthofxq@zju.edu.cn, 0099203@zju.edu.cn

SS, YY and PS contributed equally.

Received 25 January 2021
Accepted 13 May 2021

Check for updates

© Author(s) (or their employer(s)) 2021. Re-use permitted under CC BY. Published by BMJ.

To cite: Shen S, Yang Y, Shen P, *et al*. *Ann Rheum Dis* Epub ahead of print: [*please include* Day Month Year]. doi:10.1136/annrheumdis-2021-219969

ABSTRACT

Objectives Circular RNAs (circRNAs) have emerged as significant biological regulators. Herein, we aimed to elucidate the role of an unidentified circRNA (circPDE4B) that is reportedly downregulated in osteoarthritis (OA) tissues.

Methods The effects of circPDE4B were explored in human and mouse chondrocytes in vitro. Specifically, RNA pull-down (RPD)-mass spectrometry analysis (MS), immunoprecipitation, glutathione-S-transferase (GST) pull-down, RNA immunoprecipitation and RPD assays were performed to verify the interactions between circPDE4B and the RIC8 guanine nucleotide exchange factor A (RIC8A)/midline 1 (MID1) complex. A mouse model of OA was also employed to confirm the role of circPDE4B in OA pathogenesis in vivo.

Results circPDE4B regulates chondrocyte cell viability and extracellular matrix metabolism. Mechanistically, FUS RNA binding protein (FUS) was found to promote the splicing of circPDE4B, while downregulation of circPDE4B in OA is partially caused by upstream inhibition of FUS. Moreover, circPDE4B facilitates the association between RIC8A and MID1 by acting as a scaffold to promote RIC8A degradation through proteasomal degradation. Furthermore, ubiquitination of RIC8A at K415 abrogates RIC8A degradation. The circPDE4B–RIC8A axis was observed to play an important role in regulating downstream p38 mitogen-activated protein kinase (MAPK) signalling. Furthermore, delivery of a circPDE4B adeno-associated virus (AAV) abrogates the breakdown of cartilage matrix by medial meniscus destabilisation in mice, whereas a RIC8A AAV induces the opposite effect.

Conclusion This work highlights the function of the circPDE4B–RIC8A axis in OA joints, as well as its regulation of MAPK-p38, suggesting this axis as a potential therapeutic target for OA.

Key messages

What is already known about this subject?

- Circular RNAs broadly participate in normal physiology and disease, including functioning as miRNA sponges in osteoarthritis (OA).
- Protein post-translational modifications are necessary for proteins to perform physiological or pathological functions, including knee cartilage homeostasis.

What does this study add?

- circPDE4B serves as a scaffold to facilitate RIC8 guanine-nucleotide exchange factor A (RIC8A)–midline 1 binding, thereby decreasing RIC8A-dependent activation of the p38 mitogen-activated protein kinase signalling pathway and regulating OA progression.
- The role of RIC8A is first reported in chondrocytes, and K415 is found as the most important ubiquitination site of RIC8A regulated by circPDE4B.

How might this impact on clinical practice or future developments?

- The circPDE4B–RIC8A axis may serve as a potential therapeutic target for OA.

INTRODUCTION

The aetiology of osteoarthritis (OA), the most common type of arthritis, is multifactorial and is associated with obesity, ageing, strain, trauma, congenital joint abnormalities and joint deformities.[1 2] Although OA involves pathological changes in joint sites, including subchondral osteosclerosis, synovitis and osteophyte formation, destruction of cartilage represents its landmark.[3] Considering that the extracellular matrix (ECM) accounts for 90% of the dry weight of cartilage,[4] changes in its physiology directly impact the function of cartilage. Moreover, as the only cell type in cartilage, chondrocytes play an important role in maintaining ECM homeostasis.[5] Thus, characterising the molecular mechanisms of chondrocytes involved in OA development and pathogenesis is crucial for improving prognosis and developing effective therapies.[6–8]

Recently, a growing number of studies have identified various functional non-coding RNAs, including circular RNAs (circRNAs), many of which are present in the human transcriptome.[9] The expression of these circRNAs exhibits tissue specificity, while their heterocyclic structure makes them highly stable.[10] Although circRNAs are believed to participate in cell differentiation and pluripotency,[11–13] their specific functions remain largely uncharacterised. Moreover, although most identified circRNAs are non-coding, some have been recently described as protein coding.[14 15] CircRNAs also have various biological functions related to different diseases.[16] In fact, our previous report,[17] as well as those of others,[18–20] have reported a significant role for circRNAs in chondrocyte

Ann Rheum Dis: first published as 10.1136/annrheumdis-2021-219969 on 26 May 2021. Downloaded from http://ard.bmj.com/ on April 19, 2024 by guest. Protected by copyright.

regulation of OA development and progression. However, these studies focused primarily on the function of circRNAs as miRNA sponges; hence, it remains unclear whether other molecular mechanism are also associated with the role of circRNAs in OA.

In the current study, we investigated the functions and molecular mechanisms of circPDE4B in OA. We believe that our study paves the way for future research investigating circRNA as a promising therapeutic target for OA.

METHODS

Detailed experimental procedures are described in the online supplemental materials and methods and tables.

RESULTS

circPDE4B exhibits lower expression in OA tissue

We previously performed RNA-seq analyses on the chondrocytes total RNA of ribosomal RNA deletion in three clinical OA and three control samples (SRA accession: PRJNA516555). Among the 50 most abundant significantly dysregulated circRNAs, the expression level of circPDE4B ranked first, the expression of which was significantly downregulated in chondrocytes of patients with OA ($p<0.05$, online supplemental table S1). In the current study, collected cartilage was assigned to one of three groups (total n=20): normal medial, OA lateral and OA medial. The OA severity for each case was assessed using the preoperative Kellgren-Lawrence, Outerbridge and Osteoarthritis Research Society International (OARSI) grading systems for the region of interest (ROI) (figure 1A). Meanwhile, histomorphological and western blot analyses accompanied by fluorescence in situ hybridisation (FISH) staining of ROI cartilage indicated that increased degradation of cartilage corresponded to decreased expression of circPDE4B in chondrocytes (figure 1B and online supplemental figure S1A). These results were confirmed by quantitative reverse transcription PCR (RT-qPCR) analysis which detected downregulated circPDE4B RNA levels in the chondrocytes of severe OA tissues, whereas mPDE4B mRNA level remained relatively consistent (figure 1C). Taken together, these results revealed that circPDE4B expression was negatively associated with OA severity.

Considering that circPDE4B is conserved between humans and mice, we also detected circPDE4B expression in human/mouse chondrocytes (circPDE4B in human chondrocytes (HCs); circPde4b in mouse chondrocytes (MCs)) and found that interleukin-1β (IL-1β; 10 ng/mL) and tumor necrosis factor-α (TNF-α; 50 ng/mL) treatment significantly decreased circPDE4B/circPde4b expression in HCs/MCs in a time-dependent manner (figure 1D and online supplemental figure S1B). Moreover, Sanger sequencing displayed the splicing sequence of circPDE4B/circPde4b (online supplemental figure S1C,H). Meanwhile, circPDE4B/circPde4b was amplified by divergent primers from cDNA, but not in gDNA (online supplemental figure S1D,I). circPDE4B/circPde4b also exhibited a remarkable resistance to RNase R digestion (online supplemental figure S1E,J) and actinomycin D treatment (online supplemental figure S1F,K). Besides, mPDE4B/mPde4b was amplified by random primer and oligo(dT) primer, whereas circPDE4B/circPde4b was only amplified using random primers (online supplemental figure S1G,L). Nuclear separation experiments coupled with RT-qPCR analysis and FISH revealed that circPDE4B/circPde4b is primarily located in the cytoplasm of HCs/MCs (figure 1E,F and online supplemental figure S1M,N). Cumulatively, these results indicate that circPDE4B is downregulated in OA and, thus, may contribute to OA progression.

FUS RNA binding protein (FUS) regulates circPDE4B expression through direct binding to pre-mRNA

We next sought to identify circPDE4B upstream regulators. We first performed RNA pull-down (RPD)-MS assay of circPDE4B flanking sequence and found two RNA splicing related RBPs, including DExH-box helicase 9 and FUS (figure 1G). RT-qPCR results indicated that following FUS knockdown, circPDE4B was downregulated in HCs, while pPDE4B and mPDE4B did not exhibit significant changes (figure 1H and online supplemental figure S2A). In addition, infection with two FUS shRNA lentivirus served to only decrease the expression of circPDE4B (figure 1I and online supplemental figure S2B), whereas overexpressed FUS upregulated the expression of circPDE4B (figure 1I). Next, RNA immunoprecipitation (RIP) assays revealed that FUS binds to exon-adjacent sites, while remote regions elsewhere were negligible (figure 1J,K). We also searched for potential FUS response elements and found two potential motifs, A located upstream and B located downstream. We further engineered two short circPDE4B minigenes, including circPDE4B-s and circPDE4B-s-del (figure 1L). RIP revealed an overt interaction between FUS and circPDE4B-s, but not with circPDE4B-s-del (figure 1M), indicating that FUS requires the putative sites in surrounding introns for binding. We next knocked down FUS in circPDE4B-s/del expressed HCs and found that circPDE4B-s had significantly reduced circPDE4B transcripts on FUS knockdown, compared with circPDE4B-del (figure 1N). Notably, FUS was downregulated by TNF-α in HCs (figure 1O). Cumulatively, the downregulation of circPDE4B in OA was, at least in part, caused by the inhibition of FUS.

circPDE4B regulates chondrocyte cell viability and ECM metabolism

To assess the involvement of circPDE4B/circPde4b in ECM metabolism, we transfected HCs/MCs with three circPDE4B/circPde4b siRNAs, respectively (figure 2A and online supplemental figure S3A). Knockdown of circPDE4B/circPde4b expression did not affect PDE4B/Pde4b mRNA levels (online supplemental figure S3B,C).

We then assessed the influence of circPDE4B/circPde4b on chondrocytes viability using a cell counting kit-8 (CCK-8) assay. Results showed that knockdown of circPDE4B/circPde4b expression reduced chondrocytes viability (figure 2B and online supplemental figure S3D). In addition, the inhibition of circPDE4B/circPde4b by shRNA adenovirus (online supplemental figure S3E,F) significantly enhanced the expression of MMP3, MMP13 and ADAMTS4, whereas the expression of SOX9, COL2A1 (or COL2 protein) and aggrecan was downregulated in HCs/MCs, as revealed by RT-qPCR (figure 2C and online supplemental figure S3G) and western blot (figure 2D and online supplemental figure S3H). Immunofluorescence further confirmed that circPDE4B/circPde4b knockdown affected MMP3, MMP13, COL2 and aggrecan levels in HCs/MCs (figure 2E,F and online supplemental figure S3I,J). Meanwhile, Alcian blue staining of HCs/MCs revealed that circPDE4B/circPde4b inhibition led to a chondrocytes dysfunction with less blue-stained proteoglycan. (figure 2G and online supplemental figure S3K).

We then performed gain-of-function experiments (online supplemental figure S3L,M) and found that overexpression of circPDE4B/circPde4b increased the viability of chondrocyte cells, as revealed by a CCK-8 assay (figure 2H and online supplemental figure S3N). Besides, mRNA and protein levels of MMP3, MMP13 and ADAMTS4 were downregulated, whereas those of SOX9, COL2A1 (or COL2 protein) and aggrecan

Ann Rheum Dis: first published as 10.1136/annrheumdis-2021-219969 on 26 May 2021. Downloaded from http://ard.bmj.com/ on April 19, 2024 by guest. Protected by copyright.

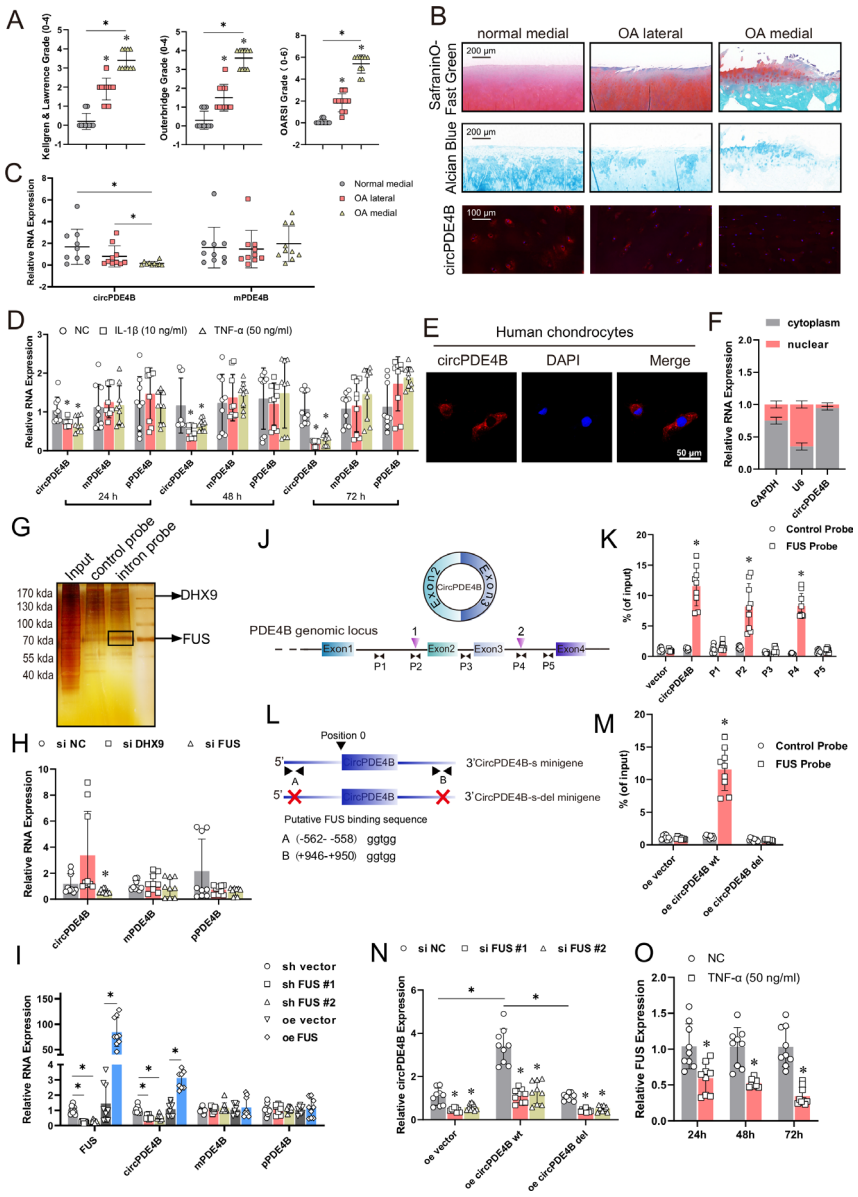

Figure 1 Characterisation of circPDE4B in human chondrocytes (HCs) and osteoarthritis tissues. (A) Preoperative Kellgren-Lawrence, Outerbridge and OARSI grading based for region of interest (ROI) cartilage (n=10 per group). *p≤0.05. (B) Histomorphological analysis and circPDE4B-labelled FISH staining for ROI cartilage. Scale bars, 200 μm. (C) circPDE4B and mPDE4B expression in ROI chondrocytes via RT-qPCR (n=10); *p≤0.05. (D) Changes in circPDE4B, mPDE4B and pPDE4B RNA levels, treated with IL-1β and TNF-α, assessed via RT-qPCR (n=9, 3 donors for three replicates); *p≤0.05. (E) Representative images of FISH staining for circPDE4B localisation in HCs. Scale bars, 50 μm. (F) Expression of circPDE4B assessed by RT-qPCR in the nuclear and cytoplasmic fractions (n=9, 3 donors for three replicates); *p≤0.05. (G) Silver staining of purified interaction proteins in the circPDE4B flanking sequence RPD experiment. (H) circPDE4B expression in HCs transfected with DExH-box helicase 9 and FUS siRNA or a negative control (n=9, 3 donors for three replicates); *p≤0.05. (I) circPDE4B, mPDE4B and pPDE4B expression after FUS inhibition or overexpression (n=9, 3 donors for three replicates); *p≤0.05. (J) Schematic of PDE4B pre-mRNA showing the locations of the two putative sites (inverted blue triangles) and amplicons (P1–P5) used for the RIP assay. (K) RIP assay performed with the PCR primers indicated in the schematic on the left. (n=9, 3 donors for three replicates); *p≤0.05. (L) Schematic illustrating the putative FUS-binding sites on the flanking introns in the circPDE4B-s minigene. The 5′ terminus of the circular exons of circPDE4B was defined as position 0. Putative FUS-binding sites A and B are located in the intron at the 5′ terminus of the circPDE4B exon (position: −562 to −558) and on the intron at the 3′ terminus of the circPDE4B exon (position: 946–950). (M) RIP analysis of FUS binding to circPDE4B-s and circPDE4B-s-del minigenes in HCs (n=9, 3 donors for three replicates); *p≤0.05. (N) Expression of circPDE4B relative to β-actin in HCs infected with circPDE4B-s or circPDE4B-s-del lentivirus followed by transfection with FUS siRNA or control siRNA (n=9, 3 donors for three replicates); *p≤0.05. (O) FUS mRNA expression level in HCs after TNF-α treatment (n=9, 3 donors for three replicates); *p≤0.05. DAPI, 4′,6-diamidino-2-phenylindole; FISH, fluorescence in situ hybridisation; FUS, FUS RNA binding protein; IL-1β, interleukin-1β; NC, negative control; RIP, RNA immunoprecipitation; RPD, RNA pull-down; RT-qPCR, quantitative reverse transcription PCR; TNF-α, tumour necrosis factor-α.

were upregulated in circPDE4B/circPde4b-overexpressing HCs/MCs (figure 2I–L and online supplemental figure S3O–R). Furthermore, Alcian blue staining of HCs/MCs indicated that circPDE4B/circPde4b overexpression and IL-1β cotreatment reduced cartilage destruction compared with IL-1β treatment alone (figure 2M and online supplemental figure S3S). These data demonstrate that circPDE4B/circPde4b in HCs/MCs can promote cell viability and inhibit the catabolic effect.

Ann Rheum Dis: first published as 10.1136/annrheumdis-2021-219969 on 26 May 2021. Downloaded from http://ard.bmj.com/ on April 19, 2024 by guest. Protected by copyright.

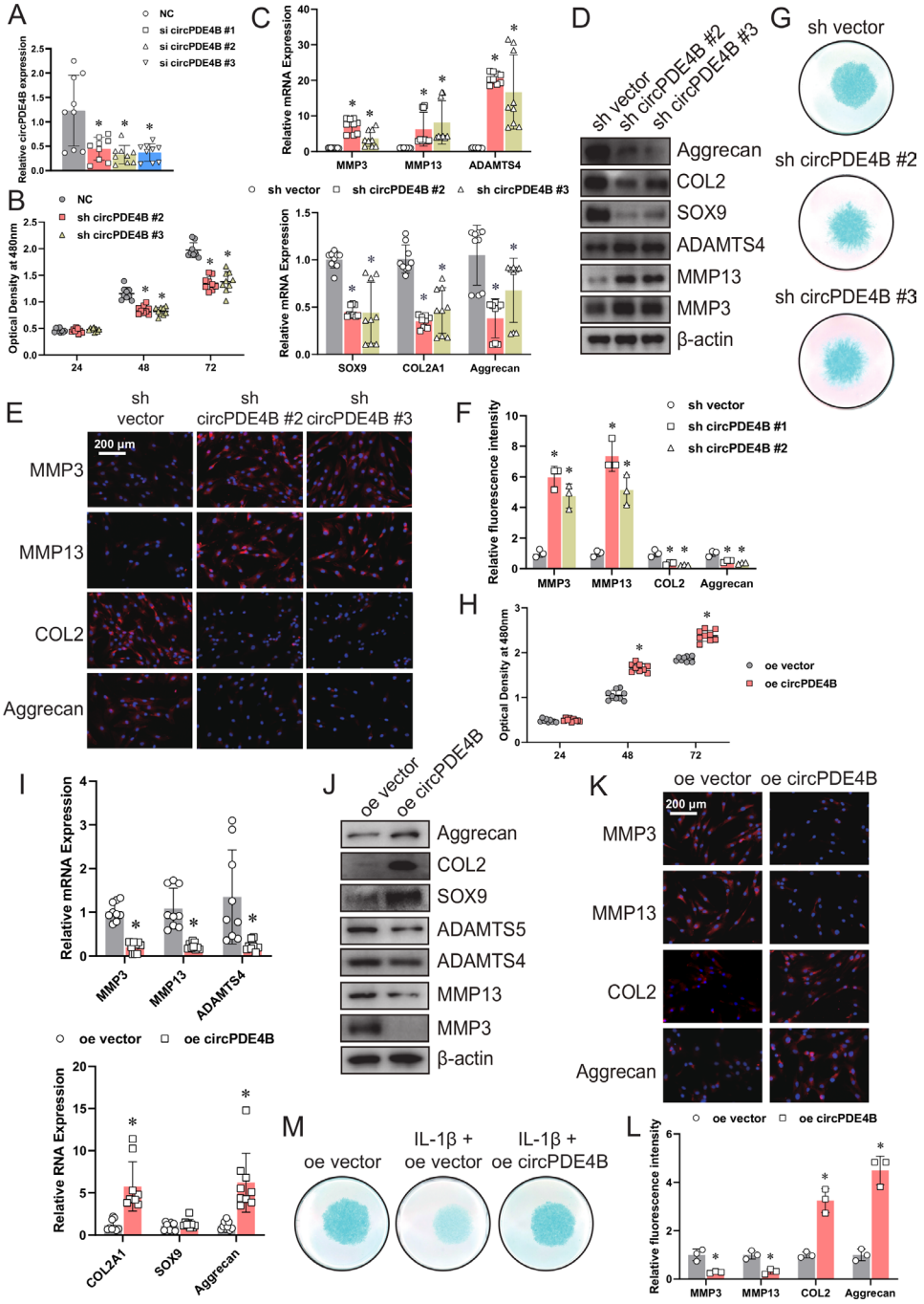

Figure 2 Targeting circPDE4B expression affects matrix-degrading and anabolic factors in human chondrocytes (HCs). (A) circPDE4B expression in HCs transfected with circPDE4B siRNAs or negative control siRNA (n=9, 3 donors for three replicates); *p≤0.05. (B) Viability of HCs infected with circPDE4B shRNA #2/#3 adenovirus or control shRNA adenovirus (n=9, 3 donors for three replicates); *p≤0.05. (C,D) mRNA and protein levels of MMP3, MMP13, ADAMTS4, COL2A1 (or COL2 protein), SOX9 and aggrecan in HCs infected with circPDE4B shRNA #2/#3 adenovirus or control shRNA adenovirus (n=9, 3 donors for three replicates); *p≤0.05. (E) Immunofluorescence analysis of MMP3, MMP13, COL2 and aggrecan. (F) Quantification of immunofluorescence analysis (n=9, 3 donors for three replicates); *p≤0.05. (G) Alcian blue staining of shRNA-treated HCs. (H) Viability of HCs infected with a circPDE4B overexpression adenovirus or control adenovirus (n=9, 3 donors for three replicates); *p≤0.05. (I,J) mRNA and protein levels of MMP3, MMP13, ADAMTS4, COL2A1 (or COL2 protein), SOX9 and aggrecan (n=9, 3 donors for three replicates); *p≤0.05. (K) Immunofluorescence of MMP3, MMP13, COL2 and aggrecan. (L) Quantification of immunofluorescence analysis (n=9, 3 donors for three replicates); *p≤0.05. (M) Alcian blue staining of HCs treated with IL-1β with or without circPDE4B overexpression. IL-1β, interleukin-1β; NC, negative control.

RIC8 guanine-nucleotide exchange factor A (RIC8A) interacts with circPDE4B and participates in OA

Cytoplasm-localised circRNAs participate in translational regulation by acting as ceRNAs, coding RNAs or as a scaffold for RBPs. AGO2 RIP assay revealed that circPDE4B does not bind to AGO2 (online supplemental figure S4A). Bioinformatics analysis of circPDE4B further revealed that it has an open reading frame (ORF) fragment (online supplemental figure S4B). Therefore, two full-length (FL) predicted ORFs were cloned into a eukaryotic expression vector, however, circPDE4B was not found to encode a protein (online supplemental figure S4C).

Ann Rheum Dis: first published as 10.1136/annrheumdis-2021-219969 on 26 May 2021. Downloaded from http://ard.bmj.com/ on April 19, 2024 by guest. Protected by copyright.

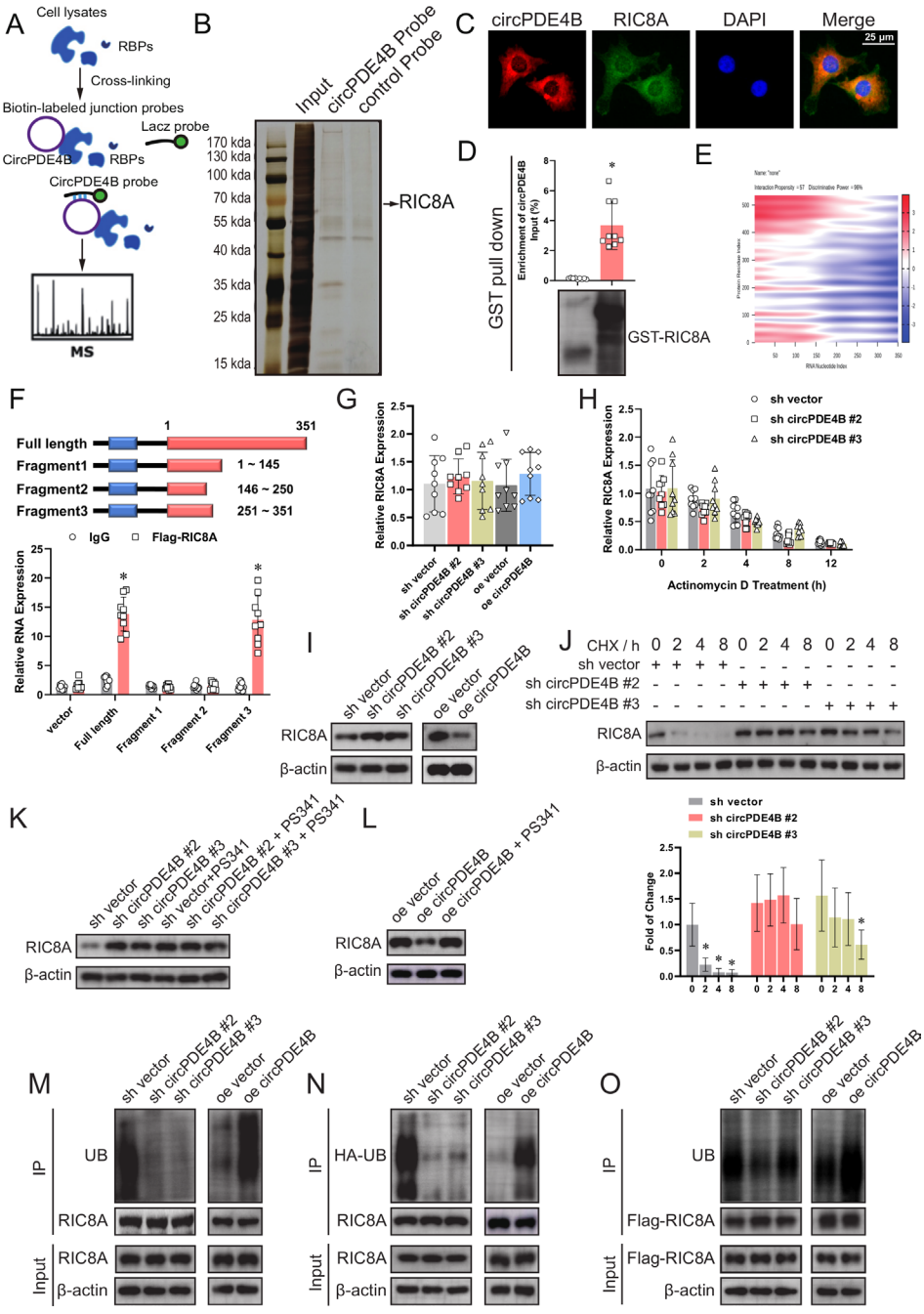

Figure 3 circPDE4B interacts with RIC8A and affects RIC8A ubiquitylation. (A) Schematic of RPD-MS experiments. (B) Silver staining of proteins binding to circPDE4B. (C) circPDE4B and RIC8A interaction in human chondrocytes (HCs) confirmed via an RNA-protein colocalisation assay. Scale bars, 50 μm. (D) RIC8A–circPDE4B interaction detected by GST pull-down assays. GST was used as a pull-down control. (E) Predicted binding sites of circPDE4B and RIC8A (catRAPID graph). (F) Binding sequence of circPDE4B for RIC8A identified by an RIP assay (n=9, 3 donors for three replicates); *p≤0.05. mRNA levels (G), mRNA stability (H) and protein levels (I) of RIC8A after circPDE4B knockdown and overexpression (n=9, 3 donors for three replicates); *p≤0.05. (J) Western blot of RIC8A in HCs treated with the transcription inhibitor CHX (200 μg/mL). (K) Effect of PS341 treatment on RIC8A protein level alteration mediated by circPDE4B knockdown. (L) Effects of PS341 treatment on RIC8A protein expression mediated by circPDE4B overexpression. (M) Immunoprecipitation (IP) analysis of ubiquitinated RIC8A in HCs treated with PS341. The lysates of circPDE4B overexpression or knockdown cells were treated with an anti-RIC8A antibody. (N) HCs were infected with HA-UB lentivirus and then treated with PS341. The lysates of circPDE4B overexpression or knockdown cells were treated with an anti-HA antibody. (O) HCs were infected with Flag–RIC8A lentivirus and then treated with PS341. The lysates of circPDE4B overexpression or knockdown cells were treated with an anti-Flag antibody. CHX, cycloheximide; DAPI, 4',6-Diamidino-2-Phenylindole; GST, glutathione-S-transferase; RBPs, RNA binding proteins; RIC8A, RIC8 guanine-nucleotide exchange factor A; RIP, RNA immunoprecipitation; UB, ubiquitination.

To identify proteins that interact with circPDE4B, we employed RPD-MS (figure 3A and online supplemental figure S5A). A total of 112 proteins interacting with circPDE4B were identified (online supplemental table S2 and figure 3B). We selected five of the highest pep _score proteins and verified their role in the regulation of ECM metabolism in HCs by siRNA knockdown. RT-qPCR results revealed that only RIC8A and ENO1 had an obvious effect on regulating MMP13 and

Ann Rheum Dis: first published as 10.1136/annrheumdis-2021-219969 on 26 May 2021. Downloaded from http://ard.bmj.com/ on April 19, 2024 by guest. Protected by copyright.

COL2A1 (online supplemental figure S5B). However, the RIP assay indicated that only RIC8A binds to circPDE4B (online supplemental figure S5C). We further confirmed the binding of RIC8A and circPde4b by RIP assay in MCs (figure S5D). RNA-protein colocalisation in HCs also verified the interaction between RIC8A and circPDE4B (figure 3C). RPD assay showed that in vitro linearly transcriptional circPDE4B was able to pull down recombinant RIC8A (figure 3D). We then used the catRAPID tool to predict the interacting regions of circPDE4B and RIC8A (figure 3E and online supplemental figure S5E). To identify the predicted binding sites, we truncated the FL circPDE4B into three segments (S1: 1–145 nt, S2: 146–250 nt, S3: 251–351 nt). In line with the prediction, RIP results indicated only FL and S3 were pulled down by RIC8A (figure 3F). Interestingly, the S3 truncation is reflected as a hairpin region 2 loop in the predicted RNA stem-loop structure (online supplemental figure S5F). Taken together, these results indicate that circPDE4B interacts with RIC8A in HCs.

To further investigate the function of RIC8A in the ECM metabolism of HCs, we infected HCs with two RIC8A shRNA adenoviruses (online supplemental figure S6A). CCK-8 assay indicated that RIC8A knockdown increased HCs viability (online supplemental figure S6B). Moreover, RIC8A knockdown cells displayed a significant decrease in the expression of MMP3, MMP13 and ADAMTS4 and increased expression of SOX9, COL2A1 (or COL2 protein) and aggrecan (online supplemental figure S6C–F).

We also performed gain-of-function experiments (online supplemental figure S6G). RIC8A overexpression decreased the viability of chondrocytes as revealed by CCK-8 assay (online supplemental figure S6H). Besides, the mRNA and protein expression of MMP3, MMP13 and ADAMTS4 were downregulated, while SOX9, COL2A1 (or COL2 protein) and aggrecan were upregulated in RIC8A-overexpressing HCs (online supplemental figure S6I–L). We further performed western blot and RT-qPCR to assess the influence of mmu_RIC8A on ECM metabolism in MCs. RIC8A also impaired ECM anabolic processes in MCs (online supplemental figure S6M,N). These data collectively support inhibition of cell viability and procatabolic effects of RIC8A in chondrocytes.

circPDE4B regulates RIC8A function through proteasome-mediated degradation

Our further investigation indicated that circPDE4B regulates RIC8A protein levels, however, not mRNA levels or stability (figure 3G–I). We also blocked RIC8A protein synthesis and observed obvious differences in RIC8A protein half-life between sh-negative control (NC) and sh-circPDE4B HCs (figure 3J), suggesting that circPDE4B decreased RIC8A protein stability. Moreover, in MCs, circPde4b also regulated mmu_RIC8A protein levels (online supplemental figure S6O). To confirm whether circPDE4B affects RIC8A function via changes in post-translational modification, we introduced a proteasome inhibitor named PS341. Accordingly, RIC8A was observed non-changed in both circPDE4B overexpression and knockdown cells after treatment with PS341 (figure 3K,L), indicating that circPDE4B regulates RIC8A through proteasomal activity. Consistently, the polyubiquitination of RIC8A decreased following circPDE4B depletion and increased following circPDE4B overexpression, regardless of endogenous or exogenous RIC8A (figure 3M–O). Cumulatively, these results showed that circPDE4B post-translationally impacts the degradation and turnover of RIC8A mediated by the proteasome.

circPDE4B facilitates the formation of a ternary complex between RIC8A and midline 1 (MID1) that promotes RIC8A degradation

We next sought to identify E3 ligases involved in the proteasomal degradation of RIC8A. Interestingly, MS results revealed that circPDE4B also binds two E3 ligases, including RNF2 and MID1. We, therefore, inferred whether circPDE4B could act as a scaffold for RIC8A and E3 ligases complex. However, since RNF2 is localised within the nucleus, we choose MID1 for further investigation. Indeed, MID1 was found to bind RIC8A, as indicated by an immunoprecipitation (IP) assay (figure 4A). Immunofluorescence staining of RIC8A and MID1 also proved their colocalisation in HCs (figure 4B).

Western blot results showed that MID1 decreased RIC8A protein levels (online supplemental figure S7A,B), while IP results indicated that MID1 knockdown effectively impaired the ubiquitylation of RIC8A and MID1 overexpression and increased RIC8A ubiquitylation (figure 4C). Co-immunoprecipitation (Co-IP) assay also revealed that binding of RIC8A and MID1 decreased in circPDE4B knockdown cells compared with control cells, while circPDE4B overexpression had the opposite effect (figure 4D). Moreover, circPDE4B did not affect MID1 levels (figure 4E). Both RPD and sequential IP assays revealed that circPDE4B promotes the binding of RIC8A and MID1 (figure 4F,G). In line with this finding, circPDE4B increased the association between recombinant RIC8A and MID1 proteins in an in vitro binding assay (figure 4H).

To further investigate these interactions, we performed domain truncation of RIC8A and MID1 for binding assays. The simple modular architecture research tool (SMART) prediction website indicated that RIC8A contains only a Pfam domain (online supplemental figure S7C). Thus, we divided the protein into two fragments, an N-terminal (1–153 amino acids) and C-terminal (154–537 amino acids) domain. Via co-IP, as expected, MID1 was shown to bind to RIC8A at the N-terminal regulatory domain (figure 4I). In addition, we detected RIC8A functional sites. RIC8A was immunoprecipitated in HCs and subjected to MS analysis, which confirmed ubiquitylation of amino acid residues in RIC8A (figure 4J). Ten ubiquitylation sites were identified in RIC8A, K143 and K187 and were not conserved between humans and mice (figure 4J). We thus mutated conserved RIC8A sites from lysine (K) to arginine (R), to exclude ubiquitylation. IP results indicated that substitution of K415 greatly reduced RIC8A ubiquitylation compared with WT (figure 4K), identifying K415 as the major ubiquitylation site of RIC8A (online supplemental figure S7D). Interestingly, K415 is highly conserved among mammals (figure 4L,M). Further, circPDE4B overexpression or inhibition no longer regulated the ubiquitylation levels of RIC8A following K415 mutation (figure 4N). These results suggest that circPDE4B serves as a scaffold to facilitate the association between RIC8A and MID1.

circPDE4B and RIC8A regulate the p38 signaling pathway in chondrocytes

To elucidate the signalling pathways downstream of RIC8A, we investigated the phosphorylation levels of mitogen-activated protein kinases (MAPKs), NF-κB and mTOR in RIC8A knockdown HCs. The phosphorylation level of p38 was significantly decreased by two RIC8A shRNAs (figure 5A). Next, HCs were pretreated with signalling molecule inhibitors, including PD98059 (extracellular regulated protein kinases 1/2 (ERK1/2) inhibitor), SB203580 (p38 inhibitor) and SP600125 (c-Jun N-terminal kinase (JNK) inhibitor), followed by RIC8A

Ann Rheum Dis: first published as 10.1136/annrheumdis-2021-219969 on 26 May 2021. Downloaded from http://ard.bmj.com/ on April 19, 2024 by guest. Protected by copyright.

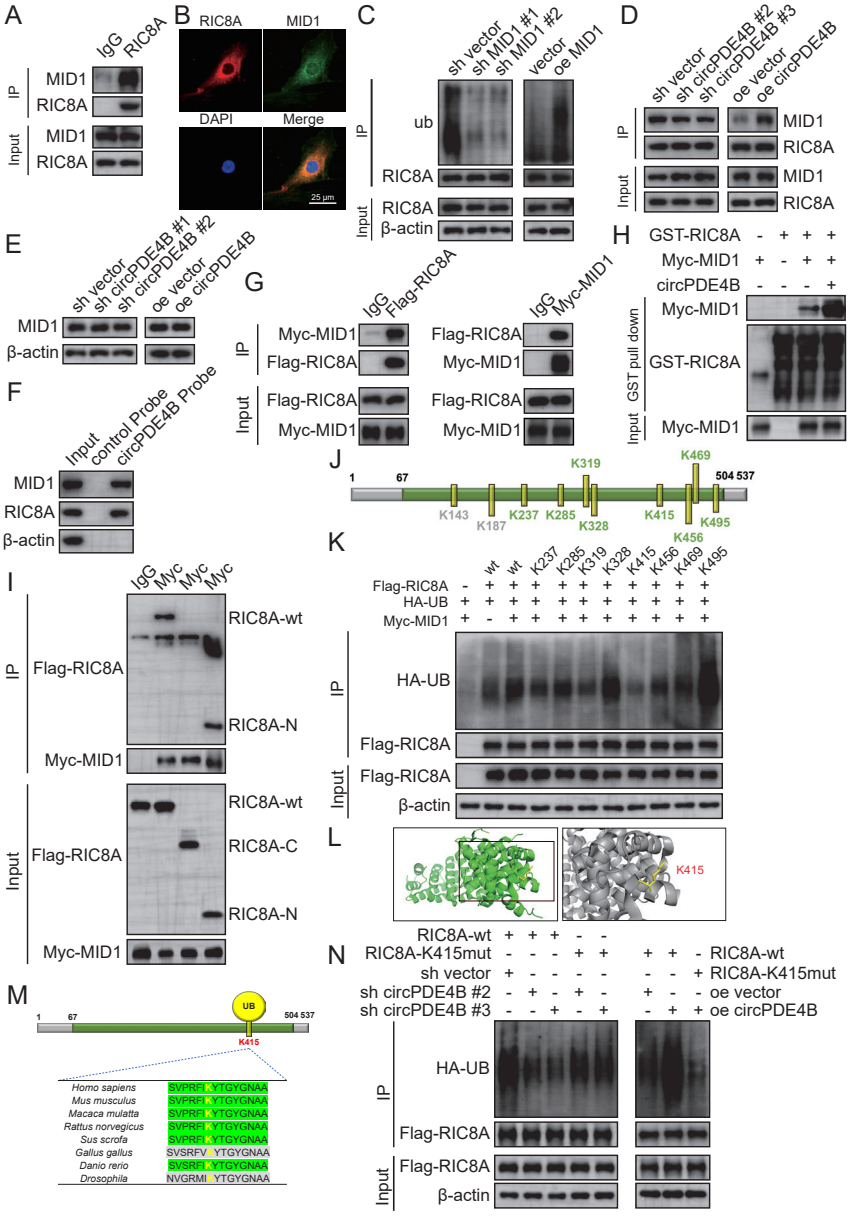

Figure 4 MID1 is an E3 ligase of RIC8A, and K415 is the primary ubiquitylation site of RIC8A. (A) Immunoprecipitation (IP) assay to verify whether E3 ligase MID1 binds to RIC8A. (B) Colocalisation in human chondrocytes (HCs) labelled with anti-RIC8A or anti-MID1 by immunofluorescence. Scale bars, 50 µm. (C) Effect of MID1 overexpression or knockdown on RIC8A ubiquitylation. (D) Effect of circPDE4B overexpression or knockdown on the interaction between RIC8A and MID1. (E) Protein expression of MID1 after circPDE4B knockdown and overexpression. (F) RPD assays using biotin-labelled linear circPDE4B probes in HC lysate before western blotting. (G) HEK-293T cells were infected with Myc–MID1 or Flag–RIC8A before consecutive IP. Rinsing with Flag peptides at first-stage Flag IPs and then eluates were subjected to secondary IP with Myc antibodies or homotypic matching IgG. Western blot was then performed to detect samples. (H) GST–RIC8A and Myc–MID1 overexpressed and purified from cells. RIC8A–MID1 interactions with or without circPDE4B were detected by GST pull-down assays. GST was used as a pull-down control. (I) Myc–MID1 and Flag–RIC8A WT, N-terminal domain and C-terminal domain plasmids were transfected into HEK-293T cells, a co-IP assay was performed and Flag expression was examined by western blotting. (J) HCs were subjected to RIC8A IP and LC–MS/MS analysis of RIC8A ubiquitylation peptide spectra. Ubiquitylated sites were identified by LC–MS analysis. (K) HCs expressing Flag-tagged wild-type or mutant RIC8A KR were first exposed to PS341 and subsequently treated with Flag IP. RIC8A ubiquitylation was analysed via western blot analysis. (L) Crystal structure of RIC8A proteins with K415. (M) Conservation ability of the K415 site of RIC8A. (N) Effect of circPDE4B inhibition and overexpression on the K415R RIC8A ubiquitylation level, as detected by an IP assay. co-IP, co-immunoprecipitation; GST, glutathione-S-transferase; HA-UB, HA-tagged ubiquitination; KR, mutation of lysine (K) to arginine (R); LC, liquid chromatography; MID1, midline 1; MS, mass spectrometry; RIC8A, RIC8 guanine-nucleotide exchange factor A; RPD, RNA pull-down.

overexpression. The overexpression of RIC8A pretreated with p38 MAPK inhibitors inhibited OA, however, it was not affected by ERK or JNK inhibitors (figure 5B). Moreover, after being infected with RIC8A shRNA or overexpression adenovirus, p38 MAPK phosphorylation and its localisation were dysregulated (figure 5C–E). These results suggest that RIC8A functions through the p38 signalling pathway in chondrocytes.

We next investigated the role of circPDE4B in regulation of the p38 signalling pathway in OA. circPDE4B overexpression decreased while circPDE4B knockdown activated p38 MAPK

Ann Rheum Dis: first published as 10.1136/annrheumdis-2021-219969 on 26 May 2021. Downloaded from http://ard.bmj.com/ on April 19, 2024 by guest. Protected by copyright.

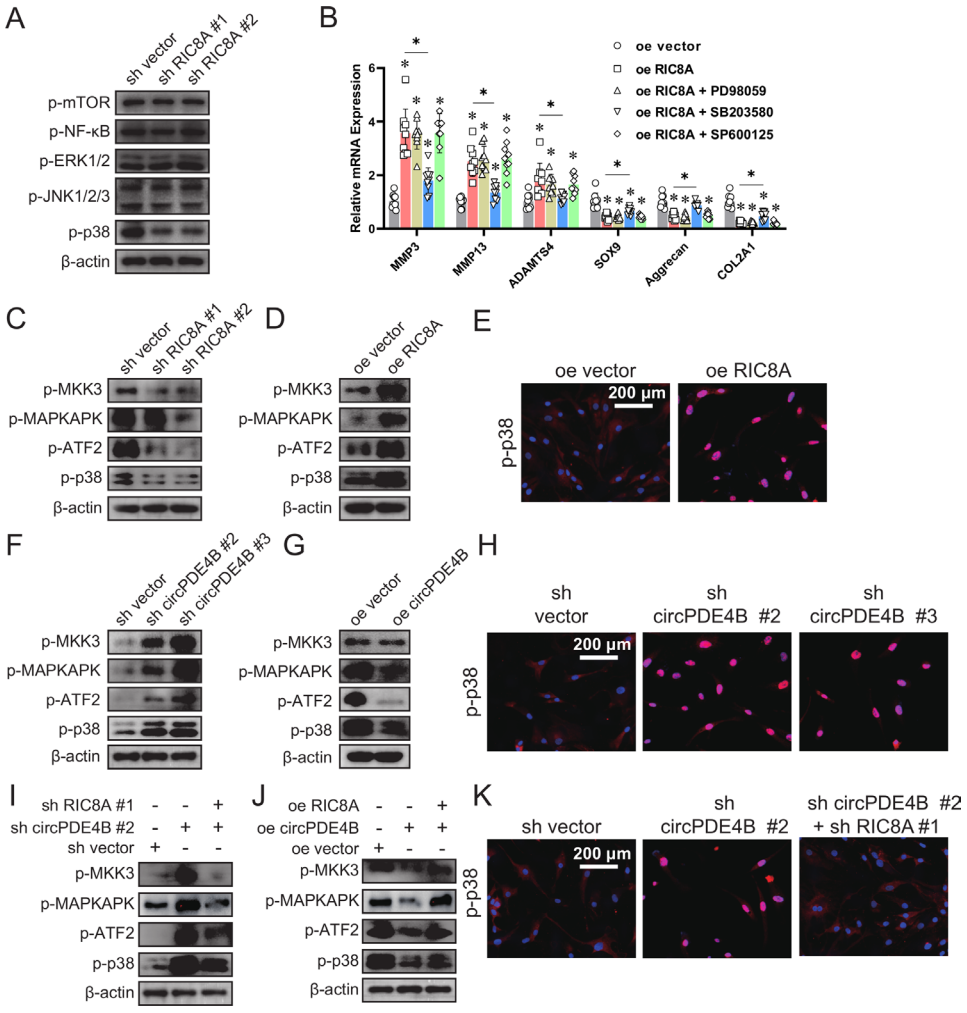

Figure 5 The p38 MAPK pathway is the downstream target of the circPDE4B–RIC8A axis. (A) Phosphorylation of MAPK, NF-κB and mTOR in human chondrocytes (HCs) infected with the vector or RIC8A shRNAs. (B) Relative mRNA expression levels of MMP3/13, ADAMTS4, SOX9, aggrecan and COL2A1 in HCs infected with RIC8A adenovirus and pretreated for 1 hour with PD98059 (ERK inhibitor), SB203580 (p38 MAPK inhibitor) or SP600125 (JNK inhibitor) (n=9, 3 donors for three replicates); *p≤0.05. (C) Phosphorylation levels of p38 MAPK signalling pathway members in HCs infected with RIC8A shRNA or vector adenovirus. Phosphorylation levels of p38 MAPK signal pathway members (D) in HCs with overexpressed RIC8A and (E) associated translocation of p38. (F) Phosphorylation levels of p38 MAPK signalling pathway members in HCs infected with circPDE4B shRNA or vector adenovirus. (G) Phosphorylation levels of p38 MAPK signalling pathway members in HCs infected with circPDE4B adenovirus. (H) Associated translocation of p38 in HCs infected with circPDE4B shRNA or vector adenovirus. (I,J) Phosphorylation levels of p38 MAPK signal pathway members in HCs coinfected with sh circPDE4B and sh RIC8A adenovirus. (I) or circPDE4B and RIC8A overexpression adenovirus. (K) Associated translocation of p38 in HCs coinfected with sh circPDE4B and sh RIC8A adenovirus. ERK, extracellular regulated protein kinases; JNK, c-Jun N-terminal kinase; MAPK, mitogen-activated protein kinase; mTOR, mechanistic target of rapamycin kinase; NF-κB, nuclear factor kappa B; RIC8A, RIC8 guanine-nucleotide exchange factor A.

signalling together with p38 phosphorylation and nuclear translocation (figure 5F–H). We then performed rescue assays. As shown in figure 5I–K, RIC8A overexpression rescued the downregulation of the p38 signalling pathway induced by circPDE4B overexpression, while RIC8A inhibition rescued the activation of p38 signalling pathway induced by circPDE4B knockdown, together with p38 phosphorylation and nuclear translocation. Based on these findings, the circPDE4B–RIC8A axis plays an important role in regulating the downstream p38 MAPK signalling pathway in chondrocytes.

circPde4b and RIC8A affect OA pathogenesis in mice

To corroborate the abovementioned findings, we further assessed the effects of circPde4b on OA in mice (online supplemental figure S8A). The specific adeno-associated virus (AAV) (approximately 1.0×10^{10}vg) efficiently infected the cartilage and synovium in the four groups (online supplemental figure S8B,C), but in vitro study showed that overexpressed circPde4b and RIC8A did not obviously promoted the inflammation of synovium (online supplemental figure S8D,E). Figure 6A shows the RNA expression of circPde4b and RIC8A after infection with the different AAV in the four groups. RT-qPCR and western blot analyses of ECM-associated proteins extracted from cartilage also suggested more severe OA in the medial meniscus destabilisation (DMM)+vector group and DMM+circPde4b+RIC8A group (figure 6B,C). Using Safranin O fast green staining (figure 6D), marked proteoglycan loss was observed in the DMM+vector group and DMM+circPde4b+RIC8A group compared with the SHAM+vector and DMM+circPDE4B groups, indicating that circPde4b AAV could rescue the OA progression caused by DMM, while RIC8A AAV could reverse this rescue. OARSI grade (figure 6E) further suggested that mice

Ann Rheum Dis: first published as 10.1136/annrheumdis-2021-219969 on 26 May 2021. Downloaded from http://ard.bmj.com/ on April 19, 2024 by guest. Protected by copyright.

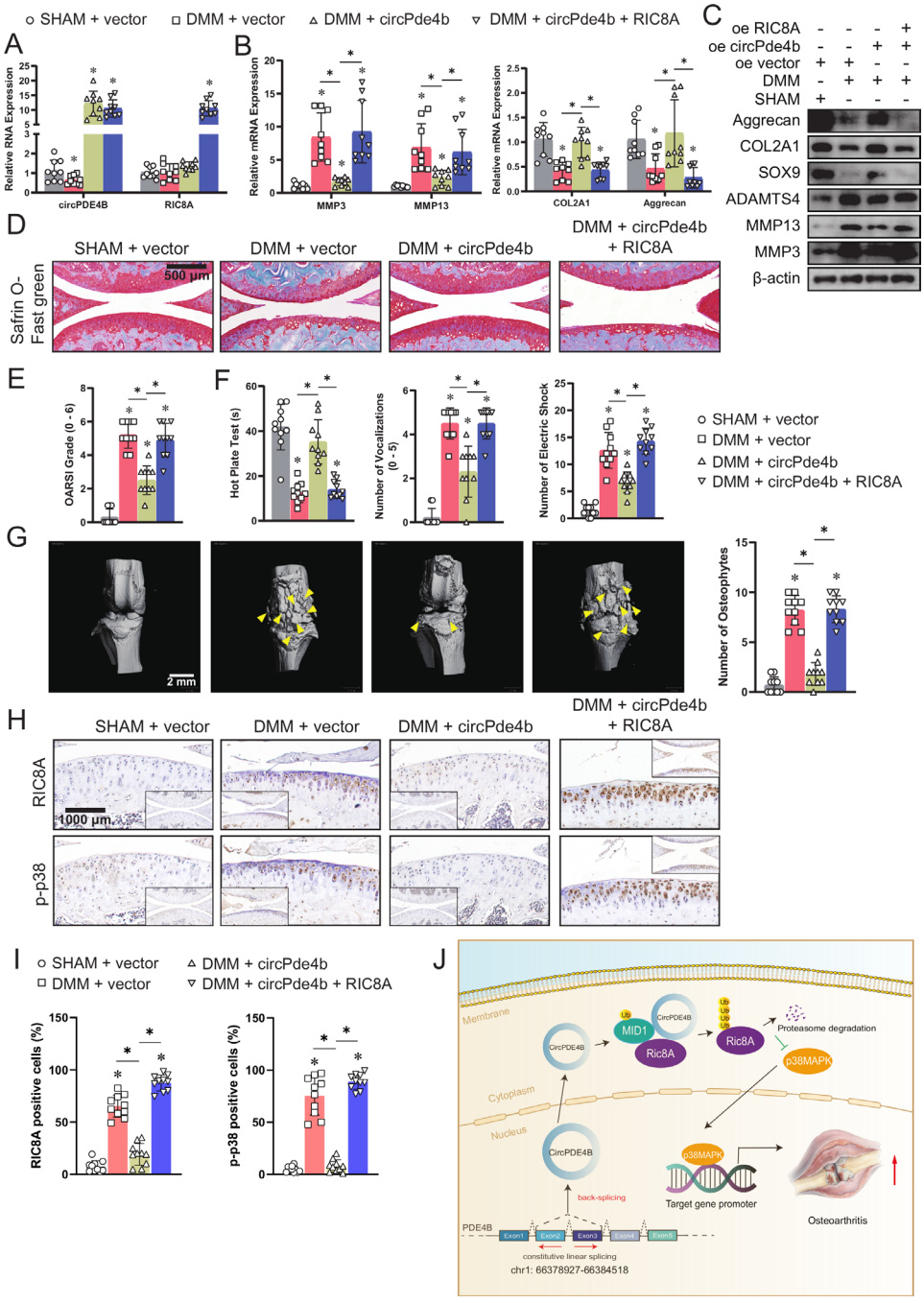

Figure 6 circPDE4B and RIC8A modulates osteoarthritis pathogenesis in a murine model. (A) RT-qPCR quantification of circPDE4B and RIC8A expression in mouse chondrocytes extracted from knee cartilage in the four groups (n=3); *p<0.05. (B) RT-qPCR quantification of MMP3, MMP13, COL2A1 and aggrecan expression in the four groups (n=3); *p<0.05. (C) Western blot analysis of extracellular matrix-associated proteins in the four groups. (D) Representative images of Safranin O fast green staining of cartilage in the four study groups. Scale bars, 500 µm. (E) OARSI grade used for evaluation of the cartilage degradation in the four groups (n=10); *p<0.05. (F) Hot plate test, knee extension test and electric shock-stimulated treadmill test used for the evaluation of knee pain (n=10); *p<0.05. (G) Left, 3D reconstruction images of micro-CT scanning of the knees and osteophytes (yellow arrow). Scale bars, 2 mm. Right, the number of osteophytes (n=10); *p<0.05. (H) Representative images of RIC8A and p-p38-labelled IHC staining. Scale bars, 1000 µm. (I) Quantitative analysis of RIC8A and p-p38 expression in the cartilage with IHC. (n=10); *p<0.05. (J) Graphic abstract of our study. DMM, medialmeniscus destabilisation; IHC, immunohistochemistry; MCs, mouse chondrocytes; OARSI, Osteoarthritis Research Society International; RIC8A, RIC8 guanine-nucleotide exchange factor A. RT-qPCR, quantitative reverse transcription PC.

in the SHAM+vector and DMM+circPde4b group displayed less cartilage degradation, whereas those in the DMM+vector and DMM+circPde4b+RIC8A exhibited the opposite. The hot plate test, knee extension test and electric shock stimulated treadmill test demonstrated more discomfort and knee pain in the DMM+vector group and DMM+circPde4b+RIC8A group than in the SHAM+vector and DMM+circPde4b groups (figure 6F). 3D reconstruction of the micro-CT of mouse knees revealed much more osteophytes in the DMM+NC group and DMM+circPde4b+RIC8A group than in the SHAM+vector and DMM+circPde4b groups (figure 6G). MMP3, MMP13, COL2 and aggrecan expression in cartilage from the four groups was

Ann Rheum Dis: first published as 10.1136/annrheumdis-2021-219969 on 26 May 2021. Downloaded from http://ard.bmj.com/ on April 19, 2024 by guest. Protected by copyright.

consistent with the above staining results (online supplemental figure S9A). Moreover, RIC8A and p-p38 labelled immunohistochemistry (IHC) staining in the four groups showed that overexpressed circPde4b downregulated the RIC8A and p-p38 expression, therefore inhibited the OA progression caused by DMM operation (figure 6H,I). Together, these results indicate that, in mice, circPde4b and RIC8A are involved in OA pathogenesis and their underlying mechanism is presented in figure 6J.

DISCUSSION

The OA pathogenesis is primarily underpinned by an imbalance in joint metabolism, for example, when catabolism exceeds anabolism, leading to the degradation of the cartilage matrix.[21] Emerging evidence has suggested several key catabolic regulators that contribute to cartilage destruction.[22] However, the mechanism underlying the cessation of matrix anabolism remains largely unknown.

Recent studies have begun to shed light on the various roles of circRNAs including a crucial role in the occurrence, development, diagnosis, prognosis and treatment of diseases.[23] Specifically, we previously reported that circSERPINE2 could inhibit the occurrence and development of OA by regulating ERG gene as ceRNA.[17] Zhou *et al*[19] reported a basic role for circRNA33186 in OA development, thus providing a latent drug target for OA therapy. However, when it comes OA, relatively few reports have focused on the importance of circRNAs. Here, we reported that circPDE4B was the most highly expressed among differentially regulated circRNAs obtained through sequencing data. We also observed that circPDE4B is downregulated in chondrocytes treated with IL-1β, as well as the cartilage of OA mice induced by DMM. Further, circPDE4B was inversely related to cartilage degeneration, suggesting that circPDE4B is likely associated with OA development. Further functional experiments revealed that circPDE4B has a key role in OA progression and could represent a therapeutic target.

circRNAs reportedly function through three well-established mechanisms: (1) regulation of parental gene expression and splicing events; (2) complex formation within proteins to perform biological functions and (3) regulating gene expression via miRNA sponging.[24–26] Herein, we describe the potential mechanism by which circPDE4B can act as a scaffold for RIC8A–MID1 complex, thus promoting RIC8A ubiquitylation. Therefore, we have discovered a distinctive function through which circRNAs can modulate protein stability in OA.

As a guanine nucleotide exchange factor for G-protein alpha subunits, RIC8A was initially identified in *Caenorhabditis elegans*.[27] RIC8A has been described as an essential protein for G-protein signalling and in centrosome movements during early embryogenesis in *C. elegans*.[28–31] In mammals, RIC8A disruption in neural progenitors leads to germinal matrix haemorrhage,[32 33] suggesting that RIC8A activation may represent a key event in human OA pathogenesis. The role of RIC8A in OA, however, remains unclear. Herein, we found that RIC8A plays an important role in OA pathogenesis by regulating p38 MAPK signalling. Previous reports have indicated that the activation of p38, ERK and JNK signalling pathways is strongly correlated with OA cartilage damage.[34–36] Moreover, MAPKs serve as pivotal signalling molecules that participate in the production of matrix metalloproteinases and regulate viability and differentiation of chondrocytes.[37] Hence, considering that circPDE4B was found to function through the RIC8A–p38 axis, disruption of this pathway may cause dysregulation of cartilage homeostasis.

Post-translational modifications are associated with disease development and may influence protein function, immunogenicity and subcellular localisation.[38–41] Ubiquitylation, a major post-translational modification, plays an important role in signal transduction, apoptosis and cell proliferation.[42–44] Herein, we demonstrated that circPDE4B could disrupt the protein stability of RIC8A and possibly functions by regulating RIC8A post-translational modification. However, such modifications of RIC8A have not been previously reported. Interestingly, we found that circPDE4B also binds to an E3 ligand protein MID1 and RIC8A is ubiquitylated by MID1, thus we infer that circPDE4B promotes RIC8A ubiquitylation by acting as a scaffold to facilitate MID1 binding to RIC8A. Besides, employing acetyl-deficient (K→R) mutants, K415 was identified as a major ubiquitylation site of RIC8A and circPDE4B overexpression or inhibition had no effect on RIC8A K415R ubiquitination.

In summary, our research describes a new circRNA mechanism in OA. We demonstrated that circPDE4B could function as a scaffold for protein degradation and play a crucial role in the progression of OA. circPDE4B was found to regulate ECM metabolism and prevent cartilage matrix construction, validating its latent therapeutic influence on OA development in preclinical animal models. Mechanistically, circPDE4B served as a scaffold to facilitate RIC8A–MID1 binding which decreased RIC8A-dependent activation of p38 signal pathway, thus regulating OA progression. Cumulatively, the results of this study provide prospects for developing novel OA therapies by focusing on reducing the imbalance between matrix synthesis and degradation.

Correction notice This article has been corrected since it published Online First. Figure 4 has been replaced.

Contributors SS and XF conceived and designed the project. SS, YY, PS and JM performed all cell and animal experiments. SS, YY and BF collected the specimens and data from humans and mice. QW, KW and PS graded the histological changes. SF, XF and SS supervised the project and wrote the manuscript.

Funding The study was supported by the National Natural Science Foundation of China (grant numbers 81871797, 81472064,81873985, 81874015 and 81601925); Key Project of Zhejiang Medical Science and Technology Plan (grant numbers 2015145597 and 2016145597); Key Project of Zhejiang Provincial Natural Science Foundation (grant number LZ15H06002) and Medical Science and Technology Project of Zhejiang Province (grant number 2017179447). No benefits in any form have been, or will be, received from a commercial party related directly, or indirectly, to the subject of this study.

Competing interests None declared.

Patient consent for publication Not required.

Ethics approval All experimental procedures involving mice were conducted with the approval of the Zhejiang University Ethics Committee. Cartilage samples were collected following informed written patient consent with approval from Sir Run Run Shaw Hospital Ethics Committee.

Provenance and peer review Not commissioned; externally peer reviewed.

Data availability statement Data are available in a public, open access repository. All data relevant to the study are included in the article or uploaded as supplementary information.

Supplemental material This content has been supplied by the author(s). It has not been vetted by BMJ Publishing Group Limited (BMJ) and may not have been peer-reviewed. Any opinions or recommendations discussed are solely those of the author(s) and are not endorsed by BMJ. BMJ disclaims all liability and responsibility arising from any reliance placed on the content. Where the content includes any translated material, BMJ does not warrant the accuracy and reliability of the translations (including but not limited to local regulations, clinical guidelines, terminology, drug names and drug dosages), and is not responsible for any error and/or omissions arising from translation and adaptation or otherwise.

Open access This is an open access article distributed in accordance with the Creative Commons Attribution 4.0 Unported (CC BY 4.0) license, which permits others to copy, redistribute, remix, transform and build upon this work for any purpose, provided the original work is properly cited, a link to the licence is given,

Ann Rheum Dis: first published as 10.1136/annrheumdis-2021-219969 on 26 May 2021. Downloaded from http://ard.bmj.com/ on April 19, 2024 by guest. Protected by copyright.

and indication of whether changes were made. See: https://creativecommons.org/licenses/by/4.0/.

ORCID iDs
Shunwu Fan http://orcid.org/0000-0002-8785-0280
Xiangqian Fang http://orcid.org/0000-0003-4500-8914

REFERENCES

1 Hunter DJ, Bierma-Zeinstra S. Osteoarthritis. *Lancet* 2019;393:1745–59.
2 Choi MC, JO JI, Park JO, *et al*. Nf-B signaling pathways in osteoarthritic cartilage destruction. *Cells* 2019;8:734. doi:10.3390/cells8070734
3 Shi Y, Hu X, Cheng J, *et al*. A small molecule promotes cartilage extracellular matrix generation and inhibits osteoarthritis development. *Nat Commun* 2019;10:1914.
4 Hardingham TE, Fosang AJ. Proteoglycans: many forms and many functions. *Faseb J* 1992;6:861–70.
5 Sanchez C, Bay-Jensen A-C, Pap T, *et al*. Chondrocyte secretome: a source of novel insights and exploratory biomarkers of osteoarthritis. *Osteoarthritis Cartilage* 2017;25:1199–209.
6 Dobson GP, Letson HL, Grant A, *et al*. Defining the osteoarthritis patient: back to the future. *Osteoarthritis Cartilage* 2018;26:1003–7.
7 Watt FE. Osteoarthritis biomarkers: year in review. *Osteoarthritis Cartilage* 2018;26:312–8.
8 Abramoff B, Caldera FE. Osteoarthritis: pathology, diagnosis, and treatment options. *Med Clin North Am* 2020;104:293–311.
9 Patop IL, Wüst S, Kadener S. Past, present, and future of circRNAs. *Embo J* 2019;38:e100836.
10 Chen L-L, Yang L. Regulation of circRNA biogenesis. *RNA Biol* 2015;12:381–8.
11 Chen X, Yang T, Wang W, *et al*. Circular RNAs in immune responses and immune diseases. *Theranostics* 2019;9:588–607.
12 Ji P, Wu W, Chen S, *et al*. Expanded expression landscape and prioritization of circular RNAs in mammals. *Cell Rep* 2019;26:3444–60.
13 Santer L, Bär C, Thum T. Circular RNAs: a novel class of functional RNA molecules with a therapeutic perspective. *Mol Ther* 2019;27:1350–63.
14 Das A, Gorospe M, Panda AC. The coding potential of circRNAs. *Aging* 2018;10:2228–9.
15 Pamudurti NR, Bartok O, Jens M, *et al*. Translation of CircRNAs. *Mol Cell* 2017;66:9–21.
16 Li D, Yang Y, Li Z-Q, *et al*. Circular RNAs: from biogenesis and function to diseases. *Chin Med J* 2019;132:2457–64.
17 Shen S, Wu Y, Chen J, *et al*. CircSERPINE2 protects against osteoarthritis by targeting miR-1271 and ETS-related gene. *Ann Rheum Dis* 2019;78:826–36.
18 Wu Y, Hong Z, Xu W, *et al*. Circular RNA circPDE4D protects against osteoarthritis by binding to miR-103a-3p and regulating FGF18. *Mol Ther* 2021;29:308–23.
19 Zhou Z-B, Huang G-X, Fu Q, *et al*. circRNA.33186 contributes to the pathogenesis of osteoarthritis by sponging miR-127-5p. *Mol Ther* 2019;27:531–41.
20 Shen P, Yang Y, Liu G, *et al*. CircCDK14 protects against osteoarthritis by sponging miR-125a-5p and promoting the expression of Smad2. *Theranostics* 2020;10:9113–31.
21 Rahmati M, Nalesso G, Mobasheri A, *et al*. Aging and osteoarthritis: central role of the extracellular matrix. *Ageing Res Rev* 2017;40:20–30.
22 Mehana E-SE, Khafaga AF, El-Blehi SS. The role of matrix metalloproteinases in osteoarthritis pathogenesis: an updated review. *Life Sci* 2019;234:116786.
23 Meng S, Zhou H, Feng Z, *et al*. CircRNA: functions and properties of a novel potential biomarker for cancer. *Mol Cancer* 2017;16:94.
24 Qu S, Yang X, Li X, *et al*. Circular RNA: a new star of noncoding RNAs. *Cancer Lett* 2015;365:141–8.
25 Conn SJ, Pillman KA, Toubia J, *et al*. The RNA binding protein quaking regulates formation of circRNAs. *Cell* 2015;160:1125–34.
26 Panda AC. Circular RNAs act as miRNA sponges. *Adv Exp Med Biol* 2018;1087:67–79.
27 Ruisu K, Meier R, Kask K, *et al*. RIC8A is essential for the organisation of actin cytoskeleton and cell-matrix interaction. *Exp Cell Res* 2017;357:181–91.
28 Srivastava D, Gakhar L, Artemyev NO. Structural underpinnings of Ric8A function as a G-protein α-subunit chaperone and guanine-nucleotide exchange factor. *Nat Commun* 2019;10:3084.
29 Zeng B, Mou T-C, Doukov TI, *et al*. Structure, function, and dynamics of the Gα binding domain of Ric-8A. *Structure* 2019;27:1137–47.
30 Saare M, Lulla S, Tõnissoo T, *et al*. Expression pattern and localization dynamics of guanine nucleotide exchange factor RIC8 during mouse oogenesis. *PLoS One* 2015;10:e0129131.
31 Peters KA, Rogers SL. Drosophila Ric-8 interacts with the Gα12/13 subunit, Concertina, during activation of the folded gastrulation pathway. *Mol Biol Cell* 2013;24:3460–71.
32 Yang F, Camp DG, Gritsenko MA, *et al*. Identification of a novel mitotic phosphorylation motif associated with protein localization to the mitotic apparatus. *J Cell Sci* 2007;120:4060–70.
33 Ma S, Santhosh D, Kumar T P, *et al*. A Brain-Region-Specific neural pathway regulating germinal matrix angiogenesis. *Dev Cell* 2017;41:366–81.
34 Latourte A, Cherifi C, Maillet J, *et al*. Systemic inhibition of IL-6/Stat3 signalling protects against experimental osteoarthritis. *Ann Rheum Dis* 2017;76:748–55.
35 Ge H-X, Zou F-M, Li Y, *et al*. JNK pathway in osteoarthritis: pathological and therapeutic aspects. *J Recept Signal Transduct Res* 2017;37:431–6.
36 Prasadam I, Mao X, Wang Y, *et al*. Inhibition of p38 pathway leads to OA-like changes in a rat animal model. *Rheumatology* 2012;51:813–23.
37 Lee SA, Moon S-M, Han SH, *et al*. Chondroprotective effects of aqueous extract of Anthriscus sylvestris leaves on osteoarthritis in vitro and in vivo through MAPKs and NF-κB signaling inhibition. *Biomed Pharmacother* 2018;103:1202–11.
38 Chakraborty J, Basso V, Ziviani E. Post translational modification of Parkin. *Biol Direct* 2017;12:6.
39 Heo K-S. Regulation of post-translational modification in breast cancer treatment. *BMB Rep* 2019;52:113–8.
40 Victorino VJ, Mencalha AL, Panis C. Post-Translational modifications disclose a dual role for redox stress in cardiovascular pathophysiology. *Life Sci* 2015;129:42–7.
41 Liu J, Qian C, Cao X. Post-Translational modification control of innate immunity. *Immunity* 2016;45:15–30.
42 Vu LD, Gevaert K, De Smet I. Protein language: post-translational modifications talking to each other. *Trends Plant Sci* 2018;23:1068–80.
43 Gan W, Dai X, Lunardi A, *et al*. SPOP promotes ubiquitination and degradation of the ERG oncoprotein to suppress prostate cancer progression. *Mol Cell* 2015;59:917–30.
44 Tan R, Nakajima S, Wang Q, *et al*. Nek7 protects telomeres from oxidative DNA damage by phosphorylation and stabilization of TRF1. *Mol Cell* 2017;65:818–31.

Ann Rheum Dis: first published as 10.1136/annrheumdis-2021-219969 on 26 May 2021. Downloaded from http://ard.bmj.com/ on April 19, 2024 by guest. Protected by copyright.

SUPPLEMENTARY MATERIALS

CircPDE4B prevents articular cartilage degeneration and promotes repair by acting as a scaffold for RIC8A and MID1

Shuying Shen#, Yute Yang#, Panyang Shen#, Jun Ma, Bin Fang, Qingxin Wang, Kefan Wang, Peihua Shi, Shunwu Fan*&Xiangqian Fang*

SUPPLEMENTARY MATERIALS AND METHODS

Human cartilage

The collection and classification of human cartilage samples was approved by the Ethics Committee of Sir Run Run Shaw Hospital (Zhejiang, China). Informed consent was obtained from all participants. Control cartilage was collected from ten amputees without a history of OA (n = 10), and damaged cartilage was obtained from individuals with a history of OA after total knee replacement surgery (n = 10). The cartilage was divided into three groups: normal medial, OA lateral and OA medial. The tibial plateau cartilage without the protection of a meniscus cover comprising an area of approximately 1 cm (width) × 2 cm (length) along the midline of the medial or lateral tibial plateau was defined as the region of interest (ROI). The Kellgren-Lawrence grade (upon preoperative imaging), Outerbridge grade (by visual observation in isolated specimens), and OARSI grade (after histomorphological staining) was exploited to evaluated specimen OA severity. Among them, Outerbrdige and OARSI grading were used to evaluate the cartilage ROI.

Plasmids

Human/mouse circPDE4B linear sequence (351/350 bp) was synthesized and subcloned into pHBAd-circRNA (HanBio., Shanghai, China). For RNA binding protein immunoprecipitation (RIP) assay, linear circPDE4B truncated mutants and wild type (WT) were cloned into the pcDNA3.1 vector. For RIP and immunoprecipitation (IP) assay, human RIC8A cDNA (1,614 bp) was synthesized and its truncations were subcloned into pcDNA3.1 vector. Mutants of RIC8A were prepared with GeneTailorTM Site-Directed Mutagenesis System (Invitrogen) and primers (table S3). Specially, RIC8A K415R was synthesized and subcloned to pcDNA3.1 vector. For HEK-293T co-IP assay, RIC8A cDNA (1614) /N/C terminal and MID1 cDNA (2,004 bp) were synthesized and then subcloned into pLVX-IRES-puro-Flag or pLVX-IRES-blasticidin-Myc (Addgene). For human chondrocytes (HCs) IP/co-IP assay, Myc-MID1 and Flag-RIC8A lentivirus were then packaged. mmu_RIC8A was also synthesized and then subcloned into pLVX-IRES-puro-Flag, further packaged. CircPDE4B-s and circPDE4B-s-del were also synthesized (circPDE4B-s comprises presumed FUS-binging sites on both flanking introns preserved; circPDE4B-s-del resembles circPDE4B-s, but with FUS sites deleted from the surrounding introns) and subcloned into pLVX-puro vector (Addgene), then packaged lentivirus. RIC8A K415R was also subcloned into pAdEasy-EF1-MCS-CMV-GFP vector and packaged adenovirus (Hanbio Co. Ltd, Shanghai, China). For recombinant adenovirus sh hsa/mmu circPDE4B and hsa/mmu universal shRIC8A construction, oligonucleotides with gene targeting sequences (table S3) were used for the cloning of small hairpin RNA (shRNA)-encoding sequences into pAdEasy-U6-CMV-EGFP vector (Hanbio Co. Ltd, Shanghai, China). For lentivirus shFUS construction, oligonucleotides with gene targeting sequences (table S3) were used for the cloning of small hairpin RNA (shRNA)-encoding sequences into pKLO.1 vector (addgene) and then packaged. HA-ubiquitin (Ubc) lentivirus and control virus were purchased from Hanbio Co. Ltd, Shanghai, China.

Chondrocyte culture

Human chondrocytes (HCs) were extracted from knee cartilage of amputees or subjects after total knee replacement, and mouse chondrocytes (MCs) were obtained from knee cartilage of 3-day-old C57BL/6. Chondrocytes were cultured in Dulbecco's modified eagle medium (DMEM) supplemented with 10% FBS (Thermo Fisher Scientific, Waltham, MA, USA) within 24 h at 37 °C. Before culture or mRNA isolation, cells were leached using the 0.075 mm filter and rinsed with sterile phosphate-buffered saline (PBS). Primary chondrocytes with 70–80% fusion were used in subsequent experiments. While culturing, cells were cultured in an environment with 5% CO_2 at 37 °C

Animal models

Adult male C57BL/6 mice (n = 40), eight weeks of age, were used for *in vivo* experiments. According to a previous study[1 2], medial meniscus destabilization (DMM) surgery was performed to induce post-traumatic OA to form the positive control. We randomly divided mice into four groups with ten mice per group: SHAM + vector, DMM + vector, DMM + circPde4b, and DMM + circPde4b + RIC8A groups. Briefly, mice (n = 10 per group) were anesthetized, and their medial joint capsules were incised to expose the medial meniscotibial ligament (MMTL). Subsequently, the MMTL was transected with microsurgical scissors to release the ligament linked to the tibial plateau, consequently destabilizing the medial meniscus. The joints were closed after being rinsed with sterile saline. At the same time, the medial knee joint capsule was incised for sham operation. HanBio (Shanghai, China) created and packaged adeno-associated virus (AAV) vectors for circPde4b and RIC8A. One week after operation, a total of 10 μL (approximately 1×10^{12} vg/mL) of vector AAV, circPde4b AAV, or a mixture including 5 μL circPde4b AAV and 5 μL RIC8A AAV was delivered intra-articularly into the knee

joints. Eight weeks later, knee pain was evaluated using a series of assessments[3], including a hot plate test, knee extension test, and electric shock stimulated treadmill test. Briefly, in the 55 °C hot plate test, latency was recorded when the hind paw of the mouse was lifting and/or flicking/licking. In the knee extension test, the number of vocalizations that occurred during five extensions was recorded. For the electric shock stimulated treadmill test, the number of electric shocks stimulating the mouse was recorded within 2 min at a speed of 50 m/min. Following the assessments, mice were sacrificed, and both knee articular cartilages were harvested for histological analysis or gene expression analyses. We conducted all animal experiments following the approval of the Institute of Health Sciences Institutional Animal Care and Use Committee (Zhejiang, China).

Immunofluorescence

Human osteoarthritis chondrocytes were fixed in 4% paraformaldehyde for 30 min, covered with PBS containing 0.25% Triton X-100 for 15 min, and sealed with 5% BSA containing 0.25% Triton X-100 at RT for 30 min. Cells were then incubated with the following primary antibodies: anti-MMP13 (18165-1-AP, proteintech, 1:50), anti-MMP3 (ab52915, abcam, 1:100), anti-COL2 (ab34712, abcam, 1:100), and anti-aggrecan (13880-1-AP, proteintech, 1:50). After overnight incubation at 4 °C, the cells were washed three times with PBS and incubated with goat anti-rabbit IgG (H&L) at room temperature for 1 h, rinsed and the nuclei were restained with DAPI for 5 min. Target proteins were visualized by fluorescence microscopy (Carl Zeiss, USA).

Micro-CT analysis

After fixation in 70% ethanol, all samples were scanned in a 16 mm scanning tube with 10.5 mm3 volume at 55,000 V, 180 mA, with a 115 min acquisition time. To avoid

dehydration, joints were wrapped in napkins dampened with PBS while scanning. The data were analyzed using Skyscan software.

***In vitro* transcription**

Biotin-labeled oligonucleotide probes targeting junction sites of circPDE4B were synthesized (RiboBio, Guangzhou, China). Linear circPDE4B was in vitro transcribed using Biotin RNA Labeling Mix (Roche) and T7 RNA polymerase, circularized using T4 RNA ligase I, treated with RNase R, and purified with RNeasy Mini kit (Qiagen Inc.).

Histological analysis, scoring system and immunohistochemistry

After fixing in 4% paraformaldehyde, paraffin was used to embed cartilage specimens. All samples were cut into 5 μm sections, and each one-tenth was stained with 0.1% Safranin O solution as well as 0.001% Fast Green solution (Sigma-Aldrich, St. Louis, MO, USA). OARSI grade[4 5] was used to grade the severity of cartilage degeneration by two observers blinded to group-identifying information. For human cartilage, the ROI was evaluated using OARSI, while the OA severity of mice cartilage was recorded with the maximal score of observed cartilage.

For immunohistochemistry, the sections were incubated with primary antibodies at 4 °C overnight. Subsequently, the sections were incubated with secondary antibodies for 1 h (Beyotime Institute of Biotechnology, Inc., Jiangsu, China) at 25 °C. All positively stained cells along the joint surface of each sample were counted in the femoral ankle and tibial plateau region, and the proportion of positive cells was evaluated using Image-Pro Plus 6.0 [6].

RNA extraction and RT-qPCR analysis

Total RNA was extracted using RNAEX reagent (Accurate Biotechnology, Hunan) from cultured or isolated chondrocytes. Reverse transcription of mRNAs to cDNA was performed using total RNA, with kits from Accurate Biotechnology (Hunan, China). Specific circRNAs or mRNAs were quantified with SYBR® Green Premix Pro Taq HS qPCR kit (Accurate Biotechnology, Hunan, China). The ABI 7500 Sequencing Detection System (Applied Biosystems, Foster City, CA, USA) was employed for amplification. To obtain circRNA, using 3 U/μg RNase R (Epicenter, San Diego, CA, USA) or not covered total RNA at 37 °C within 20 min. The RNeasy MinElute cleanup kit (Qiagen) was then used to purify RNA. Specific primers were designed to amplify circPDE4B. Agarose gel electrophoresis and sequencing were used to detect amplification products. All reactions were repeated three times. Housekeeping β-actin gene were used for standardization. All primers are listed in table S3.

Co-immunoprecipitation (co-IP)

Co-IP was performed as previously described (Jiao et al, 2018; Li et al, 2018b), with antibodies (1:100 dilution) specific for Myc (Abcam Inc), HA (Cell Signaling Technology), FLAG (Abcam Inc), anti-Ubiquitin antibody (Abcam Inc), RIC8A (Abcam Inc), or MID1 (Abcam Inc). Bead-bound proteins were released and analyzed by western blot.

RNA interference

siRNA-mediated knockdown was used to inhibit circRNA expression. Three different siRNAs (RiboBio, Guangzhou, China) were designed and examined for circPDE4B knockdown efficiency. SiRNA sequences are listed table S3. A specific analog (RiboBio, Guangzhou, China) was used to induce miRNA expression. Plasmid transfection was performed using Lipofectamine 3000 transfection reagent (ThermoFisher). The

Lipofectamine RNAiMAX transfection reagent (ThermoFisher) was applied for siRNA delivery.

RNA binding protein immunoprecipitation

RIP assay was performed using Magna RIPTM RNA Binding Protein Immunoprecipitation kit (Millipore), with antibodies (1:100 dilution) specific for FUS (Abcam Inc), Flag (Abcam Inc) or RIC8A (Abcam Inc). Co-precipitated RNAs were then extracted with TRIzol, and the amount of circPDE4B in the eluate was determined by RT-qPCR (table S3).

RNA pull-down assay and Mass Spectrometry (MS)/ qRT-PCR

The RNA pull-down kit (BersinBio) was used for the RNA pull-down assay. The assay is based on circRNA hybridization with the target-specific biotinylated probe, followed by pull-down, reverse transcription to cDNA for amplification through quantitative real-time PCR (RT-qPCR), and sequencing. After washing with PBS, a total of 10^7 HCs were exposed to ultraviolet irradiation at 254 nm, followed by lysis with 1 mL lysis buffer and homogenized with a 0.4 mm injector. A biotinylated antisense probe (0.2 nmol), which targets the adapter sequence, or Lac Z probes (control probes) were then added to the circPDE4B-RAP mixture. Incubation at 65 °C for 10 mins was carried out, followed by hybridization for 2 h at room temperature. Thereafter, 200 μL of streptavidin-coated magnetic beads was added. Washing followed to remove non-specific binding. Protein digestion yielded peptide fragments, which were then dissolved and vortexed. We used a loading tube to load the supernatants for MS identification. Probes are displayed in table S3.

***In vitro* binding assay**

For RIC8A GST pull-down assays, GST fusion proteins from *E. coli* BL21 cells were purified overnight at 4 °C and fixed on glutathione Sepharose 4B columns. HEK-293T cells transfected with Flag-MID1 were treated as indicated. Cells were then lysed in the NETN buffer with the protease inhibitor and cultured with Sepharose, and immobilized with indicated RIC8A GST protein and circPDE4B at 4 °C for 8 h. The RIC8A/MID1-circPDE4B complex were pulled down using GST beads (Sigma). Protein was detected by SDS–PAGE and western blot.

Western blot

SDS -PAGE separated total cellular protein, which was then transferred to an Immobilon-P membrane (0.2 μm pore size, Millipore, Billerica, MA, USA). The membranes were blocked and then incubated with primary antibodies (BD Biosciences, San Jose, CA, USA) overnight at 4 °C, and subsequently incubated with secondary antibodies for 1 h. β-actin served as the internal standard and Image J was used to quantify blots intensities. The antibodies used were as follows: anti-MMP13 antibody (1:1000, abcam, ab51072), anti-MMP3 antibody (1:1000, abcam, ab52915), anti-ADAMTS4 antibody (1:1000, abcam, ab185722), anti-COL2 antibody (1:1000, abcam, ab34712), anti-SOX9 antibody (1:1000, abcam, ab185966), anti-aggrecan antibody (1:1000, abcam, ab3778), anti-RIC8A antibody (1:1000, abcam, ab194941), anti-MID1 antibody (1:1000, abcam, ab70770), anti-HA antibody (1:2000, Cell Signaling Technology, 4970s), anti-FLAG antibody (1:1000, abcam, ab205606), anti-Ubiquitin antibody (1:1000, abcam, ab140601), anti-Myc antibody (1:1000, abcam, ab32) and anti-β-actin antibody (1:2000, Cell Signaling Technology, 4970s).

RNA fluorescent *in situ* hybridization (FISH)

The cells were seeded in 12-well plates with sterile glass covers and allowed to culture overnight. Cells were then fixed with PBS containing 37% formaldehyde for 15 min at 25 °C and dehydrated with 70% ethanol at 4 °C for 1 h. Slides were hybridized for 14–16 h at 37 °C. Cy3-labeled circPDE4B probes were constructed by RiboBio (Guangzhou, China). Hybridization buffer for RNA FISH dissolved the probes at a concentration of 20 nM. Following overnight hybridization, the slides were washed with 10% formamide/2× SSC at 37 °C on an oscillator for 30 min, and subsequently washed with PBS and 0.1% (v/v) Tween 20 three times. Cells were then stained with Alexa Fluor 546-conjugated streptavidin for 1 h at the same temperature as for IF. The cover glass was restained with DAPI, fixed with ProLong Gold anti-fading reagents, and observed under a Nikon A1Si Laser Scanning Confocal Microscope (Nikon Instruments Inc., Japan). For FISH of samples from in vivo experiments, ahead of hybridization, we performed the biopsy at 37° C under 0.8% pepsin processing. Slices were then deparaffinized, rehydrated, and permeated for 30 min. The primers and probe sequences are shown in table S3.

Patient and public involvement statement

Patients or the public WERE NOT involved in the design, or conduct, or reporting, or dissemination plans of our research

Statistical analysis

All statistical analyses were performed using SPSS v22.0. Data distribution was assessed using the Shapiro-Wilk test. The Levene test was used to assess the equality of variances. Statistical analysis was performed by unpaired two-tailed Student's t-test (normal distribution and equal variances, using 95% confidence intervals for between-group differences), Welch t-test (unequal variances), or Mann–Whitney U test (non-normal distribution). Multiple group comparisons were performed by one-way analysis of

variance (normal distribution) or Kruskal–Wallis (non-normal distribution) test followed by Bonferroni or Dunn post hoc test, respectively. A P value < 0.05 was considered statistically significant.

REFERENCES

1. Glasson SS, Blanchet TJ, Morris EA. The surgical destabilization of the medial meniscus (DMM) model of osteoarthritis in the 129/SvEv mouse. *Osteoarthritis Cartilage* 2007;15(9):1061-9. doi: 10.1016/j.joca.2007.03.006
2. Chen D, Shen J, Zhao W, et al. Osteoarthritis: toward a comprehensive understanding of pathological mechanism. *Bone Res* 2017;5:16044. doi: 10.1038/boneres.2016.44 [published Online First: 2017/02/06]
3. Piel MJ, Kroin JS, van Wijnen AJ, et al. Pain assessment in animal models of osteoarthritis. *Gene* 2014;537(2):184-8. doi: 10.1016/j.gene.2013.11.091
4. Glasson SS, Chambers MG, Van Den Berg WB, et al. The OARSI histopathology initiative - recommendations for histological assessments of osteoarthritis in the mouse. *Osteoarthritis Cartilage* 2010;18 Suppl 3:S17-23. doi: 10.1016/j.joca.2010.05.025 [published Online First: 2010/10/01]
5. Pritzker KP, Gay S, Jimenez SA, et al. Osteoarthritis cartilage histopathology: grading and staging. *Osteoarthritis Cartilage* 2006;14(1):13-29. doi: 10.1016/j.joca.2005.07.014
6. Chen P, Xia C, Mei S, et al. Intra-articular delivery of sinomenium encapsulated by chitosan microspheres and photo-crosslinked GelMA hydrogel ameliorates osteoarthritis by effectively regulating autophagy. *Biomaterials* 2016;81:1-13. doi: 10.1016/j.biomaterials.2015.12.006 [published Online First: 2015/12/30]

SUPPLEMENTARY TABLES

Table S1. Top 50 differentially expressed circRNAs in control and OA tissues ranked by expression level.

id	log2FC(Con-trol/OA)	pval	regulate	significant	mean_Con	mean_OA
1:65913245|65918835	2.298017962	0.013420134	up	yes	71.57389833	14.47433303

2:223998115|224001922	2.017322781	0.037510887	up	yes	57.89743315	14.2263021
6:159682474|159688242	3.277353459	0.000604761	up	yes	38.51538065	3.882709433
7:84129123|84194668	4.416423377	0.000404841	up	yes	23.89613671	1.023738907
4:102304317|102315830	3.801482647	0.003360458	up	yes	21.73943548	1.4663222
2:223991803|224001922	2.334035326	0.013161838	up	yes	18.03811377	3.497306791
13:42953948|42970670	2.907556748	0.009637056	up	yes	16.17980657	2.069638833
5:65170617|65197151	4.154129743	0.015296915	up	yes	15.86773823	0.796862253
17:27765535|27766588	7.209593338	2.94E-10	up	yes	14.70143599	0
1:102979382|102989571	7.01468859	9.33E-11	up	yes	12.83098702	0
1:32948222|32949774	1.899306098	0.048974712	up	yes	7.811225125	2.020780085
8:17558295|17562110	5.830035008	7.60E-07	up	yes	7.605289257	0.035448292
19:45025329|45025737	2.667894244	0.014344495	up	yes	6.992268417	1.016012274
7:80761616|80789528	2.166891001	0.025288244	up	yes	6.740826549	1.423384001
19:6702127|6702579	5.725610351	3.17E-08	up	yes	5.191520209	0
8:17543318|17543715	4.576294017	1.42E-05	up	yes	4.946360357	0.111532203
5:59180595|59215968	5.27607838	1.18E-07	up	yes	3.774876381	0
10:7243558|7285954	1.954291245	0.049795018	up	yes	3.444247889	0.814584431
17:27768977|27769584	5.136722549	0.000186202	up	yes	3.418095033	0
20:54157169|54171670	4.243602481	8.27E-05	up	yes	3.089979272	0.068397727
13:42917541|	3.094148388	0.011943706	up	yes	2.836359073	0.243856855

42970670						
7:84110470|84194668	4.361466685	0.000348323	up	yes	2.810081997	0.041570553
6:107503657|107533610	2.581974853	0.045526372	up	yes	2.492951616	0.333054478
20:18297985|18306393	4.687371106	0.002144755	up	yes	2.476554324	0
4:88475841|88479507	4.543128739	4.12E-06	up	yes	2.231406616	0
7:84046324|84060558	4.025668711	0.012672298	up	yes	2.160629655	0.038797737
7:90747681|90790652	4.475075842	3.16E-06	up	yes	2.123986063	0
1:27668226|27669346	3.850469968	0.001064668	up	yes	2.109467326	0.053172438
17:66513336|66514466	4.390178942	0.001302459	up	yes	1.996889514	0
18:6301903|6312056	2.876917257	0.039095578	up	yes	1.93391171	0.176881352
1:186893011|186911389	3.106673582	0.00897813	up	yes	1.899981712	0.132179616
18:6263947|6312056	3.497797506	0.00378226	up	yes	1.830524648	0.070896584
X:148661908|148662768	2.136810258	0.026904799	up	yes	1.829022055	0.338624828
3:112109543|112113145	3.347239351	0.003786519	up	yes	1.827445988	0.089392497
4:150467673|150491035	4.255549433	1.27E-05	up	yes	1.810064475	0
17:27778690|27779056	4.225978288	1.16E-05	up	yes	1.771312099	0
22:33761371|33765953	4.194653636	0.001595289	up	yes	1.731118987	0
17:80289659|80290728	2.289891436	0.029722666	up	yes	1.684744047	0.26496392
8:105419144|105561481	2.399627165	0.025199407	up	yes	1.584695203	0.219272552
19:45022053|45028992	3.28409336	0.006756638	up	yes	1.569980322	0.071435494

2:223912253|223918010	4.053146681	0.000134317	up	yes	1.560040669	0
13:42926336|42970670	2.181505031	0.034446179	up	yes	1.511971175	0.255352047
15:45476079|45476552	3.959830453	0.001227535	up	yes	1.456065035	0
1:46077515|46080750	3.950560938	8.63E-05	up	yes	1.446099152	0
5:65170617|65215487	3.94001855	6.71E-05	up	yes	1.434842326	0
5:65242104|65273447	2.83649554	0.031810662	up	yes	1.431521832	0.114413908
14:100353687|100361921	2.884414792	0.048709863	up	yes	1.424099749	0.106403957
17:80325030|80328477	3.013454971	0.006302126	up	yes	1.419825328	0.088214614
7:84110470|84134951	3.482653818	0.002962863	up	yes	1.414107802	0.035448292
1:102939035|102946956	2.892345557	0.03182733	up	yes	1.300464786	0.088620731

Table S2. Top 50 circPDE4B-binding proteins identified by mass spectrometry (ranked by pep_score).

num	prot_acc	prot_desc	pep_score
1	P07237	Protein disulfide-isomerase OS=Homo sapiens OX=9606 GN=P4HB PE=1 SV=3	118.07
2	Q9NPQ8	Synembryn-A OS=Homo sapiens OX=9606 GN=RIC8A PE=1 SV=3	96.92
3	P06733	Alpha-enolase OS=Homo sapiens OX=9606 GN=ENO1 PE=1 SV=2	95.8
4	Q16891	MICOS complex subunit MIC60 OS=Homo sapiens OX=9606 GN=IMMT PE=1 SV=1	95.59
5	P04259	Keratin, type II cytoskeletal 6B OS=Homo sapiens OX=9606 GN=KRT6B PE=1 SV=5	92.43

6	P67936	Tropomyosin alpha-4 chain OS=Homo sapiens OX=9606 GN=TPM4 PE=1 SV=3	90.97
7	P08133	Annexin A6 OS=Homo sapiens OX=9606 GN=ANXA6 PE=1 SV=3	87.9
8	Q6WCQ1	Myosin phosphatase Rho-interacting protein OS=Homo sapiens OX=9606 GN=MPRIP PE=1 SV=3	84.9
9	P27348	14-3-3 protein theta OS=Homo sapiens OX=9606 GN=YWHAQ PE=1 SV=1	83.69
10	O00458	Interferon-related developmental regulator 1 OS=Homo sapiens OX=9606 GN=IFRD1 PE=1 SV=4	82.38
11	P04181	Ornithine aminotransferase, mitochondrial OS=Homo sapiens OX=9606 GN=OAT PE=1 SV=1	81.54
12	Q9UNL2	Translocon-associated protein subunit gamma OS=Homo sapiens OX=9606 GN=SSR3 PE=1 SV=1	80.32
13	P10809	60 kDa heat shock protein, mitochondrial OS=Homo sapiens OX=9606 GN=HSPD1 PE=1 SV=2	77.24
14	Q15084	Protein disulfide-isomerase A6 OS=Homo sapiens OX=9606 GN=PDIA6 PE=1 SV=1	72.89
15	Q7Z406	Myosin-14 OS=Homo sapiens OX=9606 GN=MYH14 PE=1 SV=2	71.8
16	E9PRG8	Uncharacterized protein C11orf98 OS=Homo sapiens OX=9606 GN=C11orf98 PE=4 SV=1	71.22
17	P68871	Hemoglobin subunit beta OS=Homo sapiens OX=9606 GN=HBB PE=1 SV=2	67.41
18	P83731	60S ribosomal protein L24 OS=Homo sapiens OX=9606 GN=RPL24 PE=1 SV=1	66.31
19	P21333	Filamin-A OS=Homo sapiens OX=9606 GN=FLNA PE=1 SV=4	66.06
20	P21127	Cyclin-dependent kinase 11B OS=Homo sapiens OX=9606	65.88

		GN=CDK11B PE=1 SV=4	
21	P48444	Coatomer subunit delta OS=Homo sapiens OX=9606 GN=ARCN1 PE=1 SV=1	64.61
22	Q12965	Unconventional myosin-Ie OS=Homo sapiens OX=9606 GN=MYO1E PE=1 SV=2	62.35
23	P42766	60S ribosomal protein L35 OS=Homo sapiens OX=9606 GN=RPL35 PE=1 SV=2	61.42
24	P05783	Keratin, type I cytoskeletal 18 OS=Homo sapiens OX=9606 GN=KRT18 PE=1 SV=2	60.52
25	P05783	Keratin, type I cytoskeletal 18 OS=Homo sapiens OX=9606 GN=KRT18 PE=1 SV=2	60.52
26	P10412	Histone H1.4 OS=Homo sapiens OX=9606 GN=HIST1H1E PE=1 SV=2	58.75
27	P43246	DNA mismatch repair protein Msh2 OS=Homo sapiens OX=9606 GN=MSH2 PE=1 SV=1	57.6
28	O43707	Alpha-actinin-4 OS=Homo sapiens OX=9606 GN=ACTN4 PE=1 SV=2	57.2
29	P08865	40S ribosomal protein SA OS=Homo sapiens OX=9606 GN=RPSA PE=1 SV=4	56.12
30	Q9NX58	Cell growth-regulating nucleolar protein OS=Homo sapiens OX=9606 GN=LYAR PE=1 SV=2	55.3
31	P06396	Gelsolin OS=Homo sapiens OX=9606 GN=GSN PE=1 SV=1	55.09
32	Q9Y4I1	Unconventional myosin-Va OS=Homo sapiens OX=9606 GN=MYO5A PE=1 SV=2	54.65
33	P62937	Peptidyl-prolyl cis-trans isomerase A OS=Homo sapiens OX=9606 GN=PPIA PE=1 SV=2	54
34	Q15233	Non-POU domain-containing octamer-binding protein OS=Homo sapiens OX=9606 GN=NONO PE=1 SV=4	51.87

35	Q7KZF4	Staphylococcal nuclease domain-containing protein 1 OS=Homo sapiens OX=9606 GN=SND1 PE=1 SV=1	51.86
36	Q5BJD5	Transmembrane protein 41B OS=Homo sapiens OX=9606 GN=TMEM41B PE=1 SV=1	50.71
37	P13796	Plastin-2 OS=Homo sapiens OX=9606 GN=LCP1 PE=1 SV=6	48.92
38	Q02809	Procollagen-lysine,2-oxoglutarate 5-dioxygenase 1 OS=Homo sapiens OX=9606 GN=PLOD1 PE=1 SV=2	48.83
39	P47755	F-actin-capping protein subunit alpha-2 OS=Homo sapiens OX=9606 GN=CAPZA2 PE=1 SV=3	47.71
40	P62701	40S ribosomal protein S4, X isoform OS=Homo sapiens OX=9606 GN=RPS4X PE=1 SV=2	46.2
41	Q96D15	Reticulocalbin-3 OS=Homo sapiens OX=9606 GN=RCN3 PE=1 SV=1	46.01
42	P62241	40S ribosomal protein S8 OS=Homo sapiens OX=9606 GN=RPS8 PE=1 SV=2	45.16
43	P27797	Calreticulin OS=Homo sapiens OX=9606 GN=CALR PE=1 SV=1	44.29
44	P31946	14-3-3 protein beta/alpha OS=Homo sapiens OX=9606 GN=YWHAB PE=1 SV=3	42.45
45	P04844	Dolichyl-diphosphooligosaccharide--protein glycosyltransferase subunit 2 OS=Homo sapiens OX=9606 GN=RPN2 PE=1 SV=3	42.04
46	P46777	60S ribosomal protein L5 OS=Homo sapiens OX=9606 GN=RPL5 PE=1 SV=3	41.71
47	P14618	Pyruvate kinase PKM OS=Homo sapiens OX=9606 GN=PKM PE=1 SV=4	41.29
48	P60866	40S ribosomal protein S20 OS=Homo sapiens OX=9606 GN=RPS20 PE=1 SV=1	40.91
49	Q9Y281	Cofilin-2 OS=Homo sapiens OX=9606 GN=CFL2 PE=1 SV=1	40.89

50	Q9UN86	Ras GTPase-activating protein-binding protein 2 OS=Homo sapiens OX=9606 GN=G3BP2 PE=1 SV=2	40.52

Table S3. Primers and sequences used in this study.

Primers for qPCR		
PDE4B mRNA (hsa)	F	CACACTTGGGATCGACCTCT
	R	GGAAGCGTTGTCAAAGGCAG
circPDE4B (hsa)	F	CAGAGTGAAAGGGCAAGGACT
	R	CCGTCATCACACTCCTGCTTT
Pde4b mRNA (mmu)	F	TGCGCTTGGAACTTGAGCTT
	R	GCCGCTGTCGGATGCTTTTA
circPde4b (mmu)	F	CTGTGAGCCAGGAGTGGTCTA
	R	GGTGTAACTGGAAGAGCTGTAGGAT
Human β-actin	F	AGAGCTACGAGCTGCCTGAC
	R	AGCACTGTGTTGGCGTACAG
Mouse β-actin	F	AGCCATGTACGTAGCCATCC
	R	CTCTCAGCTGTGGTGGTGAA
Human MMP3	F	CCTACAAGGAGGCAGGCAAG
	R	CCCGTCACCTCCAATCCAAG
Human MMP13	F	TCGGCCACTCCTTAGGTCTT
	R	AAGTGGCTTTTGCCGGTGTA
Human COL2A1	F	TCCTGCCGTTTCGCTG
	R	CATTATACCTCTGCCCATCCTG
Human ADAMTS4	F	GTCCCATGTGCAACGTCAAG
	R	ATGCGGCCATCTTGTCATCT
Human ADAMTS5	F	GGGCACTGGCTACTATGTGG
	R	CGTCACAGCCAGTTCTCACA
Human Aggrecan	F	GGGACCTGCAAGGAGACAGAG
	R	TCAATCTCACACAGGTCCCCTTC
Human SOX9	F	GCTCTGGAGACTTCTGAACGA
	R	CCGTTCTTCACCGACTTCCT
Human RIC8A	F	GCTCTGCGGTCATACAACCAG
	R	GTCTCTTCCGGTCCTCCTGTT
Mouse RIC8A	F	AGATGCGGTGACAGAAGCTC
	R	CACGGTGCTTTGGTGACAAG
Mouse MMP13	F	CAAGCAGTTCCAAAGGCTACA

	R	TAGGGCTGGGTCACACTTCT
Mouse MMP3	F	ACTGTGTCCCAAGGAGAGGAG
	R	AAACCATCTACACAGTTCAGACAC
Mouse COL2A1	F	CACGCATGAGCCGAAGCTA
	R	GGGTTTCCACGTCTCACCA
Mouse ADAMTS4	F	TTGTTCTCCCAGTCACCCTCC
	R	AGCCTGGGACTAAAGATAGGCA
Mouse ADAMTS5	F	ATGCAGCCATCCTGTTCACC
	R	AAGGCCAAGTAGATGCCCAATTT
Mouse Aggrecan	F	CACTGTCAAAGCACCATGCC
	R	TAGGCTGGCTCCCATTCAGT
Mouse SOX9	F	TAATTCCCCAGGCTCTTGGAT
	R	GCAGCCGGGATTTAAGGCTC
Human MID1	F	CTGATCCGAGGCAAAGAGCC
	R	CAGGCACTCGTCACAGTAGG
Human FUS	F	TTATGGCCAGAGCCAGAACAC
	R	GCTACCGTAACTTCCCGAGG
Human DHX9	F	GTACGGCCTGGATTCTGCTT
	R	ATCACAGCATCCAAAGGGGG
Primers for Site-Directed Mutagenesis		
RIC8A K143R	F	ctctgtgagcctcaccactaggcgggc
	R	gcccgcctagtggtgaggctcacagag
RIC8A K187R	F	gcgcactcctctcagctcctgaaacagctg
	R	cagctgtttcaggagctgagaggagtgcgc
RIC8A K237R	F	acctccccctgatggagtccagggtg
	R	caccctggactccatcaggggggaggt
RIC8A K285R	F	gagaacatccagacacctgaggggcaagttccc
	R	gggaacttgcccctcaggtgtctggatgttctc
RIC8A K319R	F	tgtgcaaacgcctctctaggaagatgaggaggg
	R	ccctcctcatcttcctagagaggcgtttgcaca
RIC8A K328R	F	ctacactctccctcagcctgtgtgtcttgtgca
	R	tgcacaagacacacaggctgagggagagtgtag
RIC8A K415R	F	cccatagcctgtgtacctgatgaatcggggcac
	R	gtgccccgattcatcaggtacacaggctatggg
RIC8A K456R	F	tttatgctggctctggcttccttgtactcatctgtg
	R	cacagatgagtacaaggaagccagagccagcataaa
RIC8A K469R	F	ttaggcggcctctcctccaccctcccg
	R	cgggagggtggaggagaggccgcctaa

Primers for PCR		
Divergent- β-actin	F	CAGGGCTTACCTGTACACTGA
	R	GCGCGGCGATATCATCATCC
β-actin	F	AGAGCTACGAGCTGCCTGAC
	R	AGCACTGTGTTGGCGTACAG
CircPDE4B	F	CAGAGTGAAAGGGCAAGGACT
	R	CCGTCATCACACTCCTGCTTT
mPDE4B	F	CACACTTGGGATCGACCTCT
	R	GGAAGCGTTGTCAAAGGCAG
Divergent- β-actin (Mouse)	F	GGCCTGTACACTGACTTGAGA
	R	AAGGAGCTGCAAAGAAGCTGT
β-actin (Mouse)	F	AGCCATGTACGTAGCCATCC
	R	CTCTCAGCTGTGGTGGTGAA
CircPDE4B (Mouse)	F	CTGTGAGCCAGGAGTGGTCTA
	R	GGTGTAACTGGAAGAGCTGTAGGAT
PDE4B (Mouse)	F	TGCGCTTGGAACTTGAGCTT
	R	GCCGCTGTCGGATGCTTTTA
ShRNA		
CircPDE4B shRNA-1	F	CCGGCCAGGAGTGGTATTAAAAACTCGAGTTTTTAATACCACTCCTGGTTTTTC
	R	AATTGAAAAACCAGGAGTGGTATTAAAAACTCGAGTTTTTAATACCACTCCTGG
CircPDE4B shRNA-2	F	CCGGGGAGTGGTATTAAAAAGTGCTCGAGCACTTTTTAATACCACTCCTTTTTC
	R	AATTGAAAAAGGAGTGGTATTAAAAAGTGCTCGAGCACTTTTTAATACCACTCC
RIC8A shRNA-1	F	CCGGACCGCACAGAGGAGTTCCACTCGAGTGGAACTCCTCTGTGCGGTTTTTTC
	R	AATTGAAAAAGGAGTGGTATTAAAAAGTGCTCGAGCACTTTTTAATACCACTCC
RIC8A shRNA-2	F	CCGGCATGTTTGACAAGCTCTCCCTCGAGGGAGAGCTTGTCAAACATGTTTTTC
	R	AATTGAAAAACATGTTTGACAAGCTCTCCCTCGAGGGAGAGCTTGTCAAACATG
MID1 shRNA-1	F	CCGGACCGCATCCTAGTATCACACTCGAGTGTGATACTAGGATGCGGTTTTTTC
	R	AATTGAAAAAACCGCATCCTAGTATCACACTCGAGTGTGATACTAGGATGCGGT

MID1 shRNA-2	F	CCGGGCAACGTCACCCTACAGAACTCGAGTTCTGTAG GGTGACGTTGCTTTTTC
	R	AATTGAAAAAGCAACGTCACCCTACAGAACTCGAGTT CTGTAGGGTGACGTTGC
FUS shRNA-1	F	CCGGCAAGCAGATTGGTATTATTCTCGAGAATAATAC CAATCTGCTTGTTTTTC
	R	AATTGAAAAACAAGCAGATTGGTATTATTCTCGAGAA TAATACCAATCTGCTTG
FUS shRNA-2	F	CCGGCAGAGTTACAGTGGTTATACTCGAGTATAACCA CTGTAACTCTG TTTTTC
	R	AATTGAAAAACAGAGTTACAGTGGTTATACTCGAGTA TAACCACTGTAACTCTG
Mmu CircPDE4B shRNA-1	F	CCGGGGAGTGGTCTAATCTGCCACTCGAGTGGCAGAT TAGACCACTCCTTTTTC
	R	AATTGAAAAAGGAGTGGTCTAATCTGCCACTCGAGTG GCAGATTAGACCACTCC
Mmu CircPDE4B shRNA-2	F	CCGGGCCAGGAGTGGTCTAATCTCTCGAGAGATTAGA CCACTCCTGGCTTTTTC
	R	AATTGAAAAAGCCAGGAGTGGTCTAATCTCTCGAGAG ATTAGACCACTCCTGGC
SiRNAs		
Scramble si		UUCUCCGAACGUGUCACGUTT
Human CircPDE4B si-1		AGCCAGGAGTGGTATTAAA
Human CircPDE4B si-2		CCAGGAGTGGTATTAAAAA
Human CircPDE4B si-3		GGAGTGGTATTAAAAAGTG
Mouse CircPDE4B si-1		GGAGTGGTCTAATCTGCCA
Mouse CircPDE4B si-2		GCCAGGAGTGGTCTAATCT
Mouse CircPDE4B si-3		TGAGCCAGGAGTGGTCTAA
FUS si-1		CAAGCAGATTGGTATTATT
FUS si-2		CAGAGTTACAGTGGTTATA
DHX9 si-1		CGAACACCATTGCATGAAA
DHX9 si-2		GGACTAGTAGCAACATTGA
Human/Mouse RIC8A si-1		ACCGCACAGAGGAGTTCCA
Human/Mouse RIC8A si-2		CATGTTTGACAAGCTCTCC
Human KRT6B si		TACCATCAAGTCAACAGTTATCA
Human ENO1 si		GCATTGGAGCAGAGGTTTA

Human IMMT si		GGGTTGACTACTGGCAAAATTGC
Human P4HB si		GTCCTCTTTAAGAAGTTTGATGA
Probes for FISH		
Cy3-Hsa circPDE4B		5‘-Cy3-ACACTTTTTAATACCACTCCTGGCTTACAG-3’
Cy3- Mmu circPDE4B		5‘-CY3-GGCAGATTAGACCACTCCTGGCTCAC-3’
RAP and PCR sequences		
CircPDE4B pull-down probe		CATTGCTATTACAACTGTAAGCCAGGAGTGGTATTAAAAA GTGTCAGCAAACTGCATTGAATAACAGACATCCTAAGAGG GGATATTTTCCACCTCTATAATGAAGAAAAGCAGGAGTGT GATGACGGTGATGGCTGATGATAATGTTAAAGATTATTTT GAATGTAGCTTGAGTAAATCCTACAGTTCTTCCAGTAACA CACTTGGGATCGACCTCTGGAGAGGGAGAAGGTGTTGCTC AGGAAACTTACAGTTACCACCACTGTCTCAAAGACAGAGT GAAAGGGCAAGGACTCCTGAGGGAGATGGTATTTCCAGGC CGACCACACTGCCTTTGACAACGCTTCCAAGCATTGCTAT TACAACTGTAAGCCAGGAGTG
Lac Z pull-down probes		TGGCCGTCGTTTTACAACGTCGTGACTGGGAAAACCCTGG CGTTACCCAACTTAATCGCCTTGCAGCACATCCCCCTTTC GCCAGCTGGCGTAATAGCGAAGAGGCCCGCACCGATCGCC CTTCCCAACAGTTGCGCAGCCTGAATGGCGAATGGCGCCT GATGCGGTATTTTCTCCTTACGCATCTGTGCGGTATTTCA CACCGCATATGGTGCACTCTCAGTACAATCTGCTCTGATG CCGCATAG

1

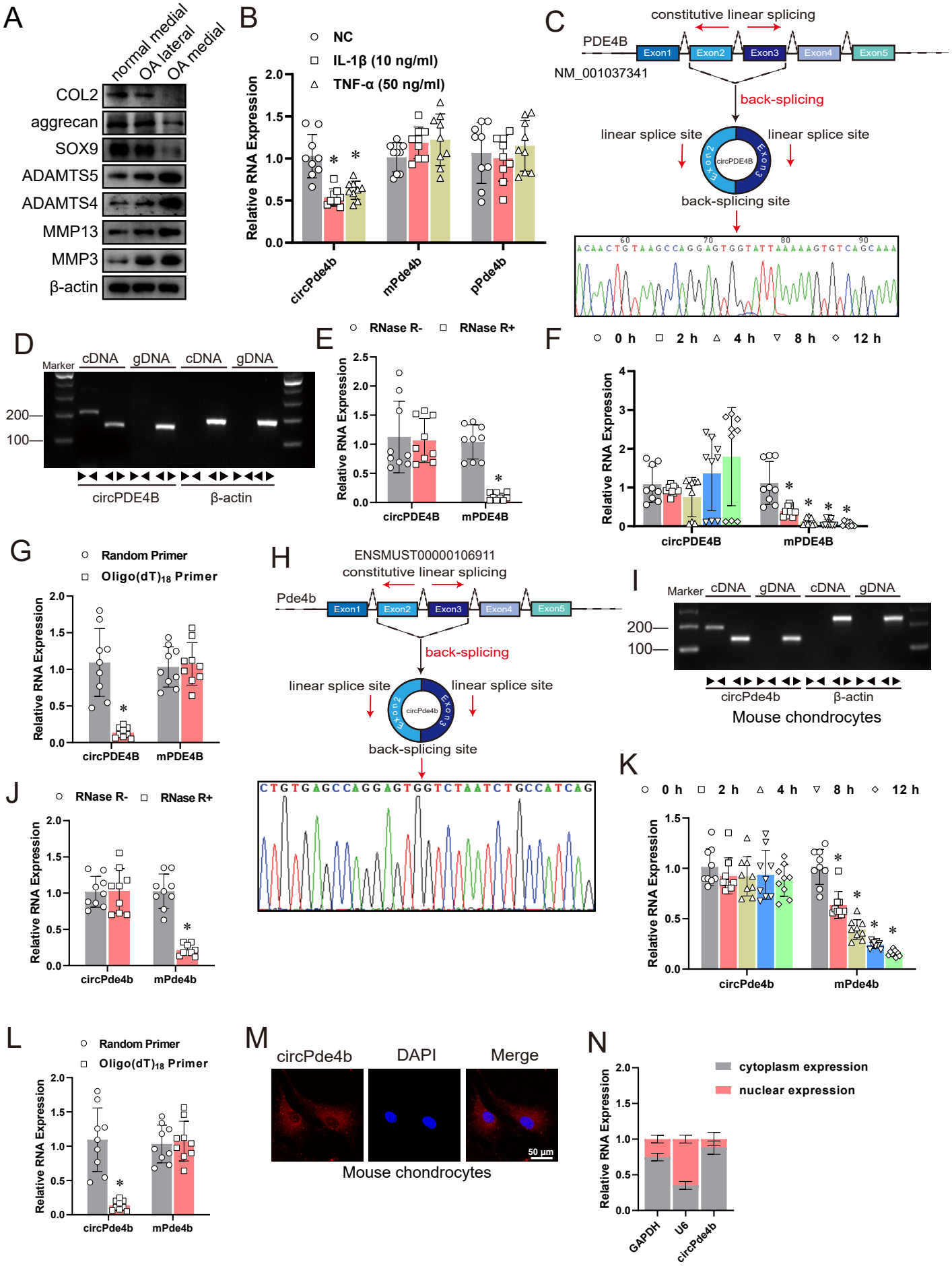
A
normal medial
OA lateral
OA medial
COL2
aggrecan
SOX9
ADAMTS5
ADAMTS4
MMP13
MMP3
β-actin
B
NC
IL-1β (10 ng/ml)
TNF-α (50 ng/ml)
Relative RNA Expression
circPde4b
mPde4b
pPde4b
C
constitutive linear splicing
PDE4B
Exon1
Exon2
Exon3
Exon4
Exon5
NM_001037341
back-splicing
linear splice site
linear splice site
circPDE4B
back-splicing site
D
Marker
cDNA
gDNA
cDNA
gDNA
200
100
circPDE4B
β-actin
E
RNase R-
RNase R+
Relative RNA Expression
circPDE4B
mPDE4B
F
0 h
2 h
4 h
8 h
12 h
Relative RNA Expression
circPDE4B
mPDE4B
G
Random Primer
Oligo(dT)18 Primer
Relative RNA Expression
circPDE4B
mPDE4B
H
ENSMUST00000106911
constitutive linear splicing
Pde4b
Exon1
Exon2
Exon3
Exon4
Exon5
back-splicing
linear splice site
linear splice site
circPde4b
back-splicing site
I
Marker
cDNA
gDNA
cDNA
gDNA
200
100
circPde4b
β-actin
Mouse chondrocytes
J
RNase R-
RNase R+
Relative RNA Expression
circPde4b
mPde4b
K
0 h
2 h
4 h
8 h
12 h
Relative RNA Expression
circPde4b
mPde4b
L
Random Primer
Oligo(dT)18 Primer
Relative RNA Expression
circPde4b
mPde4b
M
circPde4b
DAPI
Merge
50 μm
Mouse chondrocytes
N
cytoplasm expression
nuclear expression
Relative RNA Expression
GAPDH
U6
circPde4b

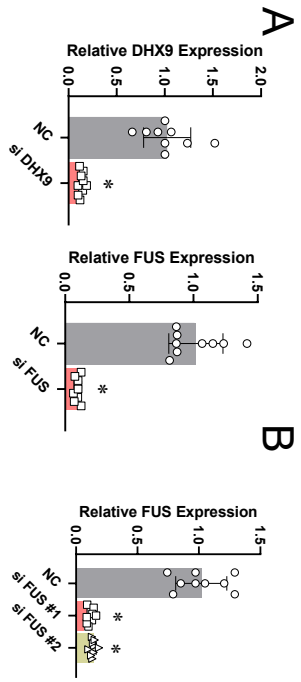
A
Relative DHX9 Expression
0.0
0.5
1.0
1.5
2.0
NC
si DHX9
*
Relative FUS Expression
0.0
0.5
1.0
1.5
NC
si FUS
*
B
Relative FUS Expression
0.0
0.5
1.0
1.5
NC
si FUS #1
si FUS #2
*
*

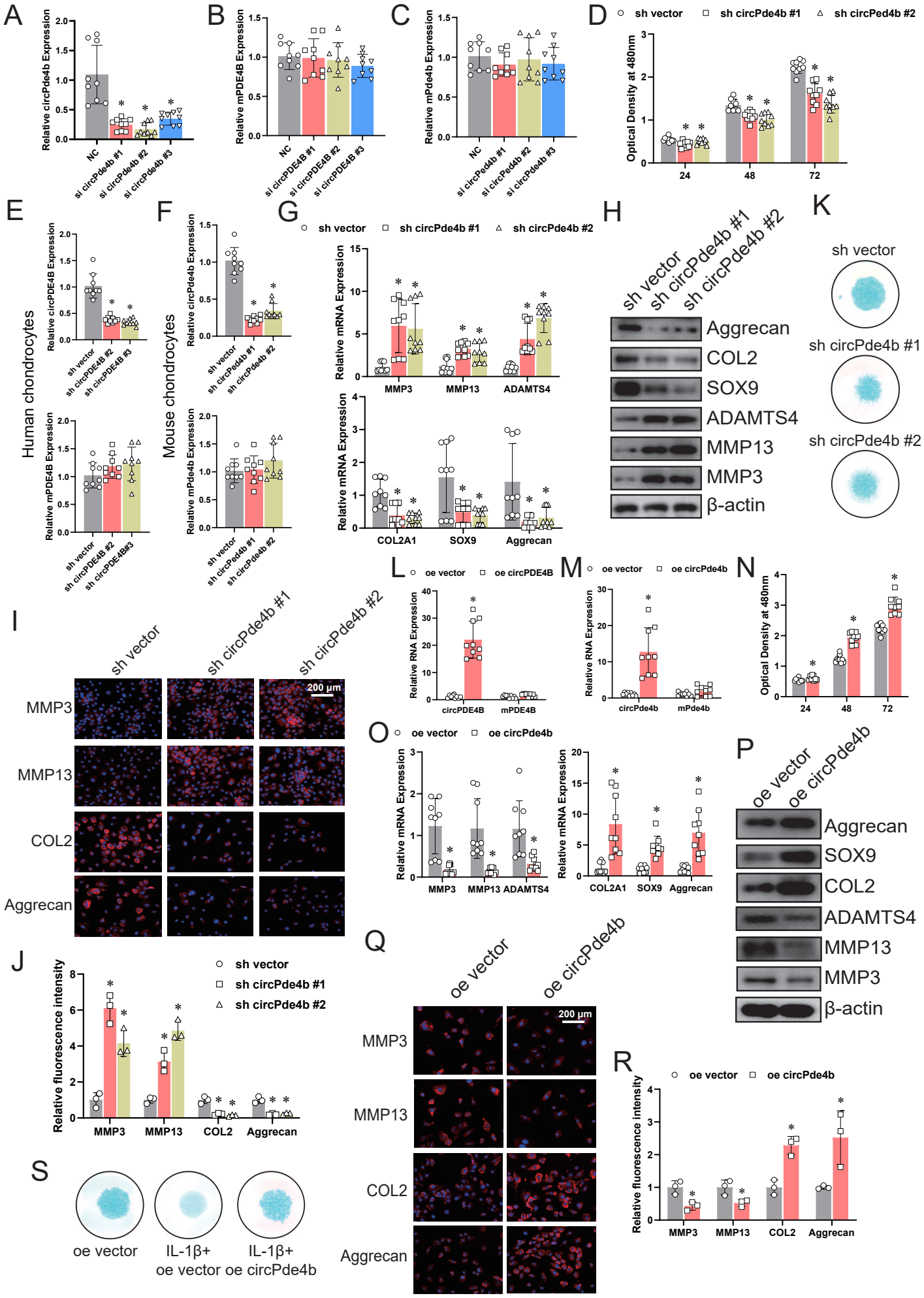
A
Relative circPde4b Expression
NC
si circPde4b #1
si circPde4b #2
si circPde4b #3
B
Relative mPDE4B Expression
si circPDE4B #1
si circPDE4B #2
si circPDE4B #3
C
Relative mPde4b Expression
D
sh vector
sh circPde4b #1
sh circPed4b #2
Optical Density at 480nm
24
48
72
E
Human chondrocytes
Relative circPDE4B Expression
sh circPDE4B #2
sh circPDE4B #3
Relative mPDE4B Expression
F
Mouse chondrocytes
Relative circPde4b Expression
sh circPde4b #1
sh circPde4b #2
Relative mPde4b Expression
G
Relative mRNA Expression
MMP3
MMP13
ADAMTS4
COL2A1
SOX9
Aggrecan
H
Aggrecan
COL2
SOX9
ADAMTS4
MMP13
MMP3
β-actin
K
sh circPde4b #1
sh circPde4b #2
L
oe vector
oe circPDE4B
Relative RNA Expression
circPDE4B
mPDE4B
M
oe circPde4b
circPde4b
mPde4b
N
I
MMP3
MMP13
COL2
Aggrecan
200 μm
O
oe circPde4b
P
Q
R
J
Relative fluorescence intensity
S
oe vector
IL-1β+ oe vector
IL-1β+ oe circPde4b

A

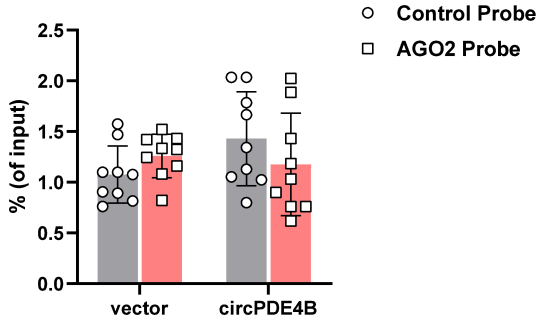

B

CPAT software: http://lilab.research.bcm.edu/cpat/calculator_sub.php

Data ID	Sequence Name	RNA Size	ORF Size	Ficket Score	Hexamer Score	Coding Probability	Coding Label
0	HSA_CIRC_0008433|NM_001037341|PDE4B	351	279	0.8886	-0.027773613549	0.076337512427542	no

ORF finder

Label	Strand	Frame	Start	Stop	Length (nt | aa)
ORF1	+	2	71	>349	279 | 92
ORF2	-	1	324	238	87 | 28

CircBank: IRES elements

ID	start	end	score
hsa_circPDE4B_003	101	274	0.60

C

ORF1-92AA
MKKSRSVMTVMADDNVKDYFECSLSKSYSSSSNTLGIDLWRGRRC
CSGNLQLPPLSQRQSERARTPEGDGISRPTTLPLTTLPSIAITTVSQE

ORF1-28AA
MLGSVVKGSVVGLEIPSPSGVLALSLCL

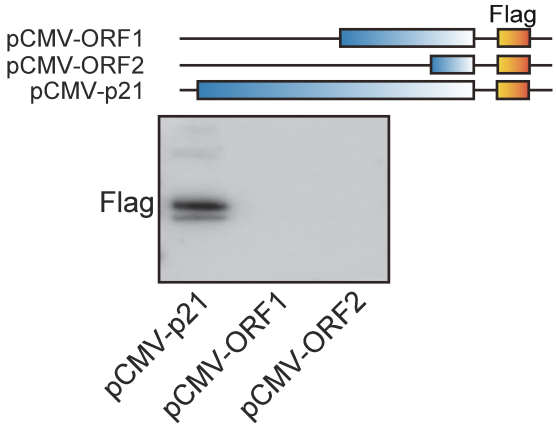

A

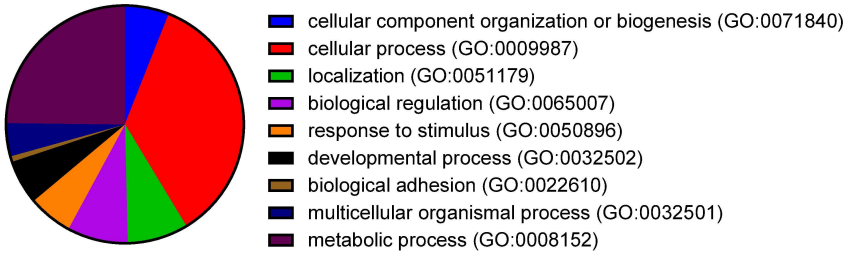

B

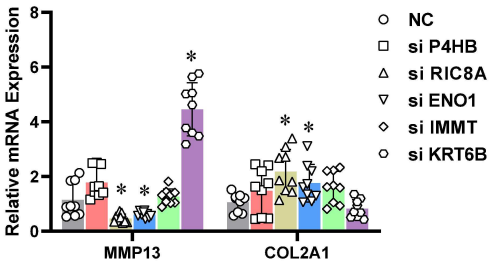

C

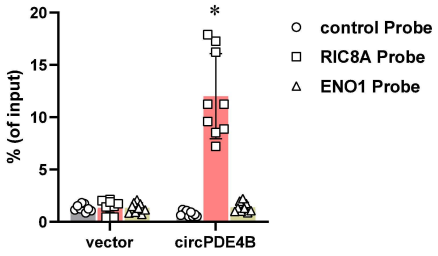

D

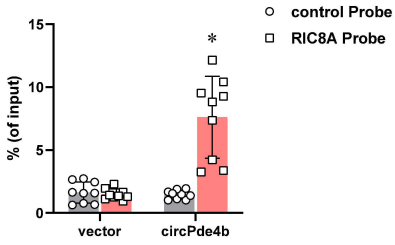

E

#	Protein region	RNA region	Interaction Propensity	Discriminative Power	Normalized Score
1	201-252	276-327	5.01	22	2.39
2	462-513	276-327	4.66	20	2.30
3	151-202	276-327	4.25	20	2.18
4	26-77	276-327	4.12	20	2.15
5	212-263	276-327	4.11	20	2.14
6	426-477	276-327	4.04	20	2.12
7	362-413	276-327	3.87	20	2.08
8	437-488	276-327	3.79	20	2.05
9	87-138	276-327	3.77	20	2.05
10	376-427	276-327	3.65	20	2.02
11	251-302	276-327	3.62	20	2.01
12	287-338	276-327	3.57	20	1.99
13	226-277	276-327	3.57	20	1.99
14	76-127	276-327	3.55	20	1.99
15	126-177	276-327	3.53	20	1.98
16	112-163	276-327	3.53	20	1.98
17	276-327	276-327	3.51	20	1.98
18	301-352	276-327	3.48	20	1.97
19	176-227	276-327	3.33	20	1.93
20	162-213	276-327	3.31	20	1.92

F

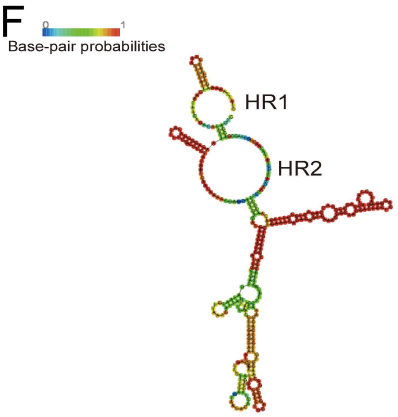

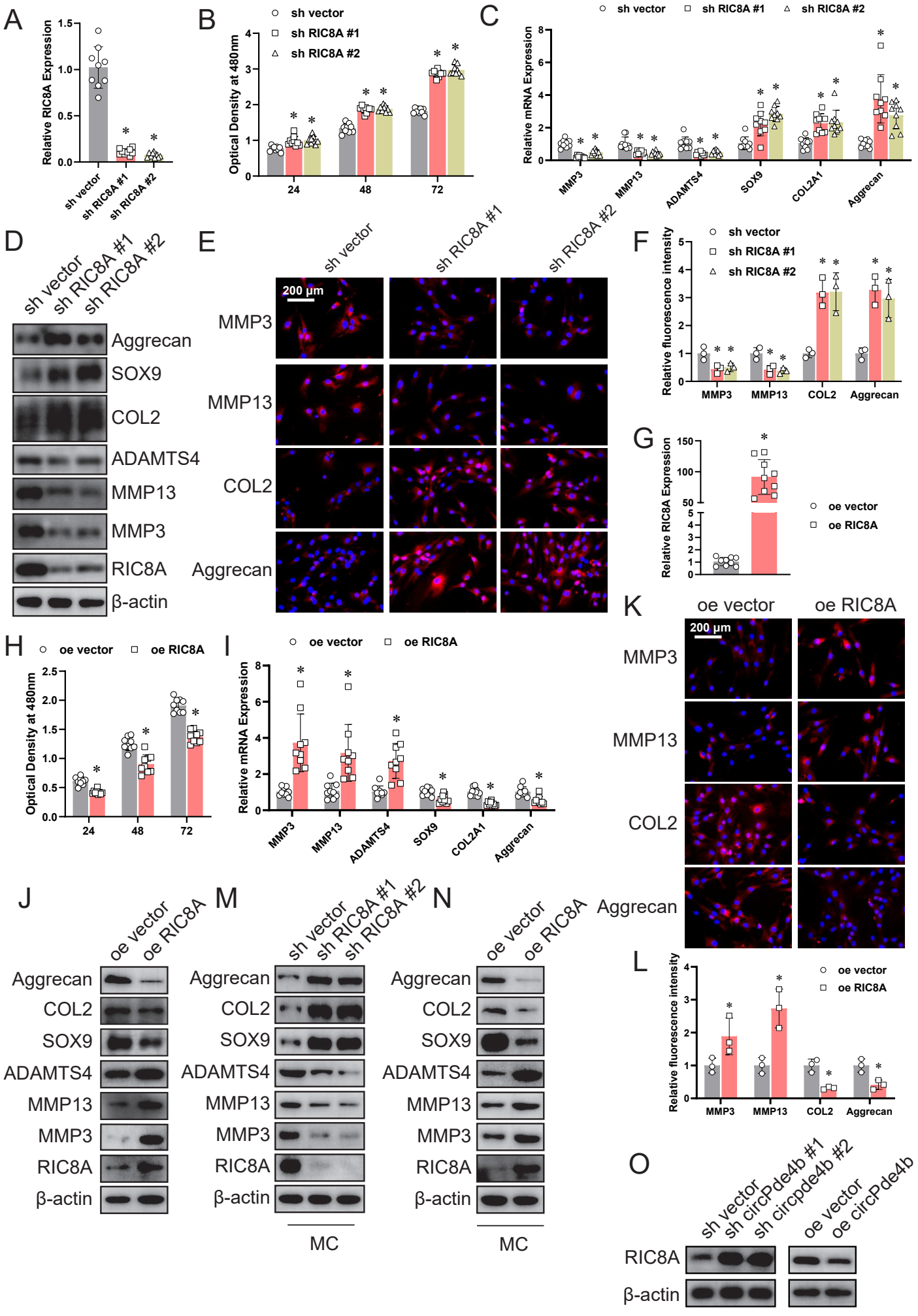
A
Relative RIC8A Expression
sh vector
sh RIC8A #1
sh RIC8A #2
B
Optical Density at 480nm
24
48
72
C
Relative mRNA Expression
MMP3
MMP13
ADAMTS4
SOX9
COL2A1
Aggrecan
D
Aggrecan
SOX9
COL2
ADAMTS4
MMP13
MMP3
RIC8A
β-actin
E
200 μm
F
Relative fluorescence intensity
COL2
G
Relative RIC8A Expression
oe vector
oe RIC8A
H
I
J
M
N
K
oe vector
oe RIC8A
L
O
sh circPde4b #1
sh circpde4b #2
oe circPde4b
MC

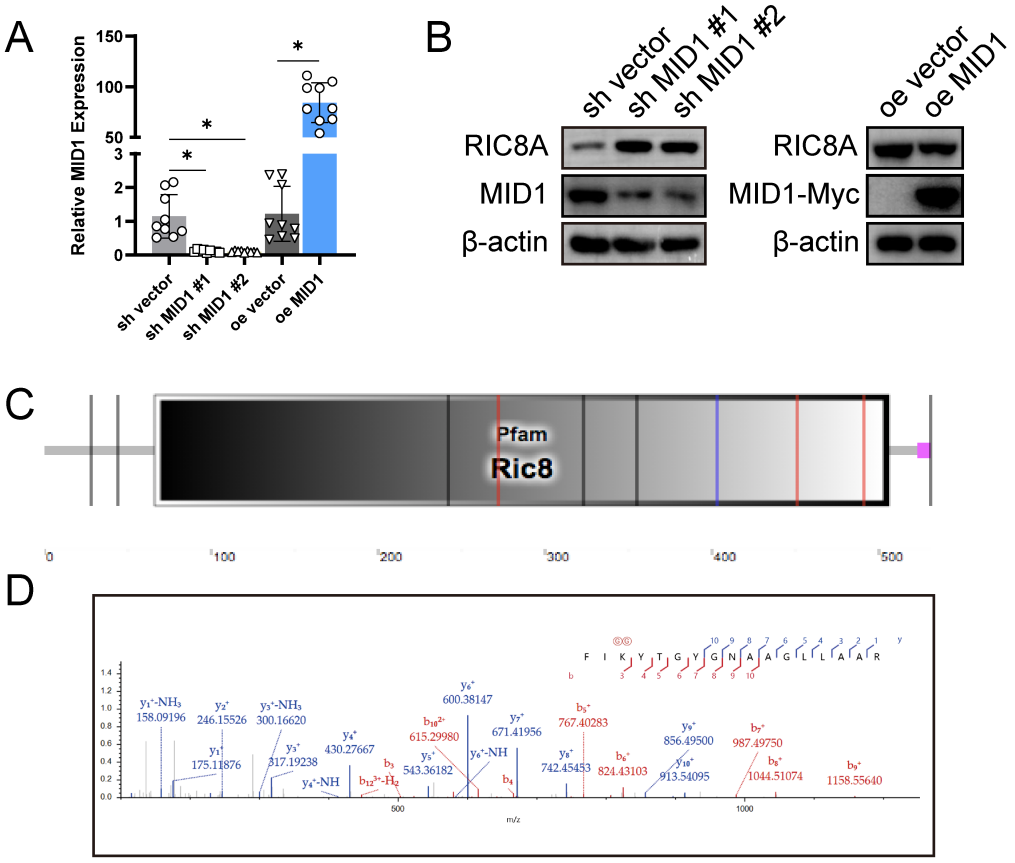
A
Relative MID1 Expression
150
100
50
3
2
1
0
*
*
*
sh vector
sh MID1 #1
sh MID1 #2
oe vector
oe MID1
B
sh vector
sh MID1 #1
sh MID1 #2
oe vector
oe MID1
RIC8A
MID1
β-actin
RIC8A
MID1-Myc
β-actin
C
Pfam
Ric8
0
100
200
300
400
500
D
F I K Y T G Y G N A A G L L A A R
y1+-NH3 158.09196
y2+ 246.15526
y3+-NH3 300.16620
y1+ 175.11876
y3+ 317.19238
y4+ 430.27667
y4+-NH
b3
b12 3+-H2
y5+ 543.36182
b18 2+ 615.29980
y6+ 600.38147
y6+-NH
b4
y7+ 671.41956
b5+ 767.40283
y8+ 742.45453
b6+ 824.43103
y9+ 856.49500
y10+ 913.54095
b7+ 987.49750
b8+ 1044.51074
b9+ 1158.55640
600
1000
m/z

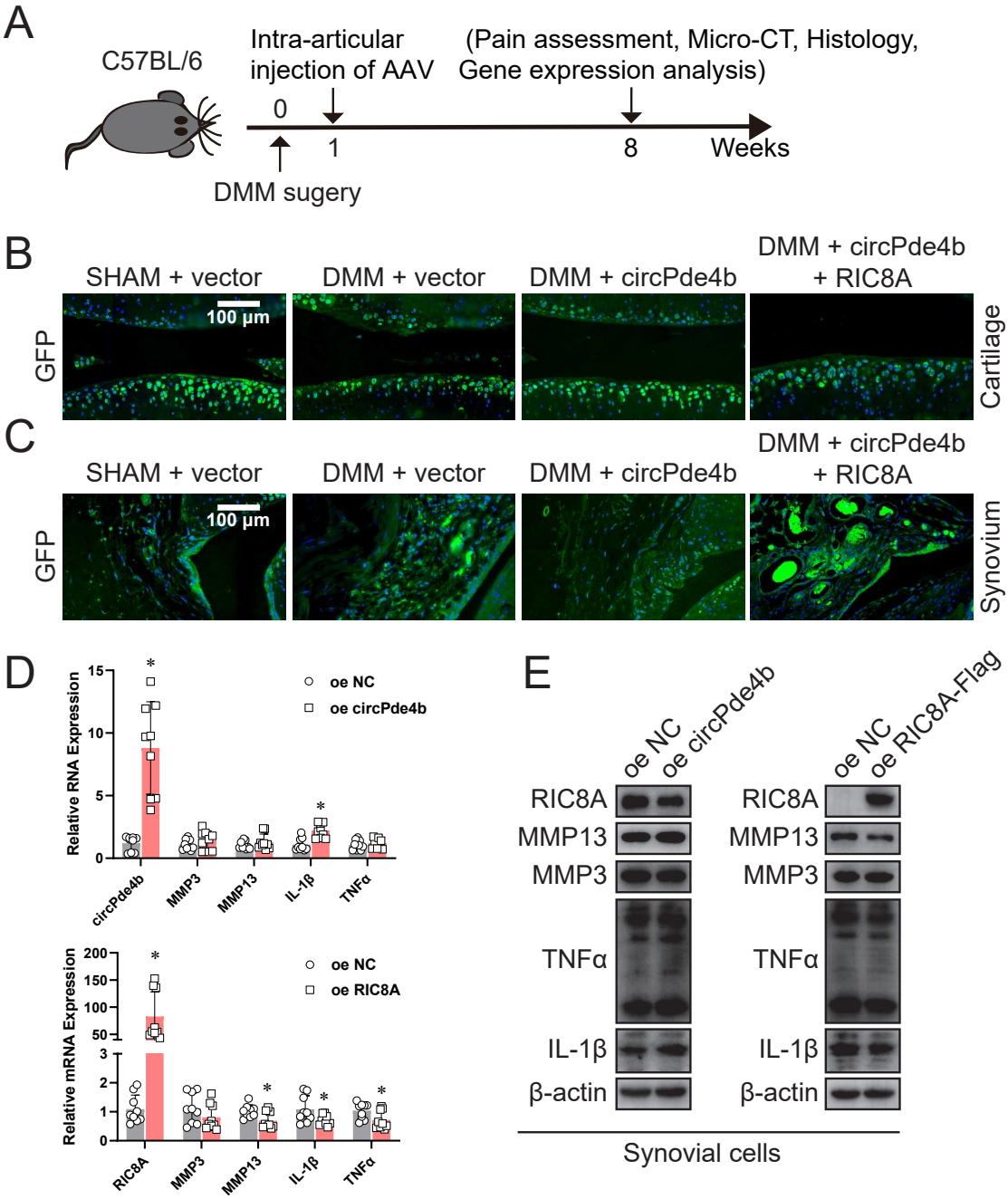
A
C57BL/6
Intra-articular injection of AAV
(Pain assessment, Micro-CT, Histology, Gene expression analysis)
0
1
8
Weeks
DMM sugery
B
SHAM + vector
DMM + vector
DMM + circPde4b
DMM + circPde4b + RIC8A
GFP
100 μm
Cartilage
C
SHAM + vector
DMM + vector
DMM + circPde4b
DMM + circPde4b + RIC8A
GFP
100 μm
Synovium
D
Relative RNA Expression
oe NC
oe circPde4b
circPde4b
MMP3
MMP13
IL-1β
TNFα
Relative mRNA Expression
oe NC
oe RIC8A
RIC8A
MMP3
MMP13
IL-1β
TNFα
E
oe NC
oe circPde4b
oe NC
oe RIC8A-Flag
RIC8A
MMP13
MMP3
TNFα
IL-1β
β-actin
Synovial cells

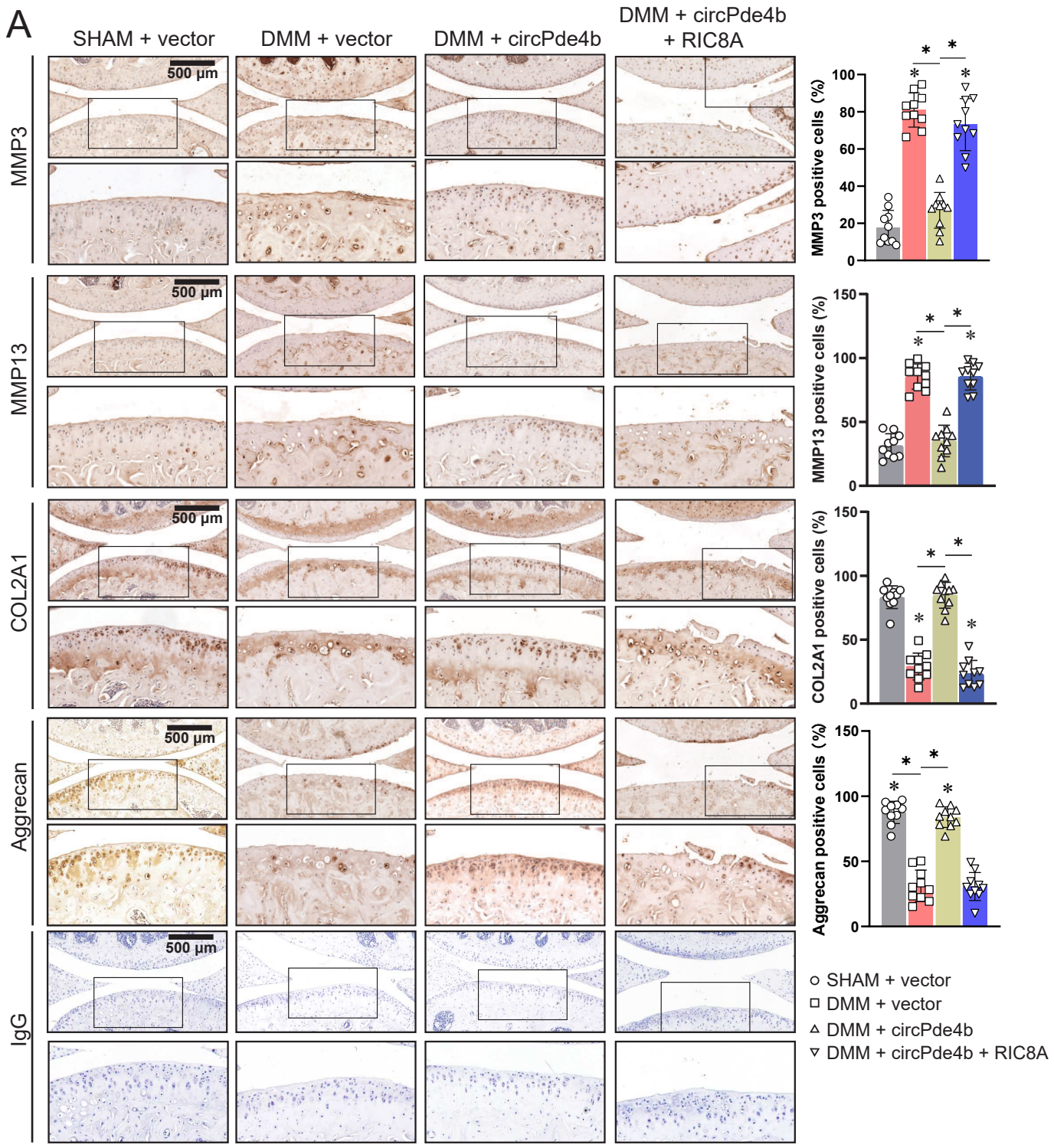
A
SHAM + vector
DMM + vector
DMM + circPde4b
DMM + circPde4b + RIC8A
MMP3
MMP13
COL2A1
Aggrecan
IgG
500 μm
MMP3 positive cells (%)
MMP13 positive cells (%)
COL2A1 positive cells (%)
Aggrecan positive cells (%)
SHAM + vector
DMM + vector
DMM + circPde4b
DMM + circPde4b + RIC8A

SUPPLEMENTARY MATERIALS

CircPDE4B prevents articular cartilage degeneration and promotes repair by acting as a scaffold for RIC8A and MID1

Shuying Shen#, Yute Yang#, Panyang Shen#, Jun Ma, Bin Fang, Qingxin Wang, Kefan Wang, Peihua Shi, Shunwu Fan*&Xiangqian Fang*

SUPPLEMENTARY MATERIALS AND METHODS

Human cartilage

The collection and classification of human cartilage samples was approved by the Ethics Committee of Sir Run Run Shaw Hospital (Zhejiang, China). Informed consent was obtained from all participants. Control cartilage was collected from ten amputees without a history of OA (n = 10), and damaged cartilage was obtained from individuals with a history of OA after total knee replacement surgery (n = 10). The cartilage was divided into three groups: normal medial, OA lateral and OA medial. The tibial plateau cartilage without the protection of a meniscus cover comprising an area of approximately 1 cm (width) × 2 cm (length) along the midline of the medial or lateral tibial plateau was defined as the region of interest (ROI). The Kellgren-Lawrence grade (upon preoperative imaging), Outerbridge grade (by visual observation in isolated specimens), and OARSI grade (after histomorphological staining) was exploited to evaluated specimen OA severity. Among them, Outerbrdige and OARSI grading were used to evaluate the cartilage ROI.

Plasmids

Human/mouse circPDE4B linear sequence (351/350 bp) was synthesized and subcloned into pHBAd-circRNA (HanBio., Shanghai, China). For RNA binding protein immunoprecipitation (RIP) assay, linear circPDE4B truncated mutants and wild type (WT) were cloned into the pcDNA3.1 vector. For RIP and immunoprecipitation (IP) assay, human RIC8A cDNA (1,614 bp) was synthesized and its truncations were subcloned into pcDNA3.1 vector. Mutants of RIC8A were prepared with GeneTailorTM Site-Directed Mutagenesis System (Invitrogen) and primers (table S3). Specially, RIC8A K415R was synthesized and subcloned to pcDNA3.1 vector. For HEK-293T co-IP assay, RIC8A cDNA (1614) /N/C terminal and MID1 cDNA (2,004 bp) were synthesized and then subcloned into pLVX-IRES-puro-Flag or pLVX-IRES-blasticidin-Myc (Addgene). For human chondrocytes (HCs) IP/co-IP assay, Myc-MID1 and Flag-RIC8A lentivirus were then packaged. mmu_RIC8A was also synthesized and then subcloned into pLVX-IRES-puro-Flag, further packaged. CircPDE4B-s and circPDE4B-s-del were also synthesized (circPDE4B-s comprises presumed FUS-binging sites on both flanking introns preserved; circPDE4B-s-del resembles circPDE4B-s, but with FUS sites deleted from the surrounding introns) and subcloned into pLVX-puro vector (Addgene), then packaged lentivirus. RIC8A K415R was also subcloned into pAdEasy-EF1-MCS-CMV-GFP vector and packaged adenovirus (Hanbio Co. Ltd, Shanghai, China). For recombinant adenovirus sh hsa/mmu circPDE4B and hsa/mmu universal shRIC8A construction, oligonucleotides with gene targeting sequences (table S3) were used for the cloning of small hairpin RNA (shRNA)-encoding sequences into pAdEasy-U6-CMV-EGFP vector (Hanbio Co. Ltd, Shanghai, China). For lentivirus shFUS construction, oligonucleotides with gene targeting sequences (table S3) were used for the cloning of small hairpin RNA (shRNA)-encoding sequences into pKLO.1 vector (addgene) and then packaged. HA-ubiquitin (Ubc) lentivirus and control virus were purchased from Hanbio Co. Ltd, Shanghai, China.

Chondrocyte culture

Human chondrocytes (HCs) were extracted from knee cartilage of amputees or subjects after total knee replacement, and mouse chondrocytes (MCs) were obtained from knee cartilage of 3-day-old C57BL/6. Chondrocytes were cultured in Dulbecco's modified eagle medium (DMEM) supplemented with 10% FBS (Thermo Fisher Scientific, Waltham, MA, USA) within 24 h at 37 °C. Before culture or mRNA isolation, cells were leached using the 0.075 mm filter and rinsed with sterile phosphate-buffered saline (PBS). Primary chondrocytes with 70–80% fusion were used in subsequent experiments. While culturing, cells were cultured in an environment with 5% CO_2 at 37 °C

Animal models

Adult male C57BL/6 mice (n = 40), eight weeks of age, were used for *in vivo* experiments. According to a previous study[1 2], medial meniscus destabilization (DMM) surgery was performed to induce post-traumatic OA to form the positive control. We randomly divided mice into four groups with ten mice per group: SHAM + vector, DMM + vector, DMM + circPde4b, and DMM + circPde4b + RIC8A groups. Briefly, mice (n = 10 per group) were anesthetized, and their medial joint capsules were incised to expose the medial meniscotibial ligament (MMTL). Subsequently, the MMTL was transected with microsurgical scissors to release the ligament linked to the tibial plateau, consequently destabilizing the medial meniscus. The joints were closed after being rinsed with sterile saline. At the same time, the medial knee joint capsule was incised for sham operation. HanBio (Shanghai, China) created and packaged adeno-associated virus (AAV) vectors for circPde4b and RIC8A. One week after operation, a total of 10 μL (approximately 1×10^{12} vg/mL) of vector AAV, circPde4b AAV, or a mixture including 5 μL circPde4b AAV and 5 μL RIC8A AAV was delivered intra-articularly into the knee

joints. Eight weeks later, knee pain was evaluated using a series of assessments[3], including a hot plate test, knee extension test, and electric shock stimulated treadmill test. Briefly, in the 55 °C hot plate test, latency was recorded when the hind paw of the mouse was lifting and/or flicking/licking. In the knee extension test, the number of vocalizations that occurred during five extensions was recorded. For the electric shock stimulated treadmill test, the number of electric shocks stimulating the mouse was recorded within 2 min at a speed of 50 m/min. Following the assessments, mice were sacrificed, and both knee articular cartilages were harvested for histological analysis or gene expression analyses. We conducted all animal experiments following the approval of the Institute of Health Sciences Institutional Animal Care and Use Committee (Zhejiang, China).

Immunofluorescence

Human osteoarthritis chondrocytes were fixed in 4% paraformaldehyde for 30 min, covered with PBS containing 0.25% Triton X-100 for 15 min, and sealed with 5% BSA containing 0.25% Triton X-100 at RT for 30 min. Cells were then incubated with the following primary antibodies: anti-MMP13 (18165-1-AP, proteintech, 1:50), anti-MMP3 (ab52915, abcam, 1:100), anti-COL2 (ab34712, abcam, 1:100), and anti-aggrecan (13880-1-AP, proteintech, 1:50). After overnight incubation at 4 °C, the cells were washed three times with PBS and incubated with goat anti-rabbit IgG (H&L) at room temperature for 1 h, rinsed and the nuclei were restained with DAPI for 5 min. Target proteins were visualized by fluorescence microscopy (Carl Zeiss, USA).

Micro-CT analysis

After fixation in 70% ethanol, all samples were scanned in a 16 mm scanning tube with 10.5 mm3 volume at 55,000 V, 180 mA, with a 115 min acquisition time. To avoid

dehydration, joints were wrapped in napkins dampened with PBS while scanning. The data were analyzed using Skyscan software.

***In vitro* transcription**

Biotin-labeled oligonucleotide probes targeting junction sites of circPDE4B were synthesized (RiboBio, Guangzhou, China). Linear circPDE4B was in vitro transcribed using Biotin RNA Labeling Mix (Roche) and T7 RNA polymerase, circularized using T4 RNA ligase I, treated with RNase R, and purified with RNeasy Mini kit (Qiagen Inc.).

Histological analysis, scoring system and immunohistochemistry

After fixing in 4% paraformaldehyde, paraffin was used to embed cartilage specimens. All samples were cut into 5 μm sections, and each one-tenth was stained with 0.1% Safranin O solution as well as 0.001% Fast Green solution (Sigma-Aldrich, St. Louis, MO, USA). OARSI grade[4 5] was used to grade the severity of cartilage degeneration by two observers blinded to group-identifying information. For human cartilage, the ROI was evaluated using OARSI, while the OA severity of mice cartilage was recorded with the maximal score of observed cartilage.

For immunohistochemistry, the sections were incubated with primary antibodies at 4 °C overnight. Subsequently, the sections were incubated with secondary antibodies for 1 h (Beyotime Institute of Biotechnology, Inc., Jiangsu, China) at 25 °C. All positively stained cells along the joint surface of each sample were counted in the femoral ankle and tibial plateau region, and the proportion of positive cells was evaluated using Image-Pro Plus 6.0 [6].

RNA extraction and RT-qPCR analysis

Total RNA was extracted using RNAEX reagent (Accurate Biotechnology, Hunan) from cultured or isolated chondrocytes. Reverse transcription of mRNAs to cDNA was performed using total RNA, with kits from Accurate Biotechnology (Hunan, China). Specific circRNAs or mRNAs were quantified with SYBR® Green Premix Pro Taq HS qPCR kit (Accurate Biotechnology, Hunan, China). The ABI 7500 Sequencing Detection System (Applied Biosystems, Foster City, CA, USA) was employed for amplification. To obtain circRNA, using 3 U/μg RNase R (Epicenter, San Diego, CA, USA) or not covered total RNA at 37 °C within 20 min. The RNeasy MinElute cleanup kit (Qiagen) was then used to purify RNA. Specific primers were designed to amplify circPDE4B. Agarose gel electrophoresis and sequencing were used to detect amplification products. All reactions were repeated three times. Housekeeping β-actin gene were used for standardization. All primers are listed in table S3.

Co-immunoprecipitation (co-IP)

Co-IP was performed as previously described (Jiao et al, 2018; Li et al, 2018b), with antibodies (1:100 dilution) specific for Myc (Abcam Inc), HA (Cell Signaling Technology), FLAG (Abcam Inc), anti-Ubiquitin antibody (Abcam Inc), RIC8A (Abcam Inc), or MID1 (Abcam Inc). Bead-bound proteins were released and analyzed by western blot.

RNA interference

siRNA-mediated knockdown was used to inhibit circRNA expression. Three different siRNAs (RiboBio, Guangzhou, China) were designed and examined for circPDE4B knockdown efficiency. SiRNA sequences are listed table S3. A specific analog (RiboBio, Guangzhou, China) was used to induce miRNA expression. Plasmid transfection was performed using Lipofectamine 3000 transfection reagent (ThermoFisher). The

Lipofectamine RNAiMAX transfection reagent (ThermoFisher) was applied for siRNA delivery.

RNA binding protein immunoprecipitation

RIP assay was performed using Magna RIPTM RNA Binding Protein Immunoprecipitation kit (Millipore), with antibodies (1:100 dilution) specific for FUS (Abcam Inc), Flag (Abcam Inc) or RIC8A (Abcam Inc). Co-precipitated RNAs were then extracted with TRIzol, and the amount of circPDE4B in the eluate was determined by RT-qPCR (table S3).

RNA pull-down assay and Mass Spectrometry (MS)/ qRT-PCR

The RNA pull-down kit (BersinBio) was used for the RNA pull-down assay. The assay is based on circRNA hybridization with the target-specific biotinylated probe, followed by pull-down, reverse transcription to cDNA for amplification through quantitative real-time PCR (RT-qPCR), and sequencing. After washing with PBS, a total of 10^7 HCs were exposed to ultraviolet irradiation at 254 nm, followed by lysis with 1 mL lysis buffer and homogenized with a 0.4 mm injector. A biotinylated antisense probe (0.2 nmol), which targets the adapter sequence, or Lac Z probes (control probes) were then added to the circPDE4B-RAP mixture. Incubation at 65 °C for 10 mins was carried out, followed by hybridization for 2 h at room temperature. Thereafter, 200 μL of streptavidin-coated magnetic beads was added. Washing followed to remove non-specific binding. Protein digestion yielded peptide fragments, which were then dissolved and vortexed. We used a loading tube to load the supernatants for MS identification. Probes are displayed in table S3.

***In vitro* binding assay**

For RIC8A GST pull-down assays, GST fusion proteins from *E. coli* BL21 cells were purified overnight at 4 °C and fixed on glutathione Sepharose 4B columns. HEK-293T cells transfected with Flag-MID1 were treated as indicated. Cells were then lysed in the NETN buffer with the protease inhibitor and cultured with Sepharose, and immobilized with indicated RIC8A GST protein and circPDE4B at 4 °C for 8 h. The RIC8A/MID1-circPDE4B complex were pulled down using GST beads (Sigma). Protein was detected by SDS–PAGE and western blot.

Western blot

SDS -PAGE separated total cellular protein, which was then transferred to an Immobilon-P membrane (0.2 μm pore size, Millipore, Billerica, MA, USA). The membranes were blocked and then incubated with primary antibodies (BD Biosciences, San Jose, CA, USA) overnight at 4 °C, and subsequently incubated with secondary antibodies for 1 h. β-actin served as the internal standard and Image J was used to quantify blots intensities. The antibodies used were as follows: anti-MMP13 antibody (1:1000, abcam, ab51072), anti-MMP3 antibody (1:1000, abcam, ab52915), anti-ADAMTS4 antibody (1:1000, abcam, ab185722), anti-COL2 antibody (1:1000, abcam, ab34712), anti-SOX9 antibody (1:1000, abcam, ab185966), anti-aggrecan antibody (1:1000, abcam, ab3778), anti-RIC8A antibody (1:1000, abcam, ab194941), anti-MID1 antibody (1:1000, abcam, ab70770), anti-HA antibody (1:2000, Cell Signaling Technology, 4970s), anti-FLAG antibody (1:1000, abcam, ab205606), anti-Ubiquitin antibody (1:1000, abcam, ab140601), anti-Myc antibody (1:1000, abcam, ab32) and anti-β-actin antibody (1:2000, Cell Signaling Technology, 4970s).

RNA fluorescent *in situ* hybridization (FISH)

The cells were seeded in 12-well plates with sterile glass covers and allowed to culture overnight. Cells were then fixed with PBS containing 37% formaldehyde for 15 min at 25 °C and dehydrated with 70% ethanol at 4 °C for 1 h. Slides were hybridized for 14–16 h at 37 °C. Cy3-labeled circPDE4B probes were constructed by RiboBio (Guangzhou, China). Hybridization buffer for RNA FISH dissolved the probes at a concentration of 20 nM. Following overnight hybridization, the slides were washed with 10% formamide/2× SSC at 37 °C on an oscillator for 30 min, and subsequently washed with PBS and 0.1% (v/v) Tween 20 three times. Cells were then stained with Alexa Fluor 546-conjugated streptavidin for 1 h at the same temperature as for IF. The cover glass was restained with DAPI, fixed with ProLong Gold anti-fading reagents, and observed under a Nikon A1Si Laser Scanning Confocal Microscope (Nikon Instruments Inc., Japan). For FISH of samples from in vivo experiments, ahead of hybridization, we performed the biopsy at 37° C under 0.8% pepsin processing. Slices were then deparaffinized, rehydrated, and permeated for 30 min. The primers and probe sequences are shown in table S3.

Patient and public involvement statement

Patients or the public WERE NOT involved in the design, or conduct, or reporting, or dissemination plans of our research

Statistical analysis

All statistical analyses were performed using SPSS v22.0. Data distribution was assessed using the Shapiro-Wilk test. The Levene test was used to assess the equality of variances. Statistical analysis was performed by unpaired two-tailed Student's t-test (normal distribution and equal variances, using 95% confidence intervals for between-group differences), Welch t-test (unequal variances), or Mann–Whitney U test (non-normal distribution). Multiple group comparisons were performed by one-way analysis of

variance (normal distribution) or Kruskal–Wallis (non-normal distribution) test followed by Bonferroni or Dunn post hoc test, respectively. A P value < 0.05 was considered statistically significant.

REFERENCES

1. Glasson SS, Blanchet TJ, Morris EA. The surgical destabilization of the medial meniscus (DMM) model of osteoarthritis in the 129/SvEv mouse. *Osteoarthritis Cartilage* 2007;15(9):1061-9. doi: 10.1016/j.joca.2007.03.006
2. Chen D, Shen J, Zhao W, et al. Osteoarthritis: toward a comprehensive understanding of pathological mechanism. *Bone Res* 2017;5:16044. doi: 10.1038/boneres.2016.44 [published Online First: 2017/02/06]
3. Piel MJ, Kroin JS, van Wijnen AJ, et al. Pain assessment in animal models of osteoarthritis. *Gene* 2014;537(2):184-8. doi: 10.1016/j.gene.2013.11.091
4. Glasson SS, Chambers MG, Van Den Berg WB, et al. The OARSI histopathology initiative - recommendations for histological assessments of osteoarthritis in the mouse. *Osteoarthritis Cartilage* 2010;18 Suppl 3:S17-23. doi: 10.1016/j.joca.2010.05.025 [published Online First: 2010/10/01]
5. Pritzker KP, Gay S, Jimenez SA, et al. Osteoarthritis cartilage histopathology: grading and staging. *Osteoarthritis Cartilage* 2006;14(1):13-29. doi: 10.1016/j.joca.2005.07.014
6. Chen P, Xia C, Mei S, et al. Intra-articular delivery of sinomenium encapsulated by chitosan microspheres and photo-crosslinked GelMA hydrogel ameliorates osteoarthritis by effectively regulating autophagy. *Biomaterials* 2016;81:1-13. doi: 10.1016/j.biomaterials.2015.12.006 [published Online First: 2015/12/30]

SUPPLEMENTARY TABLES

Table S1. Top 50 differentially expressed circRNAs in control and OA tissues ranked by expression level.

id	log2FC(Con-trol/OA)	pval	regulate	significant	mean_Con	mean_OA
1:65913245|65918835	2.298017962	0.013420134	up	yes	71.57389833	14.47433303

2:223998115|224001922	2.017322781	0.037510887	up	yes	57.89743315	14.2263021
6:159682474|159688242	3.277353459	0.000604761	up	yes	38.51538065	3.882709433
7:84129123|84194668	4.416423377	0.000404841	up	yes	23.89613671	1.023738907
4:102304317|102315830	3.801482647	0.003360458	up	yes	21.73943548	1.4663222
2:223991803|224001922	2.334035326	0.013161838	up	yes	18.03811377	3.497306791
13:42953948|42970670	2.907556748	0.009637056	up	yes	16.17980657	2.069638833
5:65170617|65197151	4.154129743	0.015296915	up	yes	15.86773823	0.796862253
17:27765535|27766588	7.209593338	2.94E-10	up	yes	14.70143599	0
1:102979382|102989571	7.01468859	9.33E-11	up	yes	12.83098702	0
1:32948222|32949774	1.899306098	0.048974712	up	yes	7.811225125	2.020780085
8:17558295|17562110	5.830035008	7.60E-07	up	yes	7.605289257	0.035448292
19:45025329|45025737	2.667894244	0.014344495	up	yes	6.992268417	1.016012274
7:80761616|80789528	2.166891001	0.025288244	up	yes	6.740826549	1.423384001
19:6702127|6702579	5.725610351	3.17E-08	up	yes	5.191520209	0
8:17543318|17543715	4.576294017	1.42E-05	up	yes	4.946360357	0.111532203
5:59180595|59215968	5.27607838	1.18E-07	up	yes	3.774876381	0
10:7243558|7285954	1.954291245	0.049795018	up	yes	3.444247889	0.814584431
17:27768977|27769584	5.136722549	0.000186202	up	yes	3.418095033	0
20:54157169|54171670	4.243602481	8.27E-05	up	yes	3.089979272	0.068397727
13:42917541|	3.094148388	0.011943706	up	yes	2.836359073	0.243856855

42970670						
7:84110470|84194668	4.361466685	0.000348323	up	yes	2.810081997	0.041570553
6:107503657|107533610	2.581974853	0.045526372	up	yes	2.492951616	0.333054478
20:18297985|18306393	4.687371106	0.002144755	up	yes	2.476554324	0
4:88475841|88479507	4.543128739	4.12E-06	up	yes	2.231406616	0
7:84046324|84060558	4.025668711	0.012672298	up	yes	2.160629655	0.038797737
7:90747681|90790652	4.475075842	3.16E-06	up	yes	2.123986063	0
1:27668226|27669346	3.850469968	0.001064668	up	yes	2.109467326	0.053172438
17:66513336|66514466	4.390178942	0.001302459	up	yes	1.996889514	0
18:6301903|6312056	2.876917257	0.039095578	up	yes	1.93391171	0.176881352
1:186893011|186911389	3.106673582	0.00897813	up	yes	1.899981712	0.132179616
18:6263947|6312056	3.497797506	0.00378226	up	yes	1.830524648	0.070896584
X:148661908|148662768	2.136810258	0.026904799	up	yes	1.829022055	0.338624828
3:112109543|112113145	3.347239351	0.003786519	up	yes	1.827445988	0.089392497
4:150467673|150491035	4.255549433	1.27E-05	up	yes	1.810064475	0
17:27778690|27779056	4.225978288	1.16E-05	up	yes	1.771312099	0
22:33761371|33765953	4.194653636	0.001595289	up	yes	1.731118987	0
17:80289659|80290728	2.289891436	0.029722666	up	yes	1.684744047	0.26496392
8:105419144|105561481	2.399627165	0.025199407	up	yes	1.584695203	0.219272552
19:45022053|45028992	3.28409336	0.006756638	up	yes	1.569980322	0.071435494

2:223912253|223918010	4.053146681	0.000134317	up	yes	1.560040669	0
13:42926336|42970670	2.181505031	0.034446179	up	yes	1.511971175	0.255352047
15:45476079|45476552	3.959830453	0.001227535	up	yes	1.456065035	0
1:46077515|46080750	3.950560938	8.63E-05	up	yes	1.446099152	0
5:65170617|65215487	3.94001855	6.71E-05	up	yes	1.434842326	0
5:65242104|65273447	2.83649554	0.031810662	up	yes	1.431521832	0.114413908
14:100353687|100361921	2.884414792	0.048709863	up	yes	1.424099749	0.106403957
17:80325030|80328477	3.013454971	0.006302126	up	yes	1.419825328	0.088214614
7:84110470|84134951	3.482653818	0.002962863	up	yes	1.414107802	0.035448292
1:102939035|102946956	2.892345557	0.03182733	up	yes	1.300464786	0.088620731

Table S2. Top 50 circPDE4B-binding proteins identified by mass spectrometry (ranked by pep_score).

num	prot_acc	prot_desc	pep_score
1	P07237	Protein disulfide-isomerase OS=Homo sapiens OX=9606 GN=P4HB PE=1 SV=3	118.07
2	Q9NPQ8	Synembryn-A OS=Homo sapiens OX=9606 GN=RIC8A PE=1 SV=3	96.92
3	P06733	Alpha-enolase OS=Homo sapiens OX=9606 GN=ENO1 PE=1 SV=2	95.8
4	Q16891	MICOS complex subunit MIC60 OS=Homo sapiens OX=9606 GN=IMMT PE=1 SV=1	95.59
5	P04259	Keratin, type II cytoskeletal 6B OS=Homo sapiens OX=9606 GN=KRT6B PE=1 SV=5	92.43

6	P67936	Tropomyosin alpha-4 chain OS=Homo sapiens OX=9606 GN=TPM4 PE=1 SV=3	90.97
7	P08133	Annexin A6 OS=Homo sapiens OX=9606 GN=ANXA6 PE=1 SV=3	87.9
8	Q6WCQ1	Myosin phosphatase Rho-interacting protein OS=Homo sapiens OX=9606 GN=MPRIP PE=1 SV=3	84.9
9	P27348	14-3-3 protein theta OS=Homo sapiens OX=9606 GN=YWHAQ PE=1 SV=1	83.69
10	O00458	Interferon-related developmental regulator 1 OS=Homo sapiens OX=9606 GN=IFRD1 PE=1 SV=4	82.38
11	P04181	Ornithine aminotransferase, mitochondrial OS=Homo sapiens OX=9606 GN=OAT PE=1 SV=1	81.54
12	Q9UNL2	Translocon-associated protein subunit gamma OS=Homo sapiens OX=9606 GN=SSR3 PE=1 SV=1	80.32
13	P10809	60 kDa heat shock protein, mitochondrial OS=Homo sapiens OX=9606 GN=HSPD1 PE=1 SV=2	77.24
14	Q15084	Protein disulfide-isomerase A6 OS=Homo sapiens OX=9606 GN=PDIA6 PE=1 SV=1	72.89
15	Q7Z406	Myosin-14 OS=Homo sapiens OX=9606 GN=MYH14 PE=1 SV=2	71.8
16	E9PRG8	Uncharacterized protein C11orf98 OS=Homo sapiens OX=9606 GN=C11orf98 PE=4 SV=1	71.22
17	P68871	Hemoglobin subunit beta OS=Homo sapiens OX=9606 GN=HBB PE=1 SV=2	67.41
18	P83731	60S ribosomal protein L24 OS=Homo sapiens OX=9606 GN=RPL24 PE=1 SV=1	66.31
19	P21333	Filamin-A OS=Homo sapiens OX=9606 GN=FLNA PE=1 SV=4	66.06
20	P21127	Cyclin-dependent kinase 11B OS=Homo sapiens OX=9606	65.88

		GN=CDK11B PE=1 SV=4	
21	P48444	Coatomer subunit delta OS=Homo sapiens OX=9606 GN=ARCN1 PE=1 SV=1	64.61
22	Q12965	Unconventional myosin-Ie OS=Homo sapiens OX=9606 GN=MYO1E PE=1 SV=2	62.35
23	P42766	60S ribosomal protein L35 OS=Homo sapiens OX=9606 GN=RPL35 PE=1 SV=2	61.42
24	P05783	Keratin, type I cytoskeletal 18 OS=Homo sapiens OX=9606 GN=KRT18 PE=1 SV=2	60.52
25	P05783	Keratin, type I cytoskeletal 18 OS=Homo sapiens OX=9606 GN=KRT18 PE=1 SV=2	60.52
26	P10412	Histone H1.4 OS=Homo sapiens OX=9606 GN=HIST1H1E PE=1 SV=2	58.75
27	P43246	DNA mismatch repair protein Msh2 OS=Homo sapiens OX=9606 GN=MSH2 PE=1 SV=1	57.6
28	O43707	Alpha-actinin-4 OS=Homo sapiens OX=9606 GN=ACTN4 PE=1 SV=2	57.2
29	P08865	40S ribosomal protein SA OS=Homo sapiens OX=9606 GN=RPSA PE=1 SV=4	56.12
30	Q9NX58	Cell growth-regulating nucleolar protein OS=Homo sapiens OX=9606 GN=LYAR PE=1 SV=2	55.3
31	P06396	Gelsolin OS=Homo sapiens OX=9606 GN=GSN PE=1 SV=1	55.09
32	Q9Y4I1	Unconventional myosin-Va OS=Homo sapiens OX=9606 GN=MYO5A PE=1 SV=2	54.65
33	P62937	Peptidyl-prolyl cis-trans isomerase A OS=Homo sapiens OX=9606 GN=PPIA PE=1 SV=2	54
34	Q15233	Non-POU domain-containing octamer-binding protein OS=Homo sapiens OX=9606 GN=NONO PE=1 SV=4	51.87

35	Q7KZF4	Staphylococcal nuclease domain-containing protein 1 OS=Homo sapiens OX=9606 GN=SND1 PE=1 SV=1	51.86
36	Q5BJD5	Transmembrane protein 41B OS=Homo sapiens OX=9606 GN=TMEM41B PE=1 SV=1	50.71
37	P13796	Plastin-2 OS=Homo sapiens OX=9606 GN=LCP1 PE=1 SV=6	48.92
38	Q02809	Procollagen-lysine,2-oxoglutarate 5-dioxygenase 1 OS=Homo sapiens OX=9606 GN=PLOD1 PE=1 SV=2	48.83
39	P47755	F-actin-capping protein subunit alpha-2 OS=Homo sapiens OX=9606 GN=CAPZA2 PE=1 SV=3	47.71
40	P62701	40S ribosomal protein S4, X isoform OS=Homo sapiens OX=9606 GN=RPS4X PE=1 SV=2	46.2
41	Q96D15	Reticulocalbin-3 OS=Homo sapiens OX=9606 GN=RCN3 PE=1 SV=1	46.01
42	P62241	40S ribosomal protein S8 OS=Homo sapiens OX=9606 GN=RPS8 PE=1 SV=2	45.16
43	P27797	Calreticulin OS=Homo sapiens OX=9606 GN=CALR PE=1 SV=1	44.29
44	P31946	14-3-3 protein beta/alpha OS=Homo sapiens OX=9606 GN=YWHAB PE=1 SV=3	42.45
45	P04844	Dolichyl-diphosphooligosaccharide--protein glycosyltransferase subunit 2 OS=Homo sapiens OX=9606 GN=RPN2 PE=1 SV=3	42.04
46	P46777	60S ribosomal protein L5 OS=Homo sapiens OX=9606 GN=RPL5 PE=1 SV=3	41.71
47	P14618	Pyruvate kinase PKM OS=Homo sapiens OX=9606 GN=PKM PE=1 SV=4	41.29
48	P60866	40S ribosomal protein S20 OS=Homo sapiens OX=9606 GN=RPS20 PE=1 SV=1	40.91
49	Q9Y281	Cofilin-2 OS=Homo sapiens OX=9606 GN=CFL2 PE=1 SV=1	40.89

50	Q9UN86	Ras GTPase-activating protein-binding protein 2 OS=Homo sapiens OX=9606 GN=G3BP2 PE=1 SV=2	40.52

Table S3. Primers and sequences used in this study.

Primers for qPCR		
PDE4B mRNA (hsa)	F	CACACTTGGGATCGACCTCT
	R	GGAAGCGTTGTCAAAGGCAG
circPDE4B (hsa)	F	CAGAGTGAAAGGGCAAGGACT
	R	CCGTCATCACACTCCTGCTTT
Pde4b mRNA (mmu)	F	TGCGCTTGGAACTTGAGCTT
	R	GCCGCTGTCGGATGCTTTTA
circPde4b (mmu)	F	CTGTGAGCCAGGAGTGGTCTA
	R	GGTGTAACTGGAAGAGCTGTAGGAT
Human β-actin	F	AGAGCTACGAGCTGCCTGAC
	R	AGCACTGTGTTGGCGTACAG
Mouse β-actin	F	AGCCATGTACGTAGCCATCC
	R	CTCTCAGCTGTGGTGGTGAA
Human MMP3	F	CCTACAAGGAGGCAGGCAAG
	R	CCCGTCACCTCCAATCCAAG
Human MMP13	F	TCGGCCACTCCTTAGGTCTT
	R	AAGTGGCTTTTGCCGGTGTA
Human COL2A1	F	TCCTGCCGTTTCGCTG
	R	CATTATACCTCTGCCCATCCTG
Human ADAMTS4	F	GTCCCATGTGCAACGTCAAG
	R	ATGCGGCCATCTTGTCATCT
Human ADAMTS5	F	GGGCACTGGCTACTATGTGG
	R	CGTCACAGCCAGTTCTCACA
Human Aggrecan	F	GGGACCTGCAAGGAGACAGAG
	R	TCAATCTCACACAGGTCCCCTTC
Human SOX9	F	GCTCTGGAGACTTCTGAACGA
	R	CCGTTCTTCACCGACTTCCT
Human RIC8A	F	GCTCTGCGGTCATACAACCAG
	R	GTCTCTTCCGGTCCTCCTGTT
Mouse RIC8A	F	AGATGCGGTGACAGAAGCTC
	R	CACGGTGCTTTGGTGACAAG
Mouse MMP13	F	CAAGCAGTTCCAAAGGCTACA

	R	TAGGGCTGGGTCACACTTCT
Mouse MMP3	F	ACTGTGTCCCAAGGAGAGGAG
	R	AAACCATCTACACAGTTCAGACAC
Mouse COL2A1	F	CACGCATGAGCCGAAGCTA
	R	GGGTTTCCACGTCTCACCA
Mouse ADAMTS4	F	TTGTTCTCCCAGTCACCCTCC
	R	AGCCTGGGACTAAAGATAGGCA
Mouse ADAMTS5	F	ATGCAGCCATCCTGTTCACC
	R	AAGGCCAAGTAGATGCCCAATTT
Mouse Aggrecan	F	CACTGTCAAAGCACCATGCC
	R	TAGGCTGGCTCCCATTCAGT
Mouse SOX9	F	TAATTCCCCAGGCTCTTGGAT
	R	GCAGCCGGGATTTAAGGCTC
Human MID1	F	CTGATCCGAGGCAAAGAGCC
	R	CAGGCACTCGTCACAGTAGG
Human FUS	F	TTATGGCCAGAGCCAGAACAC
	R	GCTACCGTAACTTCCCGAGG
Human DHX9	F	GTACGGCCTGGATTCTGCTT
	R	ATCACAGCATCCAAAGGGGG
Primers for Site-Directed Mutagenesis		
RIC8A K143R	F	ctctgtgagcctcaccactaggcgggc
	R	gcccgcctagtggtgaggctcacagag
RIC8A K187R	F	gcgcactcctctcagctcctgaaacagctg
	R	cagctgtttcaggagctgagaggagtgcgc
RIC8A K237R	F	acctccccctgatggagtccagggtg
	R	caccctggactccatcaggggggaggt
RIC8A K285R	F	gagaacatccagacacctgaggggcaagttccc
	R	gggaacttgcccctcaggtgtctggatgttctc
RIC8A K319R	F	tgtgcaaacgcctctctaggaagatgaggaggg
	R	ccctcctcatcttcctagagaggcgtttgcaca
RIC8A K328R	F	ctacactctccctcagcctgtgtgtcttgtgca
	R	tgcacaagacacacaggctgagggagagtgtag
RIC8A K415R	F	cccatagcctgtgtacctgatgaatcggggcac
	R	gtgccccgattcatcaggtacacaggctatggg
RIC8A K456R	F	tttatgctggctctggcttccttgtactcatctgtg
	R	cacagatgagtacaaggaagccagagccagcataaa
RIC8A K469R	F	ttaggcggcctctcctccaccctcccg
	R	cgggagggtggaggagaggccgcctaa

Primers for PCR		
Divergent- β-actin	F	CAGGGCTTACCTGTACACTGA
	R	GCGCGGCGATATCATCATCC
β-actin	F	AGAGCTACGAGCTGCCTGAC
	R	AGCACTGTGTTGGCGTACAG
CircPDE4B	F	CAGAGTGAAAGGGCAAGGACT
	R	CCGTCATCACACTCCTGCTTT
mPDE4B	F	CACACTTGGGATCGACCTCT
	R	GGAAGCGTTGTCAAAGGCAG
Divergent- β-actin (Mouse)	F	GGCCTGTACACTGACTTGAGA
	R	AAGGAGCTGCAAAGAAGCTGT
β-actin (Mouse)	F	AGCCATGTACGTAGCCATCC
	R	CTCTCAGCTGTGGTGGTGAA
CircPDE4B (Mouse)	F	CTGTGAGCCAGGAGTGGTCTA
	R	GGTGTAACTGGAAGAGCTGTAGGAT
PDE4B (Mouse)	F	TGCGCTTGGAACTTGAGCTT
	R	GCCGCTGTCGGATGCTTTTA
ShRNA		
CircPDE4B shRNA-1	F	CCGGCCAGGAGTGGTATTAAAAACTCGAGTTTTTAATACCACTCCTGGTTTTTC
	R	AATTGAAAAACCAGGAGTGGTATTAAAAACTCGAGTTTTTAATACCACTCCTGG
CircPDE4B shRNA-2	F	CCGGGGAGTGGTATTAAAAAGTGCTCGAGCACTTTTTAATACCACTCCTTTTTC
	R	AATTGAAAAAGGAGTGGTATTAAAAAGTGCTCGAGCACTTTTTAATACCACTCC
RIC8A shRNA-1	F	CCGGACCGCACAGAGGAGTTCCACTCGAGTGGAACTCCTCTGTGCGGTTTTTTC
	R	AATTGAAAAAGGAGTGGTATTAAAAAGTGCTCGAGCACTTTTTAATACCACTCC
RIC8A shRNA-2	F	CCGGCATGTTTGACAAGCTCTCCCTCGAGGGAGAGCTTGTCAAACATGTTTTTC
	R	AATTGAAAAACATGTTTGACAAGCTCTCCCTCGAGGGAGAGCTTGTCAAACATG
MID1 shRNA-1	F	CCGGACCGCATCCTAGTATCACACTCGAGTGTGATACTAGGATGCGGTTTTTTC
	R	AATTGAAAAAACCGCATCCTAGTATCACACTCGAGTGTGATACTAGGATGCGGT

MID1 shRNA-2	F	CCGGGCAACGTCACCCTACAGAACTCGAGTTCTGTAG GGTGACGTTGCTTTTTC
	R	AATTGAAAAAGCAACGTCACCCTACAGAACTCGAGTT CTGTAGGGTGACGTTGC
FUS shRNA-1	F	CCGGCAAGCAGATTGGTATTATTCTCGAGAATAATAC CAATCTGCTTGTTTTTC
	R	AATTGAAAAACAAGCAGATTGGTATTATTCTCGAGAA TAATACCAATCTGCTTG
FUS shRNA-2	F	CCGGCAGAGTTACAGTGGTTATACTCGAGTATAACCA CTGTAACTCTG TTTTTC
	R	AATTGAAAAACAGAGTTACAGTGGTTATACTCGAGTA TAACCACTGTAACTCTG
Mmu CircPDE4B shRNA-1	F	CCGGGGAGTGGTCTAATCTGCCACTCGAGTGGCAGAT TAGACCACTCCTTTTTC
	R	AATTGAAAAAGGAGTGGTCTAATCTGCCACTCGAGTG GCAGATTAGACCACTCC
Mmu CircPDE4B shRNA-2	F	CCGGGCCAGGAGTGGTCTAATCTCTCGAGAGATTAGA CCACTCCTGGCTTTTTC
	R	AATTGAAAAAGCCAGGAGTGGTCTAATCTCTCGAGAG ATTAGACCACTCCTGGC
SiRNAs		
Scramble si		UUCUCCGAACGUGUCACGUTT
Human CircPDE4B si-1		AGCCAGGAGTGGTATTAAA
Human CircPDE4B si-2		CCAGGAGTGGTATTAAAAA
Human CircPDE4B si-3		GGAGTGGTATTAAAAAGTG
Mouse CircPDE4B si-1		GGAGTGGTCTAATCTGCCA
Mouse CircPDE4B si-2		GCCAGGAGTGGTCTAATCT
Mouse CircPDE4B si-3		TGAGCCAGGAGTGGTCTAA
FUS si-1		CAAGCAGATTGGTATTATT
FUS si-2		CAGAGTTACAGTGGTTATA
DHX9 si-1		CGAACACCATTGCATGAAA
DHX9 si-2		GGACTAGTAGCAACATTGA
Human/Mouse RIC8A si-1		ACCGCACAGAGGAGTTCCA
Human/Mouse RIC8A si-2		CATGTTTGACAAGCTCTCC
Human KRT6B si		TACCATCAAGTCAACAGTTATCA
Human ENO1 si		GCATTGGAGCAGAGGTTTA

Human IMMT si		GGGTTGACTACTGGCAAAATTGC
Human P4HB si		GTCCTCTTTAAGAAGTTTGATGA
Probes for FISH		
Cy3-Hsa circPDE4B		5‘-Cy3-ACACTTTTTAATACCACTCCTGGCTTACAG-3’
Cy3- Mmu circPDE4B		5‘-CY3-GGCAGATTAGACCACTCCTGGCTCAC-3’
RAP and PCR sequences		
CircPDE4B pull-down probe		CATTGCTATTACAACTGTAAGCCAGGAGTGGTATTAAAAA GTGTCAGCAAACTGCATTGAATAACAGACATCCTAAGAGG GGATATTTTCCACCTCTATAATGAAGAAAAGCAGGAGTGT GATGACGGTGATGGCTGATGATAATGTTAAAGATTATTTT GAATGTAGCTTGAGTAAATCCTACAGTTCTTCCAGTAACA CACTTGGGATCGACCTCTGGAGAGGGAGAAGGTGTTGCTC AGGAAACTTACAGTTACCACCACTGTCTCAAAGACAGAGT GAAAGGGCAAGGACTCCTGAGGGAGATGGTATTTCCAGGC CGACCACACTGCCTTTGACAACGCTTCCAAGCATTGCTAT TACAACTGTAAGCCAGGAGTG
Lac Z pull-down probes		TGGCCGTCGTTTTACAACGTCGTGACTGGGAAAACCCTGG CGTTACCCAACTTAATCGCCTTGCAGCACATCCCCCTTTC GCCAGCTGGCGTAATAGCGAAGAGGCCCGCACCGATCGCC CTTCCCAACAGTTGCGCAGCCTGAATGGCGAATGGCGCCT GATGCGGTATTTTCTCCTTACGCATCTGTGCGGTATTTCA CACCGCATATGGTGCACTCTCAGTACAATCTGCTCTGATG CCGCATAG

1

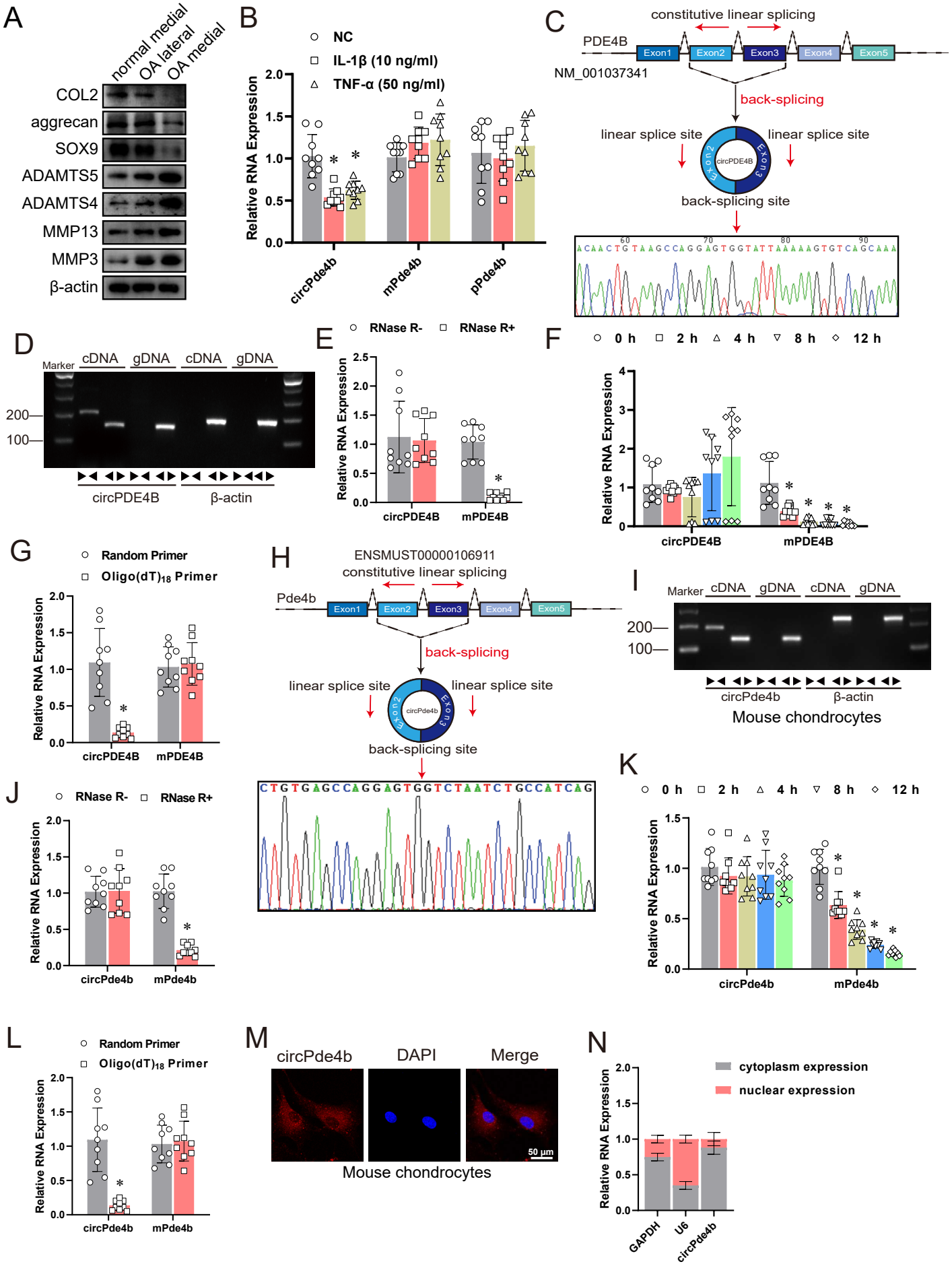
A
normal medial
OA lateral
OA medial
COL2
aggrecan
SOX9
ADAMTS5
ADAMTS4
MMP13
MMP3
β-actin
B
NC
IL-1β (10 ng/ml)
TNF-α (50 ng/ml)
Relative RNA Expression
circPde4b
mPde4b
pPde4b
C
constitutive linear splicing
PDE4B
Exon1
Exon2
Exon3
Exon4
Exon5
NM_001037341
back-splicing
linear splice site
linear splice site
circPDE4B
back-splicing site
D
Marker
cDNA
gDNA
cDNA
gDNA
200
100
circPDE4B
β-actin
E
RNase R-
RNase R+
Relative RNA Expression
circPDE4B
mPDE4B
F
0 h
2 h
4 h
8 h
12 h
Relative RNA Expression
circPDE4B
mPDE4B
G
Random Primer
Oligo(dT)18 Primer
Relative RNA Expression
circPDE4B
mPDE4B
H
ENSMUST00000106911
constitutive linear splicing
Pde4b
Exon1
Exon2
Exon3
Exon4
Exon5
back-splicing
linear splice site
linear splice site
circPde4b
back-splicing site
I
Marker
cDNA
gDNA
cDNA
gDNA
200
100
circPde4b
β-actin
Mouse chondrocytes
J
RNase R-
RNase R+
Relative RNA Expression
circPde4b
mPde4b
K
0 h
2 h
4 h
8 h
12 h
Relative RNA Expression
circPde4b
mPde4b
L
Random Primer
Oligo(dT)18 Primer
Relative RNA Expression
circPde4b
mPde4b
M
circPde4b
DAPI
Merge
50 μm
Mouse chondrocytes
N
cytoplasm expression
nuclear expression
Relative RNA Expression
GAPDH
U6
circPde4b

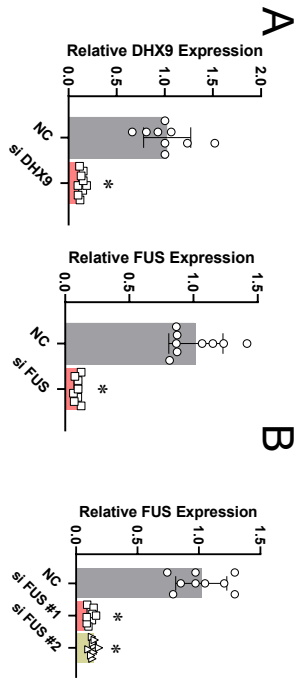
A
Relative DHX9 Expression
0.0
0.5
1.0
1.5
2.0
NC
si DHX9
*
Relative FUS Expression
0.0
0.5
1.0
1.5
NC
si FUS
*
B
Relative FUS Expression
0.0
0.5
1.0
1.5
NC
si FUS #1
si FUS #2
*
*

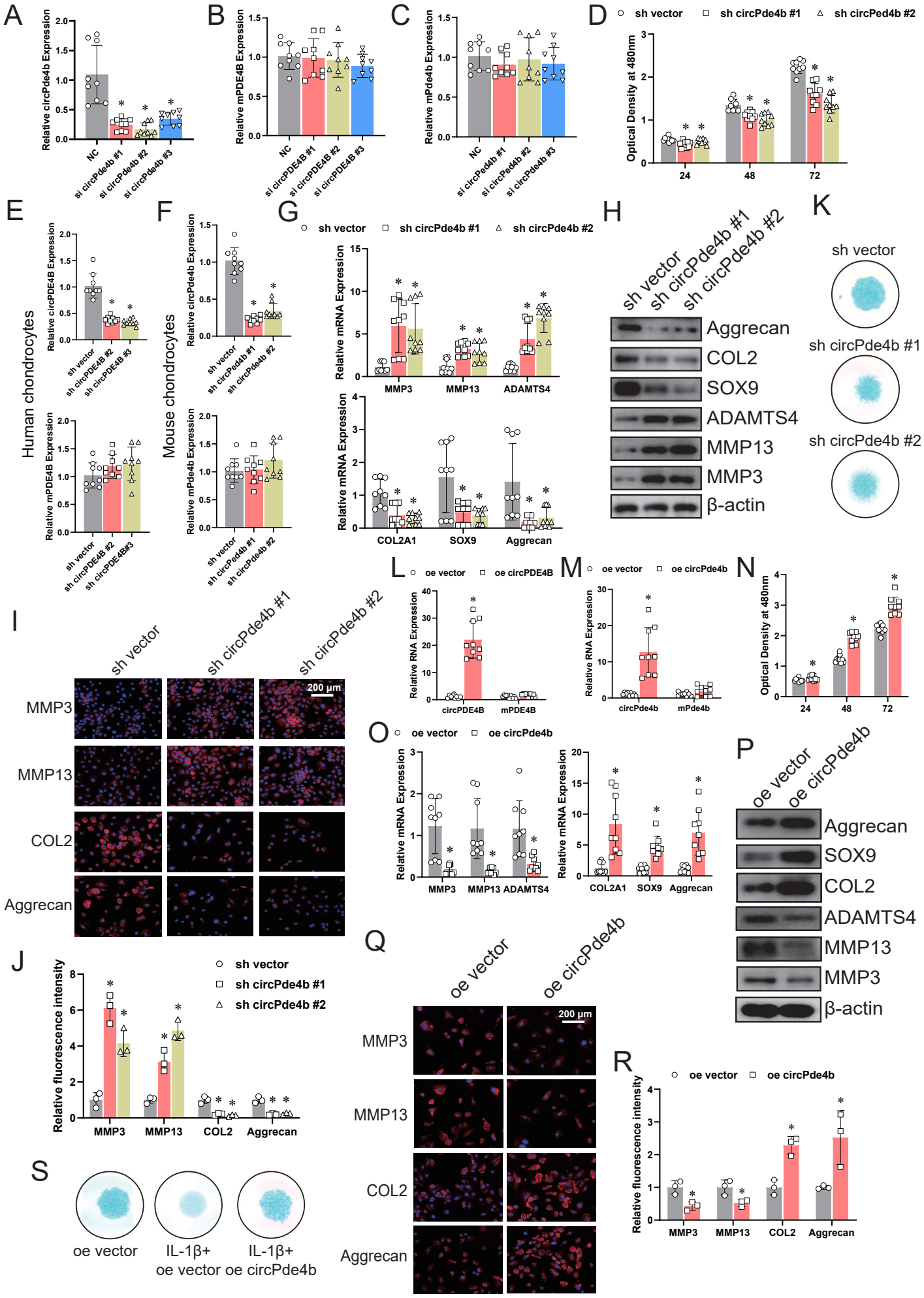
A
Relative circPde4b Expression
NC
si circPde4b #1
si circPde4b #2
si circPde4b #3
B
Relative mPDE4B Expression
si circPDE4B #1
si circPDE4B #2
si circPDE4B #3
C
Relative mPde4b Expression
D
sh vector
sh circPde4b #1
sh circPed4b #2
Optical Density at 480nm
24
48
72
E
Human chondrocytes
Relative circPDE4B Expression
sh circPDE4B #2
sh circPDE4B #3
Relative mPDE4B Expression
F
Mouse chondrocytes
Relative circPde4b Expression
sh circPde4b #1
sh circPde4b #2
Relative mPde4b Expression
G
Relative mRNA Expression
MMP3
MMP13
ADAMTS4
COL2A1
SOX9
Aggrecan
H
Aggrecan
COL2
SOX9
ADAMTS4
MMP13
MMP3
β-actin
K
sh circPde4b #1
sh circPde4b #2
L
oe vector
oe circPDE4B
Relative RNA Expression
circPDE4B
mPDE4B
M
oe circPde4b
circPde4b
mPde4b
N
I
MMP3
MMP13
COL2
Aggrecan
200 μm
O
oe circPde4b
P
Q
R
J
Relative fluorescence intensity
S
oe vector
IL-1β+ oe vector
IL-1β+ oe circPde4b

A

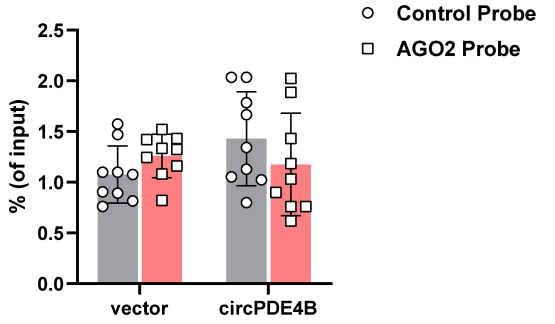

B

CPAT software: http://lilab.research.bcm.edu/cpat/calculator_sub.php

Data ID	Sequence Name	RNA Size	ORF Size	Ficket Score	Hexamer Score	Coding Probability	Coding Label
0	HSA_CIRC_0008433|NM_001037341|PDE4B	351	279	0.8886	-0.027773613549	0.076337512427542	no

ORF finder

Label	Strand	Frame	Start	Stop	Length (nt | aa)
ORF1	+	2	71	>349	279 | 92
ORF2	-	1	324	238	87 | 28

CircBank: IRES elements

ID	start	end	score
hsa_circPDE4B_003	101	274	0.60

C

ORF1-92AA
MKKSRSVMTVMADDNVKDYFECSLSKSYSSSSNTLGIDLWRGRRC
CSGNLQLPPLSQRQSERARTPEGDGISRPTTLPLTTLPSIAITTVSQE

ORF1-28AA
MLGSVVKGSVVGLEIPSPSGVLALSLCL

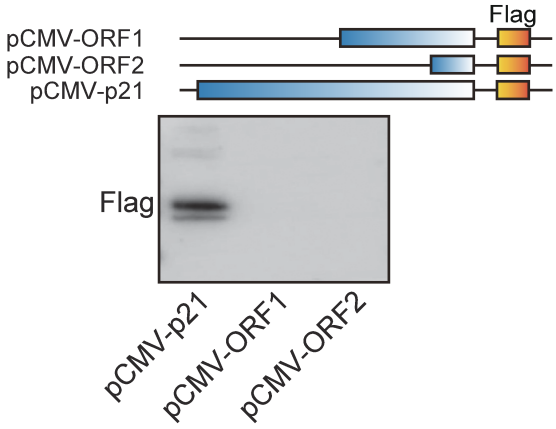

A

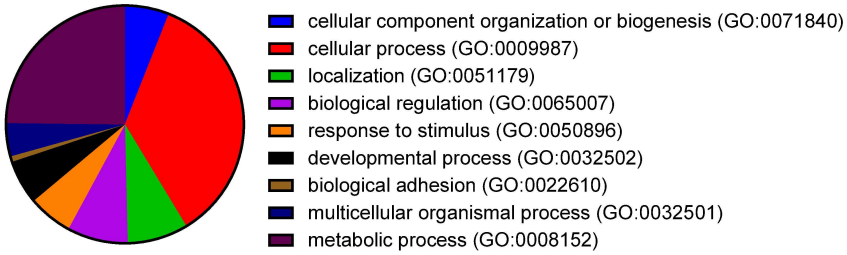

B

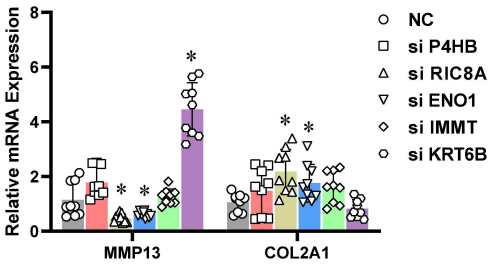

C

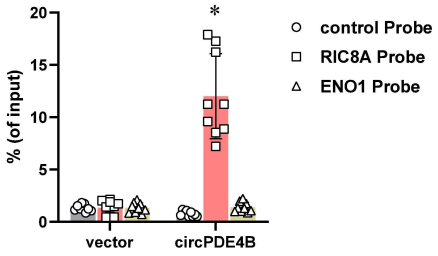

D

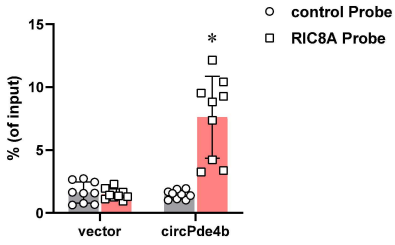

E

#	Protein region	RNA region	Interaction Propensity	Discriminative Power	Normalized Score
1	201-252	276-327	5.01	22	2.39
2	462-513	276-327	4.66	20	2.30
3	151-202	276-327	4.25	20	2.18
4	26-77	276-327	4.12	20	2.15
5	212-263	276-327	4.11	20	2.14
6	426-477	276-327	4.04	20	2.12
7	362-413	276-327	3.87	20	2.08
8	437-488	276-327	3.79	20	2.05
9	87-138	276-327	3.77	20	2.05
10	376-427	276-327	3.65	20	2.02
11	251-302	276-327	3.62	20	2.01
12	287-338	276-327	3.57	20	1.99
13	226-277	276-327	3.57	20	1.99
14	76-127	276-327	3.55	20	1.99
15	126-177	276-327	3.53	20	1.98
16	112-163	276-327	3.53	20	1.98
17	276-327	276-327	3.51	20	1.98
18	301-352	276-327	3.48	20	1.97
19	176-227	276-327	3.33	20	1.93
20	162-213	276-327	3.31	20	1.92

F

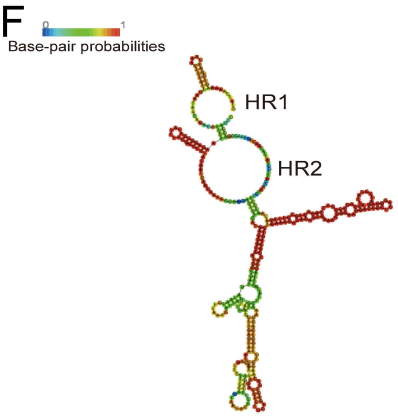

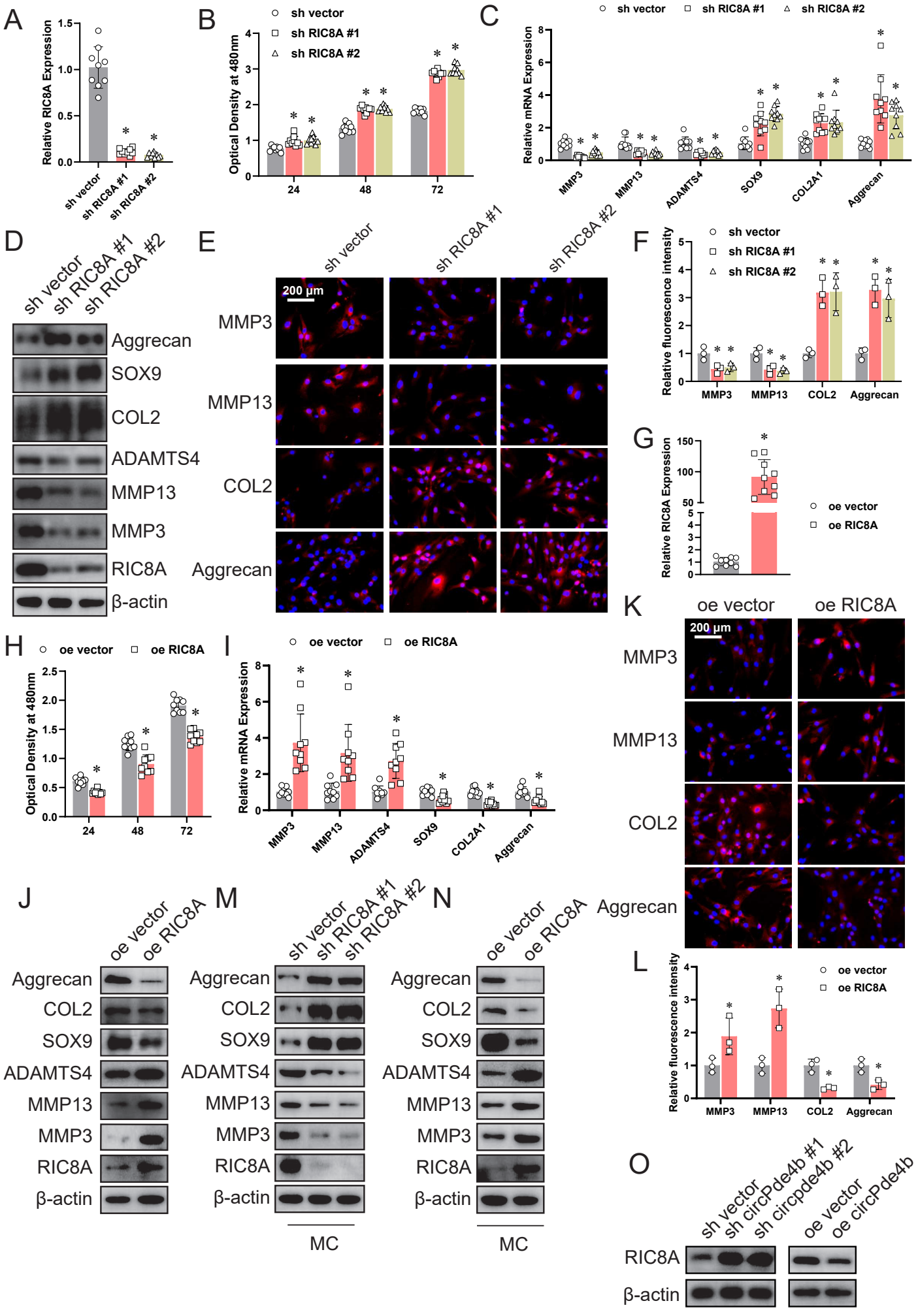
A
Relative RIC8A Expression
sh vector
sh RIC8A #1
sh RIC8A #2
B
Optical Density at 480nm
24
48
72
C
Relative mRNA Expression
MMP3
MMP13
ADAMTS4
SOX9
COL2A1
Aggrecan
D
Aggrecan
SOX9
COL2
ADAMTS4
MMP13
MMP3
RIC8A
β-actin
E
200 μm
F
Relative fluorescence intensity
COL2
G
Relative RIC8A Expression
oe vector
oe RIC8A
H
I
J
M
N
K
oe vector
oe RIC8A
L
O
sh circPde4b #1
sh circpde4b #2
oe circPde4b
MC

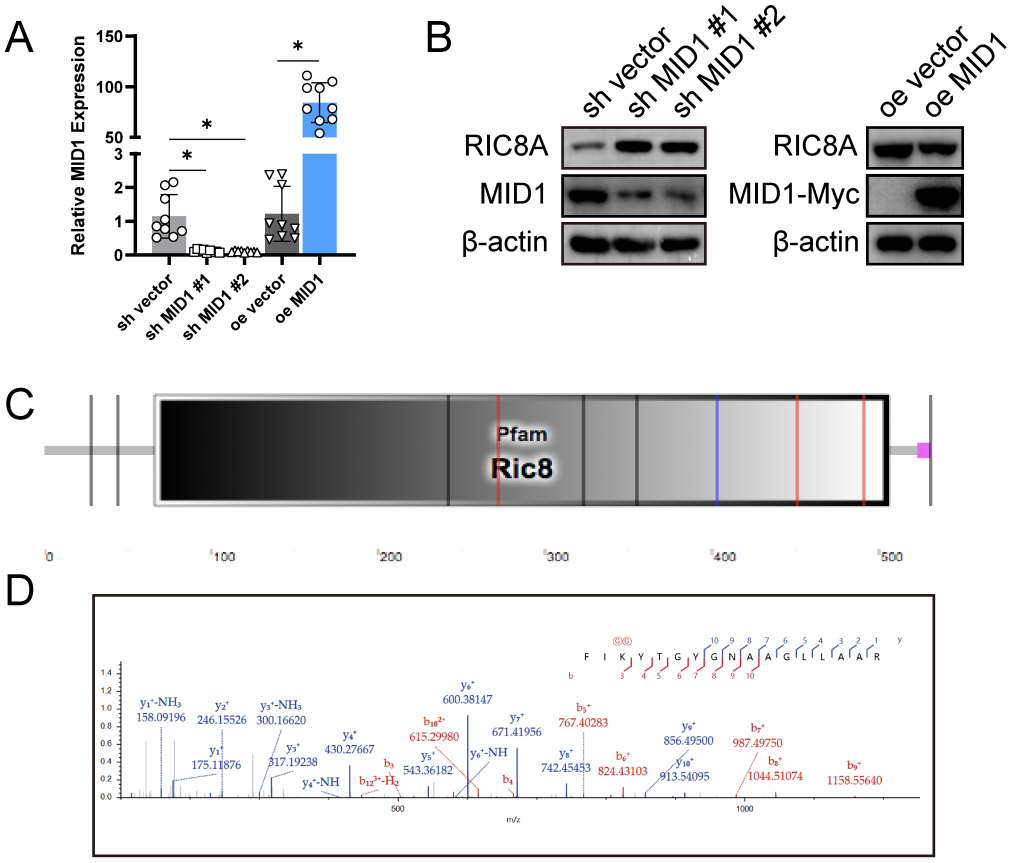
A
Relative MID1 Expression
150
100
50
3
2
1
0
*
*
*
sh vector
sh MID1 #1
sh MID1 #2
oe vector
oe MID1
B
sh vector
sh MID1 #1
sh MID1 #2
oe vector
oe MID1
RIC8A
MID1
β-actin
RIC8A
MID1-Myc
β-actin
C
Pfam
Ric8
0
100
200
300
400
500
D
F I K Y T G Y G N A A G L L A A R
y1+-NH3 158.09196
y2+ 246.15526
y3+-NH3 300.16620
y1+ 175.11876
y3+ 317.19238
y4+ 430.27667
y4+-NH
b3
b12 3+-H2
y5+ 543.36182
b18 2+ 615.29980
y6+ 600.38147
y6+-NH
b4
y7+ 671.41956
b5+ 767.40283
y8+ 742.45453
b6+ 824.43103
y9+ 856.49500
y10+ 913.54095
b7+ 987.49750
b8+ 1044.51074
b9+ 1158.55640
600
1000
m/z

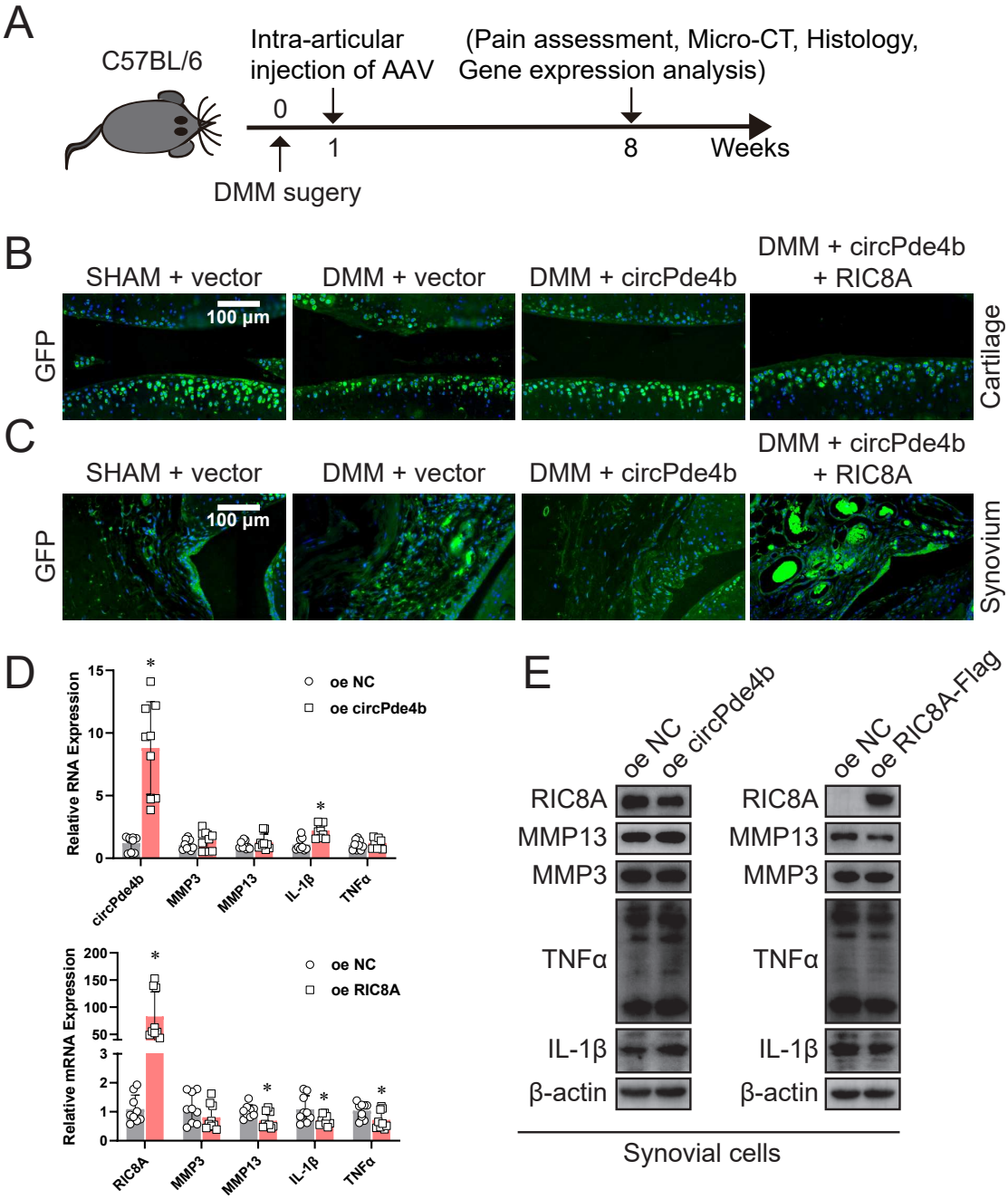
A
C57BL/6
Intra-articular injection of AAV
(Pain assessment, Micro-CT, Histology, Gene expression analysis)
0
1
8
Weeks
DMM sugery
B
SHAM + vector
DMM + vector
DMM + circPde4b
DMM + circPde4b + RIC8A
GFP
100 μm
Cartilage
C
SHAM + vector
DMM + vector
DMM + circPde4b
DMM + circPde4b + RIC8A
GFP
100 μm
Synovium
D
Relative RNA Expression
oe NC
oe circPde4b
circPde4b
MMP3
MMP13
IL-1β
TNFα
Relative mRNA Expression
oe NC
oe RIC8A
RIC8A
MMP3
MMP13
IL-1β
TNFα
E
oe NC
oe circPde4b
oe NC
oe RIC8A-Flag
RIC8A
MMP13
MMP3
TNFα
IL-1β
β-actin
Synovial cells

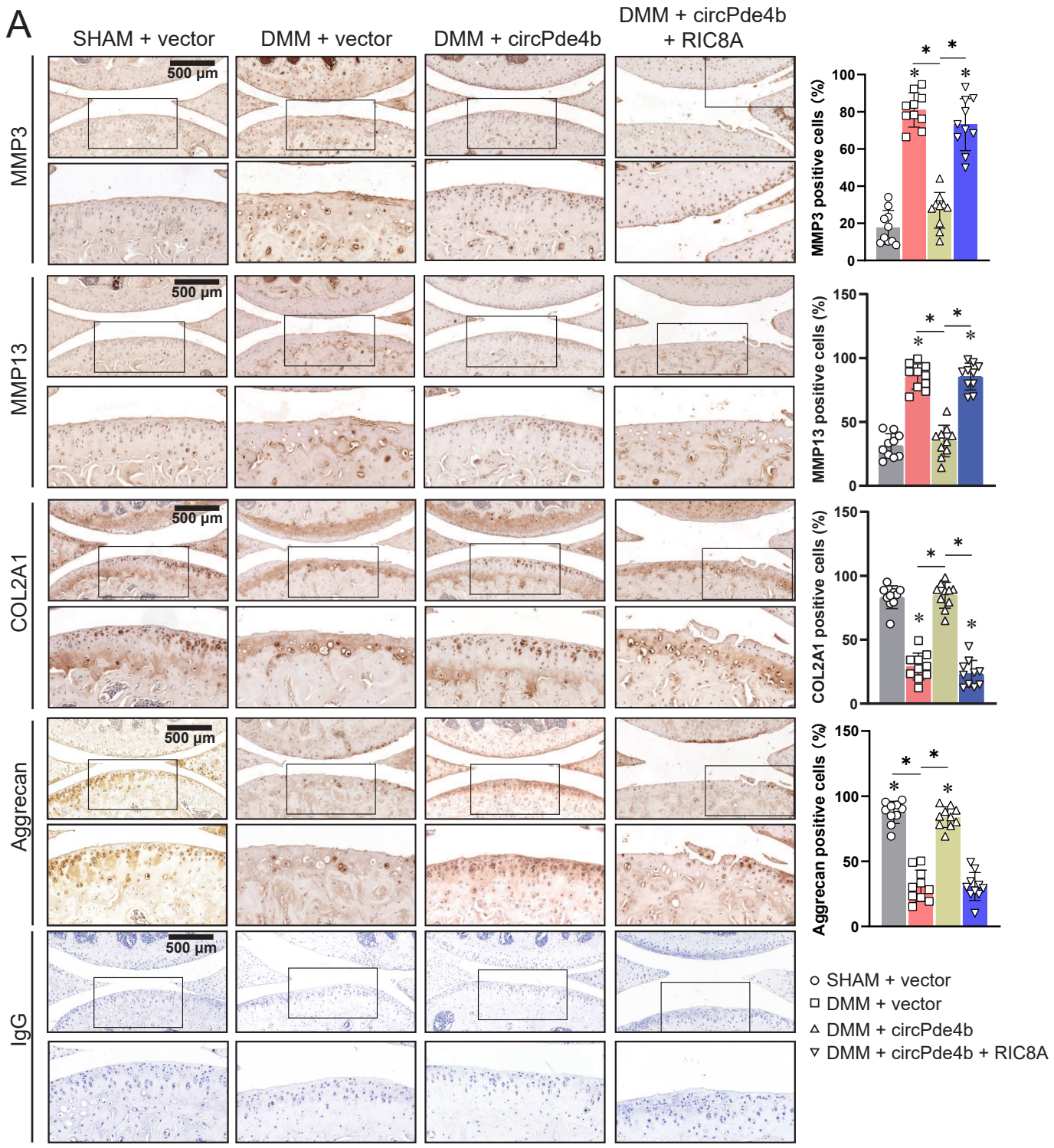
A
SHAM + vector
DMM + vector
DMM + circPde4b
DMM + circPde4b + RIC8A
MMP3
MMP13
COL2A1
Aggrecan
IgG
500 μm
MMP3 positive cells (%)
MMP13 positive cells (%)
COL2A1 positive cells (%)
Aggrecan positive cells (%)
SHAM + vector
DMM + vector
DMM + circPde4b
DMM + circPde4b + RIC8A